Norwegian University of Life Sciences
Faculty of Environmental Sciences
and Natural Resource Management

Philosophiae Doctor (PhD)
Thesis 2020:59

Leveraging non-invasive monitoring of carnivores using hierarchical models

Utvikling av ikke-invasiv overvåking av rovdyr ved hjelp av hierarkiske modeller

Mahdieh Tourani

Leveraging non-invasive monitoring of carnivores using hierarchical models

Utvikling av ikke-invasiv overvåking av rovdyr ved hjelp av hierarkiske modeller

Philosophiae Doctor (PhD) Thesis

Mahdieh Tourani

Norwegian University of Life Sciences
Faculty of Environmental Sciences and Natural Resource Management

Ås, 2020

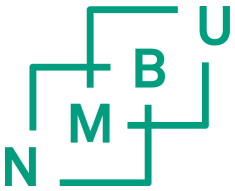

Thesis number: 2020:59
ISSN: 1894-6402
ISBN: 978-82-575-1726-7

To *Guillaume*
for the remarkable impact he had on my choices

and to fellow ecologists whom I was thinking of during my PhD:
Amirhossein Khaleghi
Taher Ghadirian
Houman Jowkar
Sam Radjabi

PhD supervisors

Richard Bischof
Faculty of Environmental Sciences and Natural Resource Management
Norwegian University of Life Sciences
P.O. Box 5003, 1432 Ås
Norway

Olivier Gimenez
CEFE, CNRS, University Montpellier
University Paul Valéry Montpellier 3, EPHE, IRD, Montpellier
France

Muhammad Ali Nawaz
Department of Animal Sciences
Quaid-i-Azam University, 4400 Islamabad
Pakistan

Adjudication committee

Beth Gardner
School of Environmental and Forest Sciences
University of Washington
Seattle, WA
USA

Erlend B. Nilsen
Norwegian Institute for Nature Research
P.O. Box 5685, Torgard, NO-74 Trondheim
Norway

Leif Egil Loe
Faculty of Environmental Sciences and Natural Resource Management
Norwegian University of Life Sciences
P.O. Box 5003, 1432 Ås
Norway

Acknowledgements

If people are asked to picture an ecologist, chances are that many will think of Jane Goodall or George Schaller; determined field workers wearing cargo pants, taking the adventures of searching for any signs of a living being. Yet, the past few decades has seen ecologists who embark on a different journey. They may still wear cargo pants, but the essential equipment is a computer full of code and statistical models, to venture through a jungle of tables filled with row upon row of data. Belonging to the latter group, my degree project was never possible without the use of computers, open source software, good instinct of those who collect data in long-term databases, and dedicated people who write books and tutorials for others to use. I would like to name Marc Kéry, Andy Royle and Michael Schaub for their invaluable books that changed my view of ecology.

Richard, I would like to thank you for all I have learned from you, for your involvement throughout my PhD project and for letting your network be my network. If it was not for your training and trust, I would have not dared to teach master-level courses and supervising master students at NMBU. You did not give me a fish but taught me to fish.

Ehsan, I mention you the second here as a colleague; You have heard all my half-cooked ideas, read all I have written, stayed awake the nights I was writing my thesis, and kept the company during the weekends I was at office. I am grateful we managed to keep our education path almost identical, and I am excited about our collaboration on many research projects to come.

Pierre, I am grateful to you for your contribution in several of my PhD chapters, and for being a thoughtful colleague. I believe every lab needs a member with your attitude and I hope we can continue working together.

Cyril, I have benefited from your developments indirectly, and you have contributed to some of my PhD chapters. Thanks to you, and to all collaborators of the projects RovQuant and WildMap: Henrik Brøseth, Joe Chipperfield, Andy Royle, Daniel Turek, Perry de Valpine, Jonas Kinberg, Soumen Dey, and Olivier Gimenez who influenced the quality of my research. Use of empirical data in chapter one was facilitated by John Odden and I am thankful for that. The names and contributions of many other individuals are given in the Acknowledgements section of each of the four articles that comprise this thesis.

Olivier, I developed a few ideas to work with you during my PhD, which unfortunately all failed due to different reasons including the COVID-19 pandemic

that cancelled my visit to Montpellier. I believe I have benefited from your ideas indirectly and I hope I can work with you more closely in the future. Thank you for making yourself available for providing feedback on my Synopsis during the last few weeks of my thesis submission. Muhammad Ali, thanks for discussions related to the Himalayan brown bear study.

Andrés Ordiz and Gabriel Pigeon were my "opponents" during the PhD transition process, and Ryan Burner, Gabriel Pigeon and Pierre Dupont read an earlier draft of my Synopsis – I am grateful for their thorough reviews and helpful comments.

I would like to thank MINA, all staff, researchers, PhD students during the past three years and the Ecology Group for organising social events and for returning smiles, in particular my office neighbours Jon Swenson and Svein Dale. During the production of this document, I received support from Grethe Delbeck, Ole Wiggo Røstad, and Jan Vermaat. Thanks to Henrik Brøseth, Monica Tronrud, Neri Thorsen, and Katrine Eldegard for discussing the Norwegian sections.

Bischof family, thank you for your generosity and welcoming smiles in many occasions. We spent many events together, even I crashed your summer vacation in 2017, and thank you Vilma for being my first person to go for advice as an expat in Norway.

The PhD position came about because of a research prize from the Norwegian University of Life Sciences (Universitetet for miljø- og biovitenskap) awarded to Richard Bischof for his performance in research, and I am honored to have been entrusted with the resulting fellowship. I have been privileged to access free higher education all way long, and been supported by family, mentors and friends to follow my dreams in academia. I dream of a world of open science and free higher education for all students.

Contents

Abstract

The development of non-invasive approaches for monitoring wildlife populations made it feasible to obtain ecological parameters across landscapes and populations, rather than a few locations or individuals. The two most popular and widespread non-invasive monitoring methods are camera trapping and genetic sampling. The technical development associated with data collection has been impressive, whilst analytical capabilities have lagged behind. Only recently are we getting close to exploiting the potentials of non-invasively obtained data. The objective of my thesis is to apply modern hierarchical analytical models to several sets of carnivore monitoring data to address a series of conceptually and methodologically connected problems, faced by applied ecologists.

The thesis consists of four articles. Two of these include simulations, and all four articles involve model fitting and case studies. The latter target a range of species including wolverine and mesocarnivores in Scandinavia and the Himalayan brown bear.

Article I quantifies detectability of mesocarnivores by camera traps and sheds light on the behavioural responses of focal species to detection devices and to olfactory lures as an important aspect of detectability. **Article II** incorporates multiple data sources with varying levels of information in a data-sparse situation and introduces a multiple observation process model in the spatial capture-recapture framework to estimate population parameters. This model is applied to multi-method monitoring data of a Himalayan brown bear population in Pakistan. The focus in **Article III** is heterogeneity in the environment and it uncovers sex-specific patterns in wolverine home range size across the species' range in Norway using solely non-invasively collected DNA data and spatial capture-recapture models. **Article IV** presents and evaluates an extension of the open-population spatial capture-recapture model to improve inferences on population parameters and showcases its application on wolverine data in central Norway.

Hierarchical modelling offers ecologists an intuitive multi-level approach to disentangle observation and ecological processes. All chapters of this thesis include hierarchical models that account for imperfect detection. Depending on the research question, I use these models to estimate time-to-detection of species, population abundance and density, survival, variation in home range size and inter-annual movement. The monitoring methods used during this thesis are often applied to studies of rare or elusive species and data sparsity is another important challenge

addressed in this thesis. Bayesian inference Using Gibbs Sampling (BUGS) language facilitates the construction of flexible models that make the incorporation of multiple types of data into one comprehensive analysis comparatively straightforward. The articles included in this thesis showcase how hierarchical models help us use non-invasively collected data to yield answers to a range of questions in applied ecology. Tackling the associated challenges increases our ability to draw inferences that more closely describe the complexity of real-world ecological systems.

Sammendrag

Utviklingen av ikke-invasive metoder for å overvåke dyrepopulasjoner har gjort det mulig å estimere økologiske parametere på tvers av landskap og populasjoner, snarere enn noen få steder eller individer. De to mest populære og utbredte ikke-invasive overvåkingsmetodene er viltkameraer og genetisk prøvetaking. Den tekniske utviklingen knyttet til datainnsamling har vært imponerende, mens analytiske evner har hengt etter. Først nylig har vi kommet i nærheten av å utnytte potensialet til ikke-invasivt innsamlede data. Målet med avhandlingen min er å bruke moderne hierarkiske analytiske modeller på flere sett med overvåkningsdata av rovdyr for å adressere en serie konseptuelt og metodisk koblede problemer, som anvendte økologer møter.

Oppgaven består av fire artikler. To av disse inkluderer simuleringer, og alle de fire artiklene involverer modelltilpassing og case-studier på en rekke arter, inkludert jerv og mesokarnivorer i Skandinavia og Himalaya brunbjørn.

Artikkel I kvantifiserer deteksjon av mesokarnivorer ved viltkameraer og kaster lys over adferdsresponsene til fokale arter på ulike deteksjonsinnretninger og luktstoff som et viktig aspekt av deteksjon. **Artikkel II** inkorporerer flere datakilder med varierende informasjonsnivå i en data-mager situasjon og introduserer en multippel observasjonsprosessmodell i den romlige fangst-gjenfangstrammen for å estimere populasjonsparametere. Denne modellen brukes til en multimetodisk overvåknings-data av en Himalaya brunbjørn i Pakistan. Fokuset i **Artikkel III** er heterogenitet i miljøet, og det avdekker kjønnsspesifikke mønstre i jervens revirstørrelse innenfor artens utbredelse i Norge ved utelukkende å bruke ikke-invasivt innsamlet DNA-data og romlige fangst-gjenfangstmodeller. **Artikkel IV** presenterer og evaluerer en utvidelse av den romlige fangst-gjenfangstmodellen med inn- og utvandring for å forbedre tolkningen til populasjonsparametere og viser hvordan den brukes på jerv-data i Midt-Norge. Hierarkisk modellering gir økologer en intuitiv tilnærming på flere nivåer for å skille observasjons prosesser og økologiske prosesser. Alle kapitler i denne oppgaven inkluderer hierarkiske modeller som korrigerer for mangelfull deteksjon. Avhengig av forskningsspørsmålene bruker jeg disse modellene for å estimere tidden det tar til en deteksjon av artene, populasjonsstørrelse og tetthet, overlevelse, samt variasjon i revirstørrelse og bevegelse mellom år. Overvåkingsmetodene som ble brukt i løpet av denne oppgaven, blir ofte brukt på studier av sjeldne eller sky arter, og begrensede data er en annen viktig utfordring i oppgaven. Bayesisk tolkning ved å bruke Gibbs Sampling (BUGS) -språk fasiliterer konstruere fleksible modeller som inkluderer flere typer data i en omfattende analyse. Artiklene

inkludert i denne oppgaven viser hvordan hierarkiske modeller hjelper oss till å bruke ikke-invasivt innsamlet data for å besvare en rekke spørsmål innen økologi. Å takle de tilhørende utfordringene øker vår evne til å trekke slutninger som bedre beskriver kompleksiteten i virkelige økologiske systemer.

چکیده

پیشرفت فناوری در دو دهه گذشته، درهای تازه‌ای را به روی پژوهشگران حیات وحش گشوده‌است. روش‌های نمونه‌برداری غیر مستقیم، امکان مطالعه گونه‌های حیات وحش را در سطح جمعیت و سرزمین فراهم آورده‌است. دوربین تله‌ای و نمونه‌برداری سرگین از پرکاربردترین روش‌های نمونه‌برداری غیر مستقیم‌اند. با اینکه دانش فنی استفاده از دوربین تله‌ای و نمونه‌های ژنتیکی پیشرفت چشمگیری داشته‌است، تحلیل چنین داده‌هایی نیازمند مدل‌های آماری پیشرفته‌ای است که با شرایط میدانی گردآوری داده و بوم‌شناسی گونه مورد مطالعه هم‌خوانی داشته باشند. رساله پیش رو، به تحلیل آماری داده‌هایی می‌پردازد که غیر مستقیم گردآوری شده‌اند. در هر چهار فصل تلاش شده‌است تا با کمک مدل‌های آماری سلسله‌مراتبی (چندلایه) به پرسش‌های رایج بوم‌شناسی درباره گوشتخواران پاسخ داده شود.

فصل نخست بر توانایی ثبت گونه‌های جانوری با دوربین تله‌ای تمرکز دارد. ثبت یا عدم ثبت حضور یک گونه می‌تواند برآیند زیست‌شناسی و رفتار گونه در رویارویی با ایستگاه دوربین تله‌ای باشد. اینکه برخی از گونه‌ها زودتر از دیگران به سراغ دوربین تله‌ای می‌روند، زمان بیشتری در برابر دوربین سپری می‌کنند یا با فاصله کمتری در برابر دوربین ثبت می‌شوند، بر موفقیت تصویربرداری از گونه‌های حاضر در محدوده دوربین‌گذاری اثرگذار است. فصل دو به برآورد فراوانی و تراکم جمعیت گونه‌های کمیاب و پنهان‌کار می‌پردازد. موضوع اصلی، تحلیل آماری داده‌هایی است که با چند روش غیر مستقیم گردآوری شده‌اند و سطح متفاوتی از دانش را شامل می‌شوند. این فصل به معرفی مدل آماری «جارو» می‌پردازد و کاربرد این مدل برای برآورد اندازه جمعیت و سایر پارامترهای جمعیتی خرس قهوه‌ای نشان داده شده‌است. فصل سه بر تخمین اندازه گستره خانگی و عوامل اثرگذار بر آن تمرکز دارد. با در نظر گرفتن محدودیت‌های استفاده از نمونه‌برداری مستقیم مانند گردنبندگذاری، در این فصل تلاش شده‌است تا گستره خانگی گونه دَله در اسکاندیناوی با نمونه‌های ژنتیکی سرگین و مدل‌های پیشرفته آماری برآورد شود. فصل چهار به معرفی مدل آماری «بازیابی جمعیت باز» و استفاده هم‌زمان از نمونه‌های ژنتیکی سرگین و بافت می‌پردازد. ثبت ژنتیکی افراد حذف‌شده از جمعیت نه تنها دقت مدل آماری را در برآورد پارامترهای جمعیتی مانند بقا افزایش می‌دهد، بلکه امکان برآورد جابه‌جایی افراد د زیستگاه را نیز فراهم می‌سازد. محدودیت توان ما در مشاهده مستقیم پدیده‌های طبیعی، انکارناپذیر است و مدلسازی بوم‌شناسی، ابزاری است برای درک بهتر از گونه‌های حیات وحش و پیرامون طبیعی.

List of articles

Article I

Tourani, M., E. N. Brøste, S. Bakken, J. Odden, and R. Bischof. Sooner, closer, or longer: detectability of mesocarnivores at camera traps. *Journal of Zoology.*

Article II

Tourani, M., P. Dupont, M. A. Nawaz, and R. Bischof. 2020. Multiple observation processes in spatial capture-recapture models: How much do we gain? *Ecology* 101(7):e03030.

Article III

Tourani, M., P. Dupont, C. Milleret, H. Brøseth, and R. Bischof. Non-invasive genetic sampling reveals landscape-level patterns in wolverine home range size. Manuscript.

Article IV

Dupont, P., C. Milleret, **M. Tourani**, H. Brøseth, and R. Bischof. Integrating dead recoveries in spatial capture-recapture models. Under review in *Ecosphere.*

Synopsis

1. Why Ecological modelling?

Key questions in ecology are often associated with substantial variability. This variability arises in part from measurement error (i.e. observation variability), because our observations of the world's phenomena are imperfect. For example, if we wish to estimate survival in a population of bears, we could use information about mortalities that are reported by hunters or dead individuals found by the public. However, bears may die without being discovered, and some individuals are presumed dead, even though they are alive but no longer detected (MacKenzie et al. 2009). Even if we manage to generate an unbiased estimate of average survival, realised survival still varies from one individual bear to another due to process variability. Process variability may be affected by measured and unmeasured factors, such as sex, age, or environmental conditions (Murray and Sandercock 2020). Measurement variability can be minimised by careful observations and process variability can, at least in theory, be reduced by studying a large population in manipulative control under laboratory settings. In field studies, however, these variabilities may remain large. Ecologists working with observational data, rather than designed experiments, increasingly acknowledge that the latter can help inform about the former, and experiments allow addressing questions that are not possible with observational studies (Bell 2017). However, experiments provide only one source of data for learning about complex processes. To address ecological questions characterized by complexity and uncertainty, we build models to simplify and ultimately understand the problems.

2. Modelling framework

While measurement variability often gets in the way of making direct inferences from the data, process variability is usually fundamental to the object of inference, since it is an attribute of the dynamics of the ecological system (Kéry and Schmidt 2008, Kellner and Swihart 2014). When surveying a population, not detecting a species may mean that it is not present at the site and hence could not be detected, or that we failed to detect it despite the species being present. Observations are the results of both observation and ecological processes. Hierarchical modelling offers ecologists an intuitive approach to disentangle these processes and their associated variability.

Most ecological models assume that there is some variability due to a combination

of unknown factors and estimate the extent of that variability from the variability observed in the field. To characterise random variability in estimating population size, variances have been used for a long time (den Boer 1968, Andrewartha and Birch 1984). Likewise, variance-mean relationships have been used to model the processes underlying these variabilities (Taylor 1961, Gaston and McArdle 1993). More sophisticated models of variability make explicit assumptions about the underlying causes of variability and can provide not only more information about the ecological processes at work, but can also better exploit collected data (Purves et al. 2013). The advantages of the hierarchical approach lie in the convenience of model parameterization, ease of interpretation, and in facilitation of model fitting (Bolker 2009). Moreover, the uncertainty is properly propagated into model inference by recognizing the uncertainty of model unknowns (Cressie et al. 2009). In ecology, understanding ecological processes is the aim, but understanding what affects our capacity to observe those ecological processes is equally important. A typical hierarchical model consists of data generated from one or more observation processes that are conditional on one or more ecological processes. Hierarchical modelling fosters and formalizes the link between observation and ecological process models.

3. Observation process

Non-invasive data collection technologies have improved our ability to collect data on rare or elusive species under natural conditions (see Fig. 1). One of the advantages emphasized by researchers is that non-invasive methods do not require capturing and handling, hence the physical integrity of the subjects is not influenced by the study (Zemanova 2020). Non-invasive methods are particularly useful in the study of wild populations, where avoidance of or habituation to human presence could be detrimental (Bezerra et al. 2014). Methods that impact study subjects are not only a concern from an animal welfare perspective (Jewell 2013), but can also impact the reliability of study results through the observer effect (Cahill et al. 2001). In addition, non-invasive methods make it more feasible to cover the entire landscape and detect a larger proportion of the study population. These survey methods are particularly useful to study species for which direct observation is often infeasible, either because the species actively avoid human and inhabit remote areas, or because they naturally occur in low densities (Box 1).

With the opportunities offered by non-invasive data collection methods, came new challenges. Observations vary due to intrinsic (differences between individuals and species), environmental (visibility) and survey-specific factors. Ignoring this vari–

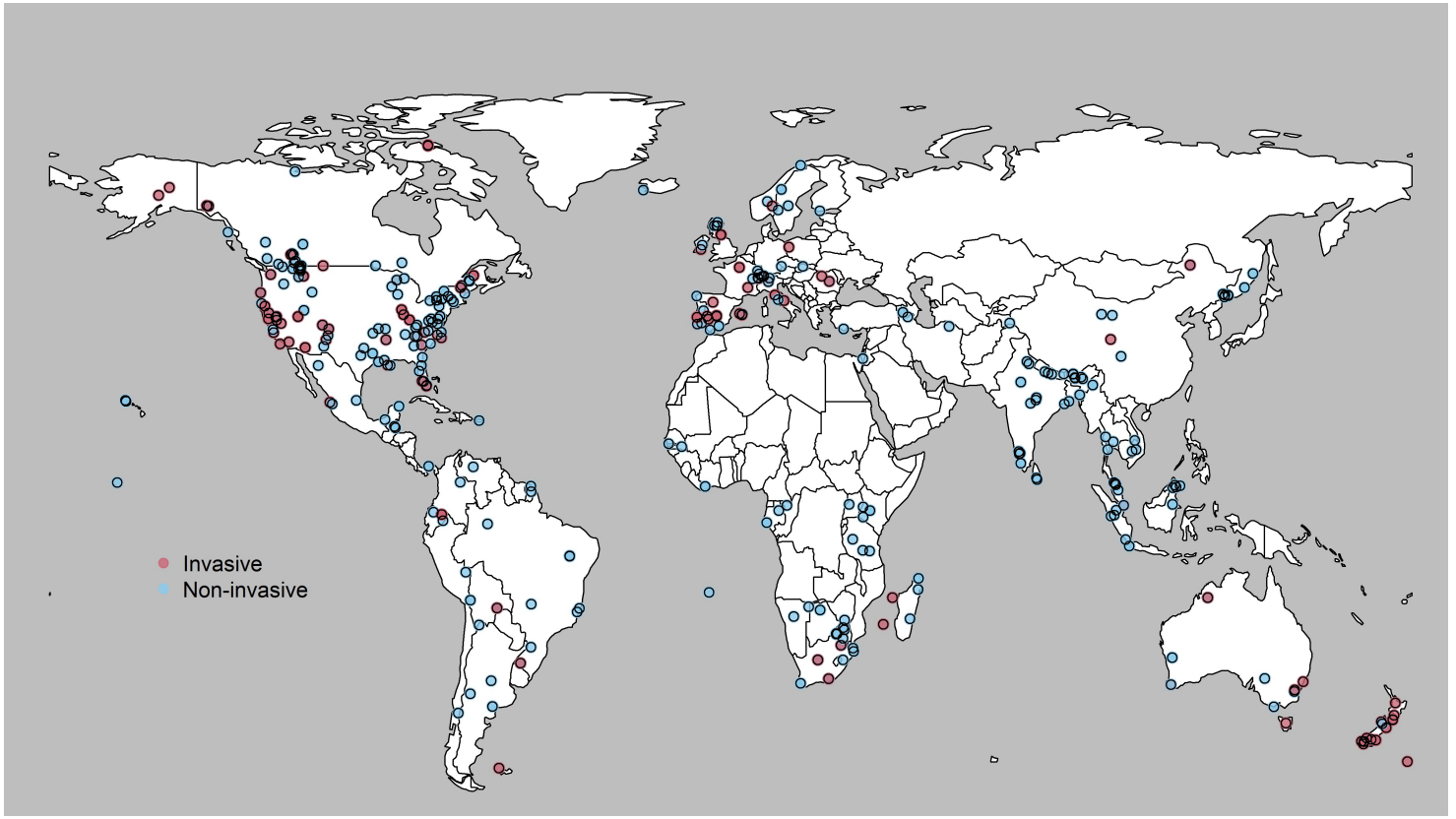

Figure 1: *Global distribution of data collection methods combined with spatial capture-recapture models based on a review of studies (journal articles) published between 2004 and 2020. Invasive methods are those involving physical capture and handling of study animals (e.g. live trapping) and non-invasive methods include camera trapping, DNA sampling, acoustic monitoring, etc.*

Box 1. Data collection methods used in this thesis

Camera traps are used worldwide as a cost-efficient tool for monitoring terrestrial mammals (Burton et al. 2015, Wearn and Glover-Kapfer 2019). Most modern camera traps are digital cameras with passive infrared motion detectors. When a moving object with a surface temperature different from the environment passes by, the sensor is triggered and the camera takes photos or records videos (Welbourne et al. 2016, Apps and McNutt 2018). Camera traps have been used for monitoring many species and to collect data on many different aspects, including recording presence or absence of species, behaviour, body condition and reproductive status (Trolle and Kéry 2003, Canu et al. 2017, Carricondo-Sanchez et al. 2017, Monterrubio-Rico et al. 2018, van Ginkel et al. 2019).

Data collection methods used in this thesis. From left to right: camera trapping (©R. Bischof), non-invasive genetic sampling (©E. Moqanaki), and dead-recovery (©R. Bischof).

Non-invasive genetic sampling (NGS) is another promising data collection method for studying wildlife species. Advancements in forensics generated new methods that can be applied to improve data collection and analysis of non-invasive genetic samples in wildlife research (Waits and Paetkau 2005, Beja-Pereira et al. 2009). By extracting genetic material from DNA sources left behind by animals, such as faeces, hair, urine, and saliva, we can record presence of species, individuals and identify sex. Non-invasive DNA has been used for sampling many species in studies on a wide range of subjects, including diet, connectivity, and population size and dynamics (Bischof et al. 2017, Monterroso et al. 2019, Lamb et al. 2019).

Dead-recoveries are additional sources of information that may arise from opportunistic recoveries, hunting surveys and citizen science, through designed protocols or from separate studies (Catchpole et al. 1998, Schaub and Pradel 2004, Kendall et al. 2006). Incorporating dead-recoveries in the analysis of ecological data has a two-fold advantage; involving the public in ecological research and gaining extra information. Studies on a range of species have included dead-recovery data (Kendall et al. 2006, Taylor et al. 2010, Proffitt et al. 2015, Hostetter et al. 2018), which provide invaluable information with little to no additional cost of sampling.

–ability can lead to bias in inferences about the ecological process. Accommodating imperfect detection as an important component of observation process is now the common thread in sampling wild populations (Kéry and Royle 2016) and is not limited to mobile organisms, but can also play a role in the study of sedentary organisms, such as plants (Kéry et al. 2006).

Aside from accounting for imperfect detection to avoid parameter bias, researchers often design studies favouring higher detection probabilities to increase sample size and thus parameter precision. Data sparsity is typically associated with studies of rare or elusive species. Non-invasively collected DNA is usually of low quality, which might make individual identification particularly challenging. Similarly, during camera trapping surveys, false-absences result from missed detections (no photo captured), late triggers (partly photo-captured animal), or blank images especially for small and fast-moving species (Glen et al. 2013). Non-invasive monitoring can be time-consuming because of the time taken to detect the presence of focal species and to reduce this cost surveys are typically designed to maximize detectability. For example, efforts to maximize detectability in camera trapping include increasing number of camera traps per site (Pease 2016, O'Connor et al. 2017, Evans et al. 2019), non-random camera trap placements (Cusack et al. 2015, Kolowski and Forrester 2017), and application of attractants (Bischof et al. 2014, Garvey et al. 2017, McLean et al. 2017, Moriarty et al. 2018). In occupancy and spatial capture-recapture models built in this thesis, detectability (of species or individual) is being estimated through repeated observations in space or time, as part of the observation process.

In **Article I**, I quantify mechanisms that affect detectability of focal species, and test the effect of olfactory lures on detectability of a mesocarnivore community. Observation variability is usually a nuisance to be dealt with, rather than the primary focus of ecological models. A practical motivation to account for detectability is that it provides a measure of sampling efficacy. For example, by modelling the time to detection of species by camera traps, one can decide on survey duration, based on study objectives.

Nowadays, many species inventories combine multiple survey methods, such as non-invasive DNA sampling, camera trapping, sign surveys, or physical mark-recapture to maximize the amount of data (Sollmann et al. 2013a,b, Blanc et al. 2014, Clare et al. 2017, Murphy et al. 2018). One way to better exploit the available information is integrated modelling, the joint analysis of multiple datasets traditionally analysed separately (Miller et al. 2019). Practical benefits of integrated modelling include improved parameter precision, reduced bias, the

ability to estimate additional parameters, and greater generality of inferences (Besbeas et al. 2002, Abadi et al. 2010, Schaub and Abadi 2011, Pacifici et al. 2017). Two articles in this thesis highlight the benefits of data-integration to improve parameter precision and reduce bias (**Article II**), but also to estimate additional parameters (**Article IV**). Specifically, in the SCR framework I discuss in **Article IV**, individuals leaving the observation area become unavailable to sampling. These individuals appear to the model as dead, hence biasing estimates of survival probability. This is especially true for studies of hunted populations with few recaptures (Hewitt et al. 2010). Integrating multiple data sources can provide vital information to increase the amount of data, and estimate demographic parameters with greater precision. Knowing individual fates by incorporating dead-recovery data helps reduce the uncertainty for the overall population and opens the door to address broader hypotheses about spatial ecology.

4. Ecological process

Ecology is inherently spatial. Spatial heterogeneity in the environment shapes life history traits across individuals, scaling up to populations through coevolutionary processes (Levin 1992). At the same time, populations and their impacts are manifested across the space they occupy. Much of the pressing problems faced by wildlife conservation and management revolve around species distribution and abundance, where these and related measures (e.g. vital rates) vary across time and space and can be associated with heterogeneity in the environment (Scheiner and Willig 2008). As a result, quantifying and describing ecological patterns in space, not only time, is pivotal for comprehending ecological systems.

Making inferences about spatial variation in demographic processes advances our understanding of natural phenomena in a changing world. However, the ability to study populations at biologically meaningful extents has been hampered by available methods (Chandler and Clark 2014). Both the interpretation and the use of information required to address applied challenges are scale dependent. The study of population dynamics benefits from fine-scale, spatio-temporal data to capture individual patterns and analytical methods to make inferences at the population level (Dunning et al. 1995, Royle et al. 2018). Novel sampling methods, such as non-invasive DNA sampling and camera trapping, have substantially increased the number of studies that collect data with a grain and extent suitable for addressing long-standing questions related to variation in demographic parameters (Fig. 2).

In ecological modelling in general, we are interested in making inferences about ecological processes (Fig. 3), given a set of observations. The process model is the–

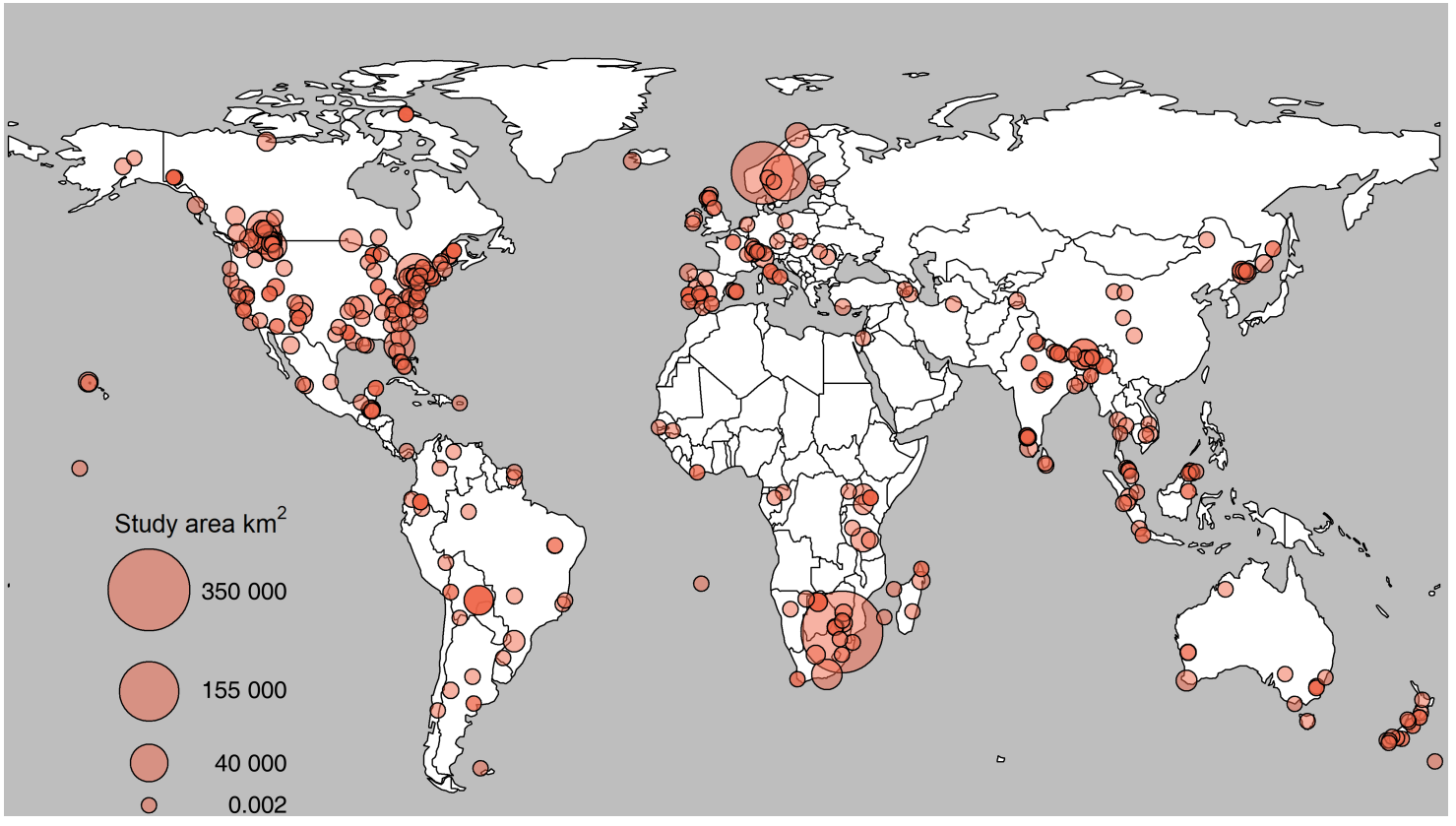

Figure 2: *Approximate spatial extent (km^2) of spatial capture-recapture studies based on a review of journal articles published between 2004 and 2020.*

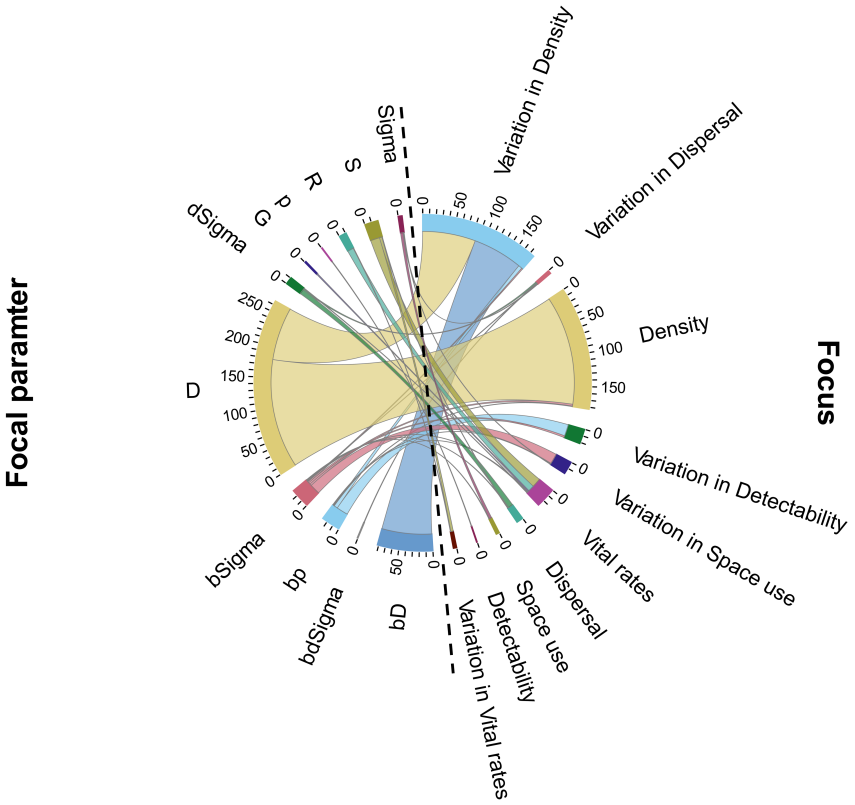

Figure 3: *Ecological insights (right) gained in spatial capture-recapture studies through modelling different population parameters (left) based on a review of journal articles published between 2004 and 2020. Focal parameters include the spatial scale parameter of the detection function (Sigma, σ), dispersal sigma (dSigma), density (D); probability of survival (S), recruitment (R), detection (p), and growth rate (G); and effects of spatial or individual covariates on σ (bSigma), detection probability (bp), dispersal sigma (bdSigma), and density (bD). Width of bands represents number of published articles reporting each of focal parameters as the focus of the study.*

–heart of most hierarchical models in ecology as it describes the dynamics of ecological system of interest. How many individuals are in the population? How are these individuals distributed in space? How do females and males use the space differently? Adopting probabilistic theory in hierarchical models allows inferences based on unobserved or partially observed variables. For example, the ecological process common to the spatial capture-recapture models usually consists of two major components: a spatial model describing the distribution of

individuals in space at a detection occasion and its movement between occasions, and a demographic model describing the true states of individuals. Individuals may be uniformly distributed across the state-space (**Article II**) or, in case of heterogeneous environment, distribution of individuals can be described through a non-homogeneous point process (**Articles III-IV**). An example demographic process describes the true states of individuals (alive or dead) and population abundance. In open-population capture recapture, this demographic process model may also describe survival process (probability of survival between occasions) and recruitment process as explained in **Article IV**.

5. Probabilistic theory of hierarchical models

A hierarchical model consists of two or more conditionally related probability models, where the probability of outcomes of one latent response depends on the outcomes of another latent or measured response (Kéry and Royle 2016). Basic probability rules are therefore fundamental for modelling variation in ecological processes through hierarchical models (Bolker 2008). For example, the probability of detecting individual A is conditional on individual A being alive. The true states (e.g. alive vs. dead) of individuals depend on observation outcomes and are partially observed random variables, i.e. probability distributions (e.g. binomial, Poisson) govern their possible values.

The simplest form of hierarchical models is a mixed-effect model, which deals with observations belonging to different clusters, where each cluster has its own properties, such as different response mean and different sensitivity to explanatory variables. For example in **Article I**, I measure minimum distance of a visitor species to camera traps. Visitors of each camera trap may have responses more similar to each other, than visitors of other camera traps because of the location of the camera trap. Without clustering in the data, a non-hierarchical model would consist of a probability distribution over outcomes, and independent draws from that distribution (i.e. observations). In a mixed-effect model, the distribution over outcomes is jointly determined by one probability distribution shared among clusters and another probability distribution shared among observations within each cluster. Both cluster-level and observation-level variations can be functions of covariates; for example in **Article I**, I test the effect of olfactory lure treatments on distance of visitors to the camera's focal point.

6. Parameter estimation

In the example above, the probability distribution parameters that govern between- or within-cluster variability are unknown, hence so are the shared parameters of probability distribution over outcomes. To estimate the parameters of interest, one can marginalise over the cluster-specific variability by introducing prior distributions over parameters of interest and computing their posterior distributions through Bayes' rule (Cressie et al. 2009). In the Bayesian approach, one assumes that the experimental outcome is the truth and the parameter values have probability distributions. One needs to define prior knowledge about the probability of different parameter values. To use the example of bear survival mentioned earlier, one specifies a parameter, the probability of survival, and asks questions about the best estimate of the probability distribution (i.e. the posterior) given the prior knowledge of the distribution and the observed data.

For computing the posterior, Markov chain Monte Carlo (MCMC) methods are efficient tools (Gelfand and Smith 1990) that I use throughout this thesis to compute the posterior distributions of different parameters. MCMCs are simulation-based methods for drawing samples from probability distributions. After a sufficient number of realizations (i.e. burn-in), generated realizations of the chain comprise a random sample from the posterior distribution. To summarise inferences on the unknowns, the sampled values from the posterior distribution are used to calculate common distributional summary statistics, such as means and variances. The uncertainty or variability in the marginal posterior distribution is conventionally characterised by the 2.5^{th} and 97.5^{th} percentile of the posterior samples (95% credible intervals) for each unknown. Although hierarchical models can be implemented using non-Bayesian approaches, the Bayesian paradigm enables exact inference and proper uncertainty assessment within the given specification (Cressie et al. 2009). Bayesian inference Using Gibbs Sampling (BUGS) language has made it possible for non-statisticians to implement MCMC methods for estimation and inference in many hierarchical models. BUGS has facilitated model specification and it allows users to focus on the statistical nature of the model, rather than implementation details and inference procedures (Kéry and Royle 2016). Dialects of BUGS are freely available through several software packages, including JAGS (Plummer 2003) and NIMBLE (de Valpine et al. 2017) that I used in different articles of this thesis. As part of the analysis in **Article I**, I use an R package in which MCMC sampling is implemented with Stan (Carpenter et al. 2017).

7. Thesis summary

In this thesis, I use hierarchical models implemented in a Bayesian framework to explore a series of ecological and methodological questions. I focus mainly on spatial capture-recapture and occupancy models and expand upon their standard model formulations to quantify observation and process variability based on data at hand and the ecological questions in mind. Observation variability is the focus of **Article I**, in which I quantify camera trapping survey efficacy in a hierarchical framework using concepts of occupancy (MacKenzie et al. 2017), time-to-event analysis, and mixed-effect models (Kéry and Royle 2016). **Articles II**, **III** and **IV** focus on process variability and concern ecological insights gained by combining spatial capture-recapture with non-invasively collected data. The focus in **Article II** is estimating density and abundance. **Article III** describes variation in home range size and **Article IV** is concerned with the estimation of density, survival, and inter-annual movement. The analyses throughout this thesis are based on data collected using two of the most common non-invasive survey methods for carnivore monitoring, i.e. DNA-sampling and camera trapping (Box 1). In **Article I**, I analyse camera trap data, whereas in **Article III**, I use DNA sampling, and **Article II** combines both sampling methods. **Article IV** uses a combination of DNA samples from non-invasive searches and dead recoveries (Fig. 4).

This thesis is about combining hierarchical models with non-invasively collected data to answer ecological questions in wild populations of carnivores at different spatial scales. Pursuing this goal led to topics from variation in detectability of different species (**Article I**), to estimating population density under data-sparse situations (**Article II**), to the cutting edge of modelling space-use and movement with spatial capture-recapture (**Articles III-IV**).

8. Concluding remarks

Hierarchical modelling has the capacity to cope with high-dimensional complex problems typically facing those seeking answers to ecological questions. The articles in this thesis exemplify the application, but also further develop such models. Throughout the articles, I combine non-invasive survey methods and hierarchical models, and I believe that advancements in these two technologies go hand in hand.

Many of the enduring elements of contemporary ecological theory, wildlife conservation and management are centred around species distributions and abundance (Scheiner and Willig 2008). Estimation of these variables is impacted by sources of variability, including imperfect detection, heterogeneity in the environment and

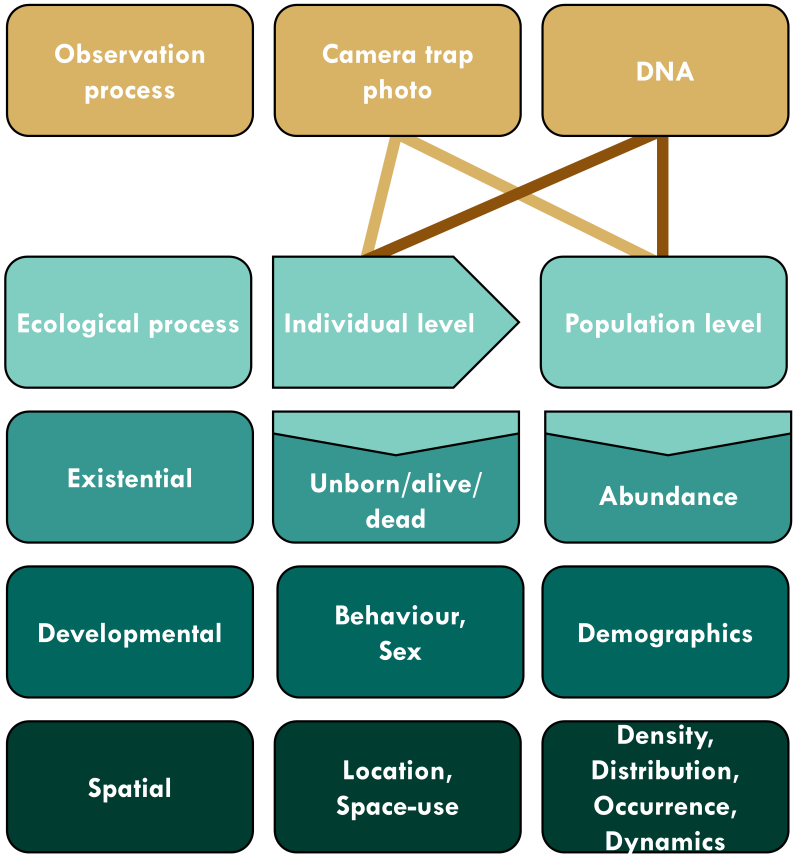

Figure 4: *A schematic representation of hierarchical models built in this thesis. The observation process provides information about the ecological processes at both individual and population levels. The ecological process pertains to individual and population level hierarchy and is further classified as Existential, Developmental, and Spatial. Adopted from McClintock et al. (2020).*

movement of individuals. Analytical methods that explicitly model this variability in both observation and ecological processes are now the basis for estimating the abundances and distributions of species (Kéry and Royle 2016). In **Article I**, I focus on detectability as a crucial component in ecological modelling. By quantifying species-specific characteristics of detectability, researchers can gain new insights that help optimise sampling design and account for some of the inherent variability in the data. Although the impact of non-invasive data collection methods on

physical integrity of the study system is generally minimal, I show here that the focal species may alter their behaviour in response to presence of detection devices or attractants.

Spatial capture-recapture (SCR) models have emerged as a particularly efficient and popular tool for studying spatial ecological processes from non-invasively collected data. These models were initially developed to exploit the spatial information contained in repeated detections of individuals at different locations to provide spatially-explicit estimates of abundance, which I use in **Article II**. However, implicit in the SCR-specific observation model is the assumption that the probability of detecting an individual in space is a function of distance to its activity centre (Royle et al. 2018). Spatial capture-recapture can also yield information about other spatial processes, such as individual space-use and movement (**Articles III-IV**). This is a prolific area of research and developments are ongoing to further expand the use of this modelling framework (Royle et al. 2018).

Data sparsity hampers our ability to make reliable inferences about population parameters, especially when studying rare or elusive species. Flexibility in model specification in BUGS is a great advantage for customising the classic model formulations when facing ecological problems (**Articles II** and **IV**). Data integration in a hierarchical framework allows incorporation of multiple sources of information. However, one should assess the gains against model complexity. Use of hierarchical models and the concept of imperfect detection is not to add yet another level of complexity to our ecological studies, i.e. statistical machismo (Welsh et al. 2013, Guillera-Arroita et al. 2014, Gimenez et al. 2014); rather it is an opportunity to incorporate our knowledge of reality into models of ecological systems.

Literature cited

Abadi, F. et al. 2010. An assessment of integrated population models: bias, accuracy, and violation of the assumption of independence. - Ecology 91: 7–14.

Andrewartha, H. G. and Birch, L. C. 1984. The Ecological Web: More on the Distribution and Abundance of Animals. - University of Chicago Press.

Bell, G. 2017. Evolutionary Rescue. - Annu. Rev. Ecol. Evol. Syst. 48: 605–627.

Besbeas, P. et al. 2002. Integrating Mark-Recapture-Recovery and Census Data to Estimate Animal Abundance and Demographic Parameters. - Biometrics 58: 540–547.

Bezerra, B. M. et al. 2014. Camera Trap Observations of Nonhabituated Critically Endangered Wild Blonde Capuchins, *Sapajus flavius* (Formerly *Cebus flavius*). - Int J Primatol 35: 895–907.

Bischof, R. et al. 2014. Being the underdog: an elusive small carnivore uses space with prey and time without enemies: Space and time use by Altai mountain weasel. - J Zool 293: 40–48.

Blanc, L. et al. 2014. Improving abundance estimation by combining capture-recapture and occupancy data: example with a large carnivore. - J Appl Ecol 51: 1733–1739.

Bolker, B. 2008. Ecological models and data in R. - Princeton University Press.

Bolker, B. 2009. Learning hierarchical models: advice for the rest of us. - Ecological Applications 19: 588–592.

Cahill, J. F. et al. 2001. The herbivory uncertainty principle: visiting plants can alter herbivory. - Ecology 82: 307–312.

Canu, A. et al. 2017. 'Video-scats': combining camera trapping and non-invasive genotyping to assess individual identity and hybrid status in gray wolf. - Wildlife Biology 2017: wlb.00355.

Carpenter, B. et al. 2017. Stan: A Probabilistic Programming Language. - J. Stat. Soft. 76(1).

Carricondo-Sanchez, D. et al. 2017. The range of the mange: Spatiotemporal patterns of sarcoptic mange in red foxes (*Vulpes vulpes*) as revealed by camera trapping. - PLoS ONE 12: e0176200.

Chandler, R. B. and Clark, J. D. 2014. Spatially explicit integrated population models. - Methods Ecol Evol 5: 1351–1360.

Clare, J. et al. 2017. Pairing field methods to improve inference in wildlife surveys while accommodating detection covariance. - Ecol Appl 27: 2031–2047.

Cressie, N. et al. 2009. Accounting for uncertainty in ecological analysis: the strengths and limitations of hierarchical statistical modeling. - Ecological Applications 19: 553–570.

Cusack, J. J. et al. 2015. Random versus Game Trail-Based Camera Trap Placement Strategy for Monitoring Terrestrial Mammal Communities. - PLoS ONE 10: e0126373.

de Valpine, P. et al. 2017. Programming With Models: Writing Statistical Algorithms for General Model Structures With NIMBLE. - Journal of Computational

and Graphical Statistics 26: 403–413.

den Boer, P. J. 1968. Spreading of risk and stabilization of animal numbers. - Acta Biotheor 18: 165–194.

Dunning, J. B. et al. 1995. Spatially Explicit Population Models: Current Forms and Future Uses. - Ecological Applications 5: 3–11.

Evans, B. E. et al. 2019. Assessing arrays of multiple trail cameras to detect North American mammals. - PLoS ONE 14: e0217543.

Garvey, P. M. et al. 2017. Exploiting interspecific olfactory communication to monitor predators. - Ecol. Appl. 27: 389–402.

Gaston, K. J. and McArdle, B. H. 1993. Measurement of Variation in the Size of Populations in Space and Time: Some Points of Clarification. - Oikos 68: 357.

Gelfand, A. E. and Smith, A. F. M. 1990. Sampling-Based Approaches to Calculating Marginal Densities. - Journal of the American Statistical Association 85.410: 398-409.

Gimenez, O. et al. 2014. Statistical ecology comes of age. - Biol. Lett. 10: 20140698.

Glen, A. S. et al. 2013. Optimising Camera Traps for Monitoring Small Mammals. - PLoS ONE 8: e67940.

Guillera-Arroita, G. et al. 2014. Ignoring Imperfect Detection in Biological Surveys Is Dangerous: A Response to 'Fitting and Interpreting Occupancy Models'. - PLoS ONE 9: e99571.

Jewell, Z. 2013. Effect of Monitoring Technique on Quality of Conservation Science: Ethics and Science in Conservation. - Conservation Biology 27: 501–508.

Kellner, K. F. and Swihart, R. K. 2014. Accounting for Imperfect Detection in Ecology: A Quantitative Review. - PLoS ONE 9: e111436.

Kéry, M. and Schmidt, B. 2008. Imperfect detection and its consequences for monitoring for conservation. - Community Ecology 9: 207–216.

Kéry, M. and Royle, J. A. 2016. Applied hierarchical modeling in ecology: analysis of distribution, abundance and species richness in R and BUGS. - Elsevier/AP.

Kéry, M. et al. 2006. How biased are estimates of extinction probability in revisitation studies? - Journal of Ecology 94: 980–986.

Kolowski, J. M. and Forrester, T. D. 2017. Camera trap placement and the potential for bias due to trails and other features. - PLoS ONE 12: e0186679.

Levin, S. A. 1992. The Problem of Pattern and Scale in Ecology. - Ecology 73: 1943–1967.

McClintock, B. T. et al. 2020. Uncovering ecological state dynamics with hidden Markov models. - arXiv preprint arXiv:2002.10497.

MacKenzie, D. I. et al. 2009. Modeling species occurrence dynamics with multiple states and imperfect detection. - Ecology 90: 823–835.

MacKenzie, D. I. et al. 2017. Occupancy estimation and modeling: inferring patterns and dynamics of species occurrence. - Elsevier.

McLean, W. R. et al. 2017. Visual lures increase camera-trap detection of the southern cassowary (*Casuarius casuarius johnsonii*). - Wildl. Res. 44: 230–237.

Miller, D. A. W. et al. 2019. The recent past and promising future for data integration methods to estimate species' distributions. - Methods Ecol Evol 10: 22–37.

Monterrubio-Rico, T. C. et al. 2018. Use of remote cameras to evaluate ocelot (*Leopardus pardalis*) population parameters in seasonal tropical dry forests of central-western Mexico. - Mammalia 82: 113–123.

Moriarty, K. M. et al. 2018. Seeking Efficiency With Carnivore Survey Methods: A Case Study With Elusive Martens. - Wildl. Soc. Bull. 42: 403–413.

Murphy, S. M. et al. 2018. Integrating multiple genetic detection methods to estimate population density of social and territorial carnivores. - Ecosphere 9: e02479.

Murray, D. L. and Sandercock, B. K. 2020. - Population Ecology in Practice. 450 pp.

O'Connor, K. M. et al. 2017. Camera trap arrays improve detection probability of wildlife: Investigating study design considerations using an empirical dataset. - PLoS ONE 12: e0175684.

Pacifici, K. et al. 2017. Integrating multiple data sources in species distribution modeling: a framework for data fusion. - Ecology 98: 840–850.

Pease, B. S. 2016. Single-Camera Trap Survey Designs Miss Detections: Impacts on Estimates of Occupancy and Community Metrics. - PLoS ONE: 11, e0166689.

Plummer, M. 2003. JAGS: A Program for Analysis of Bayesian Graphical Models Using Gibbs Sampling - Proceedings of the 3rd international workshop on distributed statistical computing. 124(125.10): 1-10.

Purves, D. et al. 2013. Time to model all life on Earth. - Nature 493: 295–297.

Royle, J. A. et al. 2018. Unifying population and landscape ecology with spatial capture-recapture. - Ecography 41: 444–456.

Schaub, M. and Abadi, F. 2011. Integrated population models: a novel analysis framework for deeper insights into population dynamics. - J Ornithol 152: 227–237.

Scheiner, S. M. and Willig, M. R. 2008. A general theory of ecology. - Theor Ecol 1: 21–28.

Sollmann, R. et al. 2013a. A spatial mark–resight model augmented with telemetry data. - Ecology 94: 553–559.

Sollmann, R. et al. 2013b. Using multiple data sources provides density estimates for endangered Florida panther. - J Appl Ecol 50: 961–968.

Taylor, L. R. 1961. Aggregation, Variance and the Mean. - Nature 189: 732–735.

Trolle, M. and Kéry, M. 2003. Estimation of ocelot density in the Pantanal using capture-recapture analysis of camera-trapping data. - Journal of Mammalogy 84: 8.

van Ginkel, H. A. L. et al. 2019. Behavioral response of naïve and non-naïve deer to wolf urine. - PLoS ONE 14: e0223248.

Welsh, A. H. et al. 2013. Fitting and Interpreting Occupancy Models (EP White, Ed.). - PLoS ONE 8: e52015.

Zemanova, M. A. 2020. Towards more compassionate wildlife research through the 3Rs principles: moving from invasive to non-invasive methods. - Wildlife Biology in press.

Article I

Sooner, closer, or longer: detectability of mesocarnivores at camera traps

Mahdieh Tourani[1,*], Ellen Nordrum Brøste[1], Sigurd Bakken[1], John Odden[2], and Richard Bischof[1]

1. *Faculty of Environmental Sciences and Natural Resource Management, Norwegian University of Life Sciences, P.O. Box 5003, 1432 Ås, Norway*
2. *Norwegian Institute for Nature Research, NO-0349 Oslo, Norway*
∗ Email: mahdieh.tourani@gmail.com

Abstract. Camera trapping, paired with analytical methods for estimating species occurrence, population size or density, can yield information with direct consequences for wildlife management and conservation. Detectability, the ability to detect a species or individual if it is present, affects the reliability and efficiency of camera trap surveys and, in turn, varies across species, space, and time. Greater detectability means greater sample size, and a common approach to boost detectability of wildlife by camera traps involves the application of olfactory lures. Using a camera-trap study on sympatric mesocarnivores (European badger *Meles meles*, red fox *Vulpes vulpes*, pine marten *Martes martes*, and domestic cat *Felis catus*), we quantified three elements of detectability: i. the time until first detection ("sooner", conditional on being present), ii. the proximity to a focal point in front of the camera ("closer", conditional on being detected), and iii. the duration of exposure to the camera ("longer", conditional on being detected). A hierarchical analytical approach and a quasi-experimental setup allowed us to test for and quantify the species-specific effect of olfactory lures on these aspects of detectability. Depending on species, average median time to first detection ranged from 4 to 28 days, distance to the focal point from 0.3 to 0.8 body lengths, and median

time to departure from 2 to 6 seconds. Credible intervals overlapped substantially between most species in all three measures and variation between observations was extensive. We detected effects of lures on time to detection for cats (castoreum), distance to focal point for badgers (striped skunk *Mephitis mephitis* scent) and martens (castoreum-, fox- and skunk-based lures), and the duration of exposure for foxes (fox- and skunk-based lures). We discuss how a multifaceted perspective on detectability in camera trap studies, linked with species biology, can give investigators a more structured approach to selecting and testing measures intended to boost detection probability.

Keywords: *camera trap, detection, Bayesian hierarchical model, time to event, survival analysis, proportional hazards, mixed effect model*

Introduction

Camera trapping is used worldwide as a non-invasive and cost-efficient tool for monitoring terrestrial mammals (Burton et al., 2015). The goals vary between studies, but chief among them are estimates of species distribution and relative or absolute abundance, all of which are useful in guiding wildlife management and conservation (Ahumada, Hurtado & Lizcano, 2013; Rovero et al., 2013).

Photographic detections (e.g. number of visits or photos during a survey) continue to be used as proxies for certain focal parameters, such as species diversity or abundance, but there is a growing recognition for the need to cope with imperfect detection (Burton et al., 2015; Sollmann, 2018). The inability to detect every species or individual present in the study area (i.e. false-negatives), together with heterogeneous detection probability, has direct consequences for the reliability of inferences drawn from camera trap and other field surveys (Archaux, Henry & Gimenez, 2012; Guillera-Arroita et al., 2014). Analytical approaches such as capture-recapture and occupancy models account for imperfect detection when estimating focal parameters (MacKenzie et al., 2017; Sollmann, 2018; Hofmeester et al., 2019).

Despite the availability of hierarchical methods that estimate and control for imperfect and variable detection, investigators are keenly interested in maximizing detection probability. Increased detection probability results in larger sample sizes, thereby boosting precision (Gerber, Karpanty & Kelly, 2012) and in some cases accuracy of parameter estimates (Guillera-Arroita et al., 2014). Increased detection

probability can also reduce the cost of surveys, for example by allowing shorter sampling periods in cases where a single detection of an individual or species at a given site is sufficient, such as occupancy studies (Hamel et al., 2013; Bischof et al., 2014b; Kays et al., 2020).

The biology of study species is an important determinant of detectability (Fig. 1). The probability of encounter with a camera trap is directly affected by the density of a species and its use of the landscape (Neilson et al., 2018). Behavioural characteristics, such as exploratory behaviour and diel activity patterns also determine if and when an animal enters the viewshed of a camera (Rowcliffe et al., 2011). Speed of movement, size and appearance of a species influence whether the camera is triggered, and if so, whether a sufficiently clear image is captured to allow detection and identification. For example, rarity, shyness, furtiveness, and small size are all characteristics that make species challenging camera trapping subjects (Fig. 1).

Investigators can address these challenges and take steps to boost detection probability. Cameras are often placed at microhabitat sites that are more likely to be visited by the focal species (or community), based on habitat selection and use of landscape features during travel (O'Connor et al., 2017). Many studies employ baits (Moriarty et al., 2018) or visual (McLean, Goldingay & Westcott, 2017), acoustic (Read et al., 2015), and olfactory lures (Bischof et al., 2014a; Garvey et al., 2017; Ferreras, Diaz-Ruiz & Monterroso, 2018), with the goal of attracting animals to the site and keeping it there long enough for photographic capture. Furthermore, camera design has improved substantially during the past decade, with features such as silent shutters and infrared (IR) or stealth IR mitigating the risk of spooking shy species (Glen et al., 2013; Rovero et al., 2013). These measures, like the biological characteristics that they implicitly target, affect different aspects of the process of photographic capture, which are either directly or indirectly related to detectability (Fig. 1).

We conducted a quasi-experimental camera trapping study of the mesocarnivore guild in southeast Norway and asked three questions: 1) How soon is a given species detected at a camera trap?, 2) How close do individuals approach a target within the cameras field of view?, and 3) How long do individuals remain within the camera's field of view? We used hierarchical models to quantify 'how soon', 'how close', and 'how long', thereby disentangling these three important aspects of detectability. Furthermore, we evaluated how these metrics are influenced by the study species and by using a widespread measure for boosting detectability: olfactory lures.

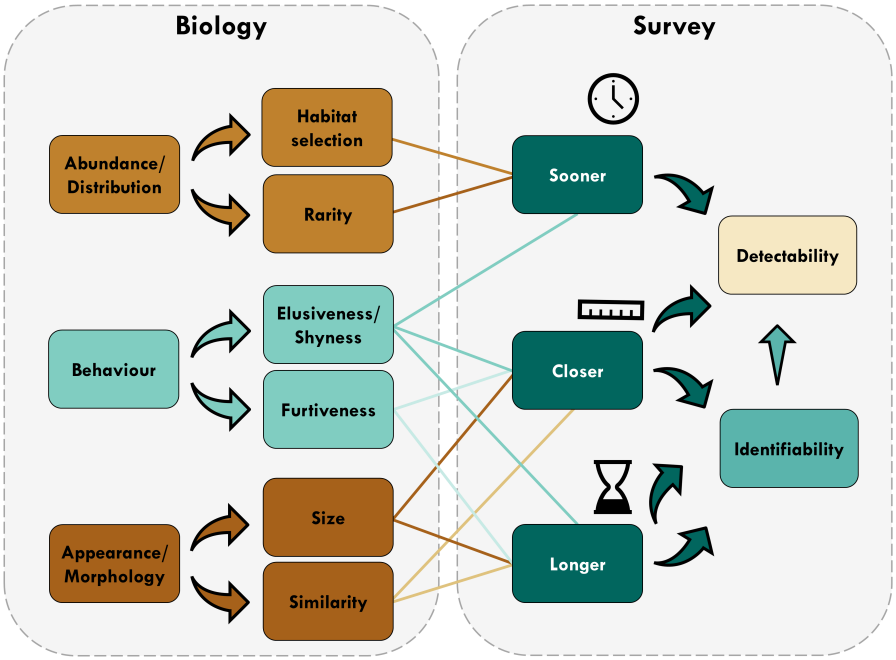

Figure 1: *Conceptual diagram showing different aspects of detectability during camera trap surveys and the modulating effect of biological characteristics. In addition to direct impacts on detectability, a longer visit and a closer image of focal species increases the chance of identifying the visitor hence increases detectability.*

Material and methods

Study area and camera trapping

The study area (2,400 km^2) is situated in south-eastern Norway (59.36-59.81°N, 10.60-11.60°E) where camera traps were placed to monitor the Eurasian lynx (*Lynx lynx*) as part of the SCANDLYNX project (`http://viltkamera.nina.no/`). The landscape varies from coastline, lakes, and agricultural fields to valleys and wooded hills, between 0 and 400 meters above sea level (Kartverket, 2017). Boreal forests dominate the area, and the climate is milder than in other areas of similar latitude, primarily due to warm winds and oceanic currents (Dannevig & Harstveit, 2013). The temperature varies throughout the year, with a mean temperature between –3 and –5°C in January and up to between 16 and 17°C in July (Dannevig, 2009). Average annual precipitation rate is 700–1000 mm (Moen, 1999), and the duration of snow cover (when snow covers minimum 50% of the ground) ranges between 50 and 125 days per year (Moen, 1999).

We deployed 30 motion-triggered digital Reconyx cameras (five different models: HC500 HyperFire Semi-Covert IR, HC600 HyperFire High Output Covert IR, PC800 HyperFire Professional Semi-Covert IR, PC900 HyperFire Professional Covert IR, and PC850 HyperFire Professional White Flash LED) from 15 September to 20 December 2017, specifically with the goal to photo-capture lynx. Therefore, cameras were installed in steep terrain, on ledges or at the base of (and facing) cliffs. Placement was often close to wildlife trails, with one camera trap per location and a minimum distance of 2.3 km between neighbouring camera trap sites. Cameras were aimed perpendicular to the wildlife trail at locations where a wildlife trail was present. Each camera was mounted on a tree between 0.2 and 1 m above the ground, depending on terrain. Notwithstanding occasional failures (empty batteries, etc.), all cameras were operating for 24 hours per day every day during the study period. Cameras were set to take three photos per trigger event with up to two photos per second. The no-delay function was used to enable the cameras to continue taking photos while being triggered. In addition to motion-triggered capture, the time-laps mode was used to take one photo per day to allow identification of time periods during which cameras were non-functional.

Lure treatment

At each camera trap location, a scent station was installed at 2 to 6 m from the camera. The area between the scent station and the camera was cleared by removing tall grass and branches. The scent station consisted of one scent lure stick (untreated Norway spruce *Pica abies*; 40 x 4.7 x 2.2 cm), hammered 20 cm into the ground (tapered end), leaving 20 cm exposed above the ground (Fig. 2). As a lure receptacle, a 3-cm deep and 1-cm wide hole angled 45 degrees downwards was drilled into each lure stick on the narrow side 2.5 cm from the top of the stick. The lure sticks were placed with the drilled hole facing the wildlife trail if the trail was present in front of the camera and facing the camera where wildlife trails were absent. The lure sticks were treated with a scent lure, applied with one cotton swab (with paper core) cut in half and soaked in the lure, containing ∼0.5 mL of lure (or control), and placed in the drilled hole of the lure stick. The five treatments were (i) skunk-based scent lure (essence of striped skunk *Mephitis mephitis* anal scent glands), (ii) fox-based scent lure (ground red fox *Vulpes vulpes* scent glands), (iii) castor-based scent lure (castoreum; essence of anal sacs from American beaver *Castor canadensis*), (iv) synthetic fermented egg (SFE), and (v) distilled water as a control. All four scent lures are commercially available products and were obtained from F&T Fur Harvester's Trading Post, Alpena, MI, USA.

Figure 2: *Example camera trap photos of the four study species in southeast Norway; clockwise from the top left: European badger (*Meles meles*), red fox (*Vulpes vulpes*), domestic cat (*Felis catus*), and pine marten (*Martes martes*). We measured distance as the number of body lengths between the lure stick and the part of the animal closest to the lure stick in each photo (indicated by arrows).*

As the lure sticks were novel objects in the environment, they may influence animal behaviour even without scent lures; we thus used distilled water instead of lures on scent poles as the control treatment. Each scent station was randomly assigned to one lure (or water) at a time, which was replaced with a different treatment and a fresh scent stick every 14 days (± 3 days) until all 5 treatments had been used at each site. After use, the lure sticks were disposed outside the study area. Clean plastic gloves were used in all handling of cameras, lure sticks, and lures to prevent cross contamination between lure treatments.

Analysis

We only included photos of European badger (*Meles meles*), red fox, pine marten (*Martes martes*), and domestic cat (*Felis catus*) in the analysis, as these were the most common free-ranging mesocarnivores in the study area. Photos of a given species that were taken within a five-minute interval were classified as belonging to the same visit. We performed three Bayesian analyses as explained below

and assessed model convergence by inspecting trace plots and by using the R-hat statistic, where models with R-hat $\leq$1.1 are considered converged (Brooks & Gelman 1998). The number of Markov chain Monte Carlo (MCMC) samples/iterations was based on convergence requirements identified in preliminary analyses. Parameter estimates were provided as the mean and 95% credible interval (CI) of their respective posterior distribution.

Sooner - time to first detection

We fitted separate occupancy models for each species in a Bayesian framework following (Bornand et al., 2014). We estimated the effect of lure treatments on the time (in days since lure treatment application) until the first photographic capture of the focal species at each camera, conditional on occupancy of the site by the focal species.

The occupancy state z_i of a given site i is the result of a Bernoulli trial where ψ is the probability of occurrence:

$$z_i \sim Bernoulli(\psi) \tag{1}$$

We adopted an exponential distribution and modelled the time to detection as a censored random variable stratified by lure treatment (Poisson rate λ for a given lure l) and a constant hazard in continuous time. Detection probability p until time t is a function of the detection rate λ and the survey time t:

$$p_l = 1 - exp(-\lambda_l t) \tag{2}$$

We defined a censoring indicator variable d, where $d = 1$ indicated that the time-to-detection observation at site i was censored (hence, the species had not been detected before the end of the survey period T) for a given lure and $d = 0$, otherwise. There were two ways in which an observation could become censored ($d = 1$) at a given site i, either because the species was absent at that site ($z_i = 0$) or because the species was present ($z_i = 1$) but was not detected by the end of the observation period (following a given lure treatment).

We fitted species-specific models using the R2jags package in R (version 3.5.2, R Development Core Team, 2017; Su & Yajima, 2015) and JAGS (Plummer, 2003). We drew 200,000 MCMC samples from three chains, thinned by three and we discarded the initial 50,000 samples as burn-in. The model definition is provided in the electronic Supporting Information Appendix S1.

Closer - distance to the focal point

To obtain a relative measure of an individual's proximity to the lure stick, we measured distance in units of body lengths of the animal visible in the photo (Fig. 2). When an event resulted in several photos, we measured distance as the minimum distance over all photos of the event. Body length has been used as a measuring unit in other studies in behavioural ecology (Macdonald et al., 2004). We measured the body length from the base of the ear to the base of the tail. We recorded distance as the number of body lengths (with ½ body length resolution) between the lure stick and the part of the animal closest to the lure stick (Figs. 2-3). Contact between the animal and the lure was recorded as zero body lengths. We fitted species-specific Bayesian generalised linear mixed models using brms R package (Burkner, 2018), with an identity link (Gaussian family), to quantify the effect of lure treatment on log of distance of the focal species to the camera (+0.01 body lengths to deal with zeros). We included camera station as a random effect on the intercept to account for non-independence between observations associated with the same camera trap. Individual animals may be detected during multiple visits at one or multiple camera trap; this source of non-independence could not be accounted for here, due to the inability to distinguish individuals. We also fitted one model testing differences between species (regardless of lure treatment) with the specifications described above. We drew 2,000 MCMC samples from four chains, and we discarded the initial 1,000 samples as burn-in.

Longer - duration of exposure

Apparent time spent at camera stations was defined as the time difference (in seconds) between the first and last photograph showing the species during a visit. The time an animal spent at scent lures has been used to evaluate attraction and avoidance in both captive (Saunders & Harris, 2000) and wild carnivores (Andersen, Johnson & Jones, 2016), suggesting that longer visits at a scent station could indicate attraction, while shorter visits could indicate avoidance. We fitted species-specific Cox proportional hazard models using the spBayesSurv package in R (Zhou, Hanson & Zhang, 2018) to quantify the effect of lure treatments on duration of exposure for the focal species. We used treatment as a categorical covariate (5 levels) and compared effect of the 4 lure treatments to water. In addition, we included a random effect of camera trap (station) in our model. We drew 20,000 MCMC samples from four chains, and we discarded the initial 5,000 samples as burn-in.

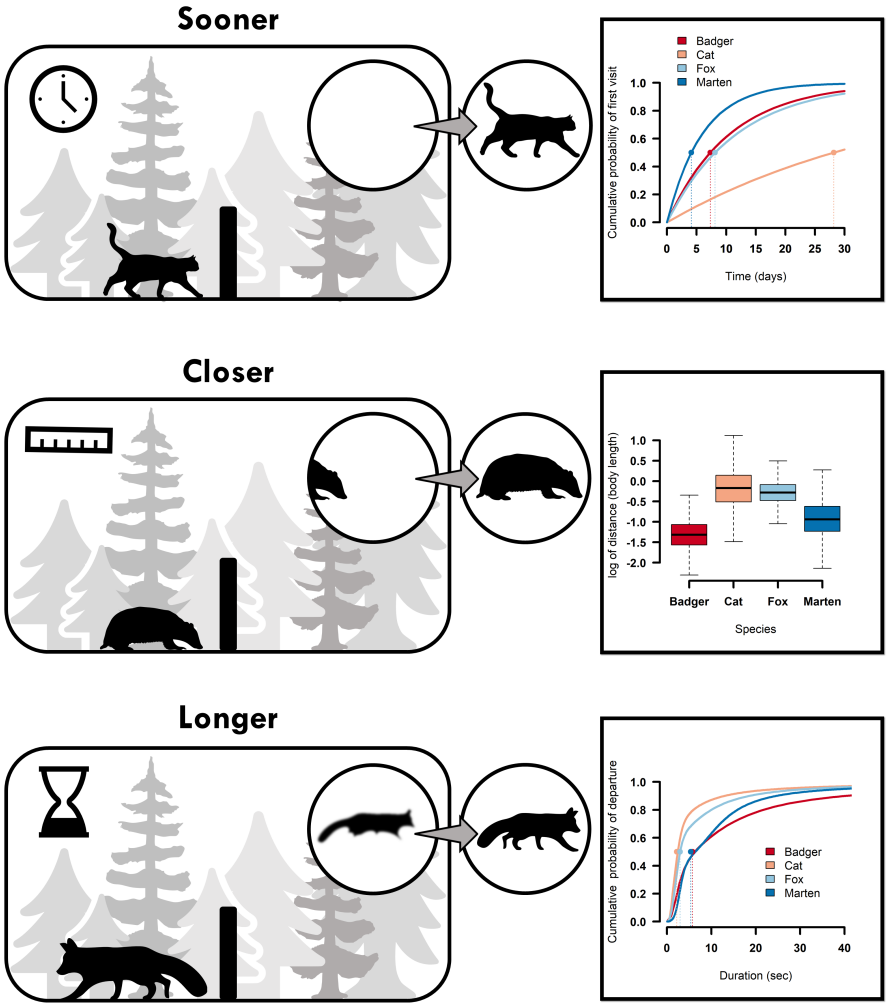

Figure 3: *The workflow of our study and potential impact of behavioural response to reduce false absences in camera trapping. Boxes on the right show posterior time to first detection (days), distance from camera's focal point (body length) and duration of visits (seconds) for the focal species: European badger (*Meles meles*), red fox (*Vulpes vulpes*), domestic cat (*Felis catus*), and pine marten (*Martes martes*). Time to detection (top-right) is conditional on a site being occupied.*

Results

Of 1876 trap nights (operational cameras), 336 were associated with the control treatment (water), 357 with SFE, 369 with castor-based lures, 360 with fox-based lures, and 420 with skunk-based lures. Focal species were recorded in 1279 (68.2%) camera trap photos (520 badger, 122 cat, 560 fox and 199 marten). We recorded 40 camera station visits by cats, 60 by badger, 108 visits by fox, and 32 by marten across all treatments. Red foxes were photo-captured at 27 of the 30 camera trap locations, badgers at 14, domestic cats at 10, and pine martens at 12 camera trap locations. Based on R-hat values, convergence was reached by all Bayesian models used for inferences.

Sooner - time to first detection

Median time to first detection, i.e. the time by which 50% of occupied sites had made their first detection of the focal species were 4 days with 95% Credible Interval (CI) of 2.2 to 41.4 for martens, 28 days for cats (95% CI = 4.1 to 108), 7.3 days (95% CI = 3.3 to 49) for badgers and 8 days (95% CI = 5 to 18) for foxes (Fig. 3). These estimates assume an exponential hazard function. In addition, they are conditional on the site being occupied and thus accounting for imperfect detection. The only species for which we detected a significant effect of lure on time to first detection was the domestic cat. Exponential hazard rate (λ) of domestic cat was higher at stations treated with castor-based lure (mean $\lambda = 1.5$, 95% CI = 0.3 to 3.6) compared to control treatment water (mean $\lambda = 0.2$, 95% CI = 0.03 to 0.5). This translates into a 4.3-day reduction (95% CI = 1 to 27 days) in the median time to first detection (Fig. 4).

Closer - distance to the focal point

The shortest distance from the focal point within the cameras viewshed (expressed in body lengths of the individual in the image; Figs. 2-3) varied substantially between observations and their posteriors overlapped between species: 0.84 median body lengths for cats (95% CI = 0.3 to 2.1), 0.75 median body lengths for fox (95% CI = 0.43 to 1.4), 0.3 median body lengths for badger (95% CI = 0.13 to 0.55), and 0.4 median body lengths for marten (95% CI = 0.2 to 1). Martens kept a longer distance from the lure stick when the scent station was treated by fox-based lure (mean regression coefficient $\beta = 4$, 95% CI = 1.9 to 6.3), skunk-based lure (mean β = 3.2, 95% CI = 0.8 to 5.6) or castor-based lure (mean $\beta = 4$, 95% CI =0.7 to 7.4) compared with the control treatment (water). Conversely, badgers moved closer to

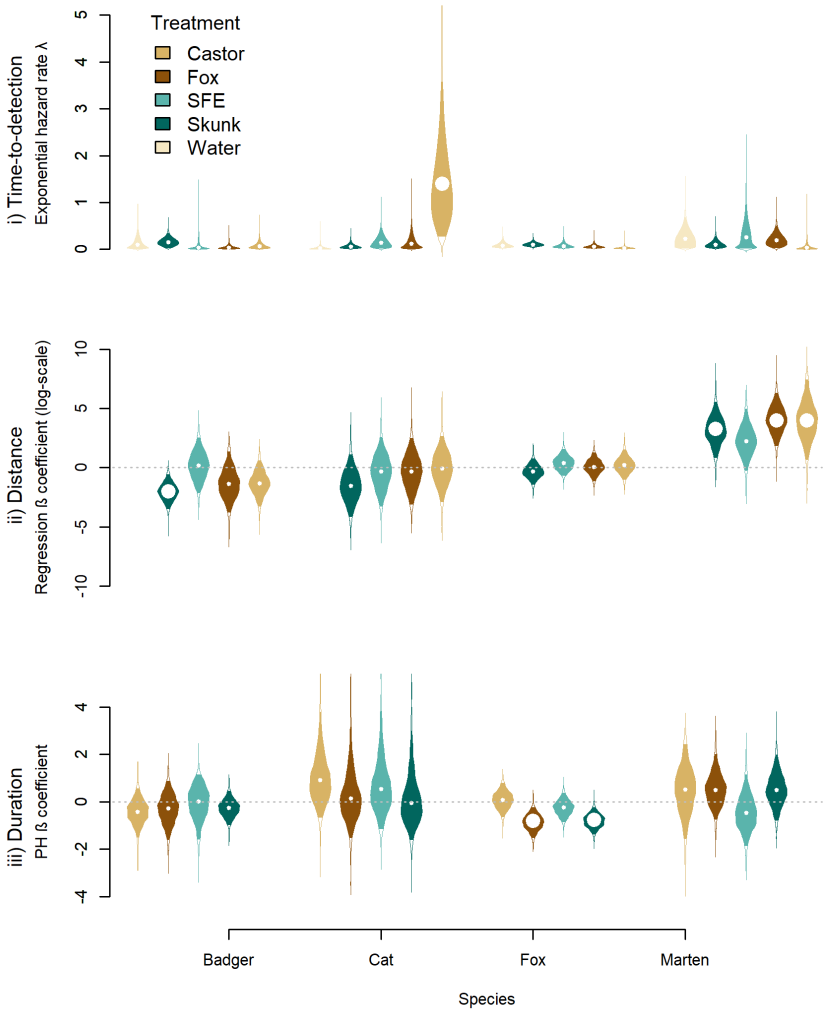

Figure 4: *The effect of scent lure treatment (castoreum, fox gland, synthesized fermented egg [SFE], skunk gland) on i) time to first photo-capture of the study species (λ: exponential hazard rate), ii) distance of focal species to the lure stick (linear regression β coefficient of each lure treatment on log of distance), and iii) duration of visit (proportional hazard β coefficient of each lure treatment effect on time to departure; higher coefficients mean shorter durations). Each violin shows posterior distribution (with 95% credible interval) of coefficients of one lure treatment (colour coded) effect on one species and the median is shown by a white dot (larger dots for results that are significantly different from 0). Violins for the control (water) are only shown in the "time to first detection" analysis; violins in the other two plots are coefficients, compared with the control.*

lure sticks when they were treated with skunk-based lure (mean β = –2, 95% CI = –3.5 to –0.5) compared to the control treatment (Fig. 4, Appendix S2 Table S1-S4).

Longer - duration of exposure

Median time to departure (i.e. the time by which half of the documented visits by the focal species had ended) was 6 sec for badgers (95% CI = 3 to 16 sec), 5 sec for martens (95% CI = 3 to 14), 3 sec for foxes (95% CI = 0 to 4), and 2 sec for cats (95% CI = 0 to 4; Fig. 3). Foxes had the longest visits at scent stations that were treated with fox-based lure (mean hazard coefficient = –0.8, 95% CI = –1.5 to –0.2) or skunk-based lures (mean hazard coefficient = –0.8, 95% CI = –1.4 to –0.2) compared to the control (water). We detected no significant difference in duration of visits between control and lure treatments for the other species (Fig. 4, Appendix S3 Table S1-S4).

Discussion

Our study yielded quantitative information about three different aspects of detectability during camera trapping (Figs. 1 and 3): 1) the time until first detection, 2) the proximity of the subject to a focal point in the viewshed of the camera, and 3) the duration of exposure to the camera. Variation in these measures was substantial, and to some extent explained by species and lure treatment (Fig. 4).

Sooner - time to detection

Time to detection is directly related to the probability of detection (Garrard et al., 2008). Factors that influence the propensity for and frequency of visits (e.g. density, movement patterns, curiosity) affect the time until the initial detection or the interval between consecutive detection events. We found that time to detection varied substantially between observations in our study but detected only one significant effect: free-ranging domestic cats appeared to visit sites with the castoreum-based lure sooner than other sites (Fig. 4). An affinity of felines to castoreum lures has been reported previously (McDaniel et al., 2000). However, given the spectrum of scents used in this study and previous reports from similar work (Bischof et al., 2014b), a lack of additional effects on time to detection was surprising. Our study was conducted late autumn to early winter which might have influenced the effective sampling distance by cold weather. Alternatively, we used a comparatively small amount of lure ($\sim$0.5 ml) which could explain the paucity of effects.

Investigators have multiple options for manipulating the time to detection. They can try to reduce it, as we attempted here, by using olfactory or other attractants which may draw animals from a wider area or increase the propensity for approaching the camera by exploiting the interest in food, potential mates, or curiosity in general. Although the effect was not pronounced in our study, based on findings from other studies, lures can be an effective tool for increasing detectability and thus decreasing time to detection (Bischof et al., 2014b; Ferreras et al., 2018; Mills et al., 2019). Other measures are aimed at reducing the risk of avoidance behaviour by preventing contamination of the site with human scent, hiding or camouflaging cameras, using illumination outside the visible spectrum of the target species, and minimizing sounds generated by the camera. Most important is perhaps is the selection of sites (O'Connor et al., 2017); placing cameras at locations the target species' range and in preferred microhabitat increases exposure to individuals in the population and thus reduces time to detection (Fig. 1).

Regardless of the biological characteristics that influence time to detection and the measures taken to reduce it, it has already been recognized as an intuitive and useful measure of detectability (Garrard et al., 2008; Bischof et al., 2014b; Halstead, Kleeman & Rose, 2018). Specifically, time to event analysis has been used previously in wildlife camera trapping studies to quantify the effect of lures and other covariates on time to detection (Bischof et al., 2014b). Among previous studies that employed time to detection, we can make a coarse distinction based on accounting for imperfect detection (Garrard et al., 2008; Bischof et al., 2014b; Bornand et al., 2014). Accounting for imperfect detection, which includes the present study, has the distinct advantage that we estimate time to detection conditional on the site being occupied, rather than apparent time to detection conditional on the detection having been made. Time to detection without accounting for imperfect detection is liable to underestimate time to detection, as it ignores sites without detections (Bischof et al., 2014b). Alternatively, one may estimate time to detection using right-censoring of sites without detections, which leads to overestimation of time to detection.

Here we included an exponential hazard model for time to detection besides a binomial component to account for detection conditional on presence (Garrard et al., 2008; Bornand et al., 2014). This allowed us to account for non-detections that were due to true absences, while analysing the effect of lure treatment on the time to detection. The hazard rate parameter (λ) estimated by the model translates directly into detection probability (Equation 2) but offers a different perspective on detectability (Garrard et al., 2008).

Regardless of the type of time-to-detection model used, we recommend that it is made part of a hierarchical approach that accounts for imperfect detection. When it comes to measures intended to reduce time to detection, investigators should consider not only the strength of the effect, but also potential unintended consequences these measures may have for the interpretation of survey results. For example, lures may change the size of the area sampled, thereby affecting assumptions of the analytical methods (Larrucea et al., 2007; Rowcliffe et al., 2008) or they could cause changes in the study population (e.g. territory maintenance, energy expenditure). Furthermore, many camera trap studies target multiple species and lures that attract one, may repel another (Rocha, Ramalho & Magnusson, 2016; Mills et al., 2019).

Closer - distance to the focal point

Once an individual has been attracted to a camera trap site, detection will depend on whether the individual enters the camera's field of view in a way that a) triggers the camera and b) results in a photo (or video) with enough detail to make an identification. Distance of a visitor to the camera trap is one of the most important covariates of a successful trigger (Randler & Kalb, 2018). Since most camera traps in use today operate on a passive infrared sensor that detects heat of a moving object, the probability of missing a visit increases with distance from the sensor.

Our analysis showed species-specific differences in proximity to the focal location at camera trap stations, modulated by lure type. When lure sticks were treated with the control (distilled water), pine martens approached the sticks more closely than the other three species (Appendix S2 Table S1-S4). This pattern reversed, when lures were applied, with marten exhibiting avoidance behaviour towards gland-based lures (castoreum, fox, and skunk). Certain species could display aversion towards lures; e.g. odours from predators or potential competitors can act as deterrent to subordinate species, hence their detectability could decrease when using lures (Rocha et al., 2016). Red foxes represent an interspecific threat to the smaller marten, which may explain apparent avoidance behaviour (Lindström, Brainerd & Overskaug, 1995; Monterroso et al., 2020). The similar response to skunk-scented sticks is more difficult to explain, as striped skunks are not native to Europe and do not occur in our study area.

By contrast, badgers approached lure sticks treated with skunk anal scent gland significantly more closely than the control. Similar communication systems in closely related species (Hughes, Price & Banks, 2010) may facilitate bidirectional olfactory communications within species assemblage (Nielsen et al., 2015). Although striped

skunk does not occur in our study area, both skunk and badger are mustelids, which may explain interest by badgers. Alternatively, skunk-based lure, a novel stimulus, may elicit curiosity (Harrington, Harrington & Macdonald, 2009). Other studies have reported little effect of scent lures from sympatric predators on badger attraction (Monterroso et al., 2011; Suárez-Tangil & Rodríguez, 2017), possibly indicating a greater role of the novelty and curiosity aspects.

Detection probability decreases or becomes biased as the chance of misidentification (i.e. false-positive) increases with the number of related and similar-looking species co-occurring in the same area (Rowcliff & Carbone 2008). Similarly, animals that are hesitant to fully enter the camera's viewshed or keep their distance are less likely to trigger the camera or yield photos that allow identification, which translates into lowered detection probability. These challenges are further amplified for small-bodied (Tobler et al., 2008) and furtive species (Glen et al., 2013). The choice of camera (focal length, shutter speed or frame rate, image resolution, choice of still vs. video, etc.), camera placement (e.g. relative to a path), installation (height, aim), and the application of attractants give investigators some control over the position of target animals within the camera's viewshed. Attractants may in addition help keep fast-moving species still enough to minimize motion blur.

As our results show, lures may not only facilitate increased proximity but could also prompt avoidance behaviour, manifested as increased distance from the focal point. As mentioned earlier, this could be especially relevant in studies targeting multiple species, where finding a lure or bait that attracts some or all, but does not repel any target species may be challenging if not impossible (Rocha et al., 2016). Furthermore, leaving DNA at the camera's focal point (e.g. scats or hair samples), where it can be detected and used as an additional source of information can aid individual identification (see also next section).

Longer - duration of exposure

In many cases, the time spent in the camera's viewshed is directly related to the number of images or the number or length of video recordings. More abundant visual documentation translates into a higher probability of making an identification and ultimately greater detection probability. We found that red foxes spent significantly more time getting their picture taken at stations treated with skunk and red fox scent gland lures than at stations with the control (Fig. 4). Fox reaction to conspecifics and skunk can be attributed to information gathering (e.g. communication with conspecifics and competitors) or novelty investigation behaviour.

We detected no significant response to SFE by foxes or any other species in our

study. SFE contains some of the components of carrion scent (Bullard, 1982), and has been reported as effective for attracting canids such as red fox (Saunders & Harris, 2000; Hunt, Dall & Lapidge, 2007), kit fox *V. macrotis*, and coyote *Canis latrans* (Roughton, 1982; Bullard, Turkowski & Kilburn, 1983), as well as dingo *C. lupus dingo* and feral dog *C. l. familiaris* (Hunt et al., 2007). The lack of a response to SFE in our study may be due to the very small amount of lure used at scent stations (∼0.5 ml), compared with other studies, i.e. 2-10 ml (Monterroso et al., 2011; Stratman & Apker, 2014; Suárez-Tangil & Rodríguez, 2017). In addition, our study was conducted during the autumn, whereas others reported that red fox spent more time with SFE during winter and spring than summer and autumn (Saunders & Harris, 2000).

There is another potentially important and unaccounted-for aspect that could have influenced behaviour during our study: the mutual influence between species visiting the camera trap. Carnivores, intentionally or unintentionally, leave scent at camera trap stations which is liable to be picked up during subsequent visits to the same station by conspecifics and other species. For example, a lure that attracts species A and prompts it to leave a scent mark, may attract or repel species B. This is also one of the reasons (aside from the inability to distinguish individuals) we refer to our study as quasi-experimental, as mutual interactions were neither controlled for during the study nor accounted for during the analysis but may have contributed to the observed patterns.

Investigators may be especially interested in measures to increase the duration of visits to camera traps when working with fast-moving species or species that are difficult to identify due to their morphology (similarity with conspecifics, lack of unique markings, etc.). Particularly capture-recapture methods that require individual identification and rely on unique markings such as pelt patterns, may benefit from boosting the number of images taken and thus the chance of identification (Garrote et al., 2012; Gerber et al., 2012; Dorning & Harris, 2019). For species without visible markings, longer visits may increase the probability and amount of DNA left behind, such as in hair (Burki et al., 2010), faeces and urine (Wikenros et al., 2017), and glandular secretion in case of marking (Clapham et al., 2014).

While lengthening exposure time to the camera will increase detection probability, sample size (visual documentation), and detail, it may also artificially increase encounters between individuals of the same or different species, thus impacting the study system. In addition, it may constitute a manipulation of time budgets. These and other potential impacts should be considered when measures are taken to keep animals in front of the camera for an extended time.

Conclusions

An important conclusion regarding measures to boost detection probability in camera trapping studies is that one measure does not fit all. Biological differences – e.g. distribution, density, behaviour, morphology – mean different challenges to detectability (Fig. 1) requiring different measures to overcome them. Disentangling and quantifying components of detectability, as we did here, offers investigators a framework for organizing study and species-specific impediments to detection and come up with strategies to cope with them.

In addition to biological considerations, the impediments and choice of measure for overcoming them will depend on the goals of a given camera-trapping study. Studies that require individual identification, such as capture-recapture for abundance estimation, may place high importance on "closer" and "longer" in order to make reliable individual assignments (Guthlin, Storch & Kuchenhoff, 2014). Similarly, studies focusing on assessments of behaviour (Caravaggi et al., 2017; van Ginkel, Smit & Kuijper, 2019), and body condition (Carricondo-Sanchez et al., 2017) that want to distinguish reproductive status (Trolle & Kéry, 2003; Canu et al., 2017) and sex (Monterrubio-Rico et al., 2018) will be interested in boosting the quantity and level of detail of information obtained during a given visit to a camera trap. Conversely, studies on presence-absence or species assemblages (Kays et al., 2020) will initially be focused on maximizing the probability of a visit to the camera trap station, especially when rare species are involved ("sooner").

Finally, measures taken to boost different aspects of detectability may have other, unintended effects. Camera trapping is generally hailed as a non-invasive ecological survey method (Burton et al., 2015), but see Meek et al., 2016). The use of lures and baits, as discussed above, could have unintentional consequences for movement and activity patterns, as well as intra and interspecific communication (Neilson et al., 2018). Such changes not only make camera trapping intrusive but could also impact the assumptions of the approach used for drawing inferences (e.g. the size of the site in occupancy analysis). In addition, a measure that improves detection of one species or demographic group, may have the opposite effect for another species or group. We recommend that investigators take a comprehensive look at both the biological and study-specific impediments to detectability and strategies taken to overcome them.

Acknowledgment

This research was partly based on E.B. and S.B. master's degree project at NMBU. We thank H. Weber for camera trapping instructions, N. H. Thorsen for his help with choosing camera sites, and R. Økseter for helping with the preparation of the lure sticks. We are grateful to all students and volunteers that assisted with classification of the camera trap images. This study was funded by the Norwegian Environment Agency, the Research Council of Norway (grant 281092), and the Nature Protection Division of the County Governor's Office for Oslo, Akershus and Østfold Counties. We thank two anonymous reviewers for their constructive comments on an early version of this manuscript, E. Moqanaki for his contribution to Figures 1-3 and P. Dupont for fruitful discussions. Any use of product names in this study is for descriptive purposes only and does not imply endorsement.

References

Ahumada, J.A., Hurtado, J. & Lizcano, D. (2013). Monitoring the Status and Trends of Tropical Forest Terrestrial Vertebrate Communities from Camera Trap Data: A Tool for Conservation. PLoS ONE.

Andersen, G.E., Johnson, C.N. & Jones, M.E. (2016). Sympatric predator odour reveals a competitive relationship in size-structured mammalian carnivores. Behav. Ecol. Sociobiol. 70, 1831–1841.

Archaux, F., Henry, P.-Y. & Gimenez, O. (2012). When can we ignore the problem of imperfect detection in comparative studies?: Detectability in comparative studies. Methods Ecol. Evol. 3, 188–194.

Bischof, R., Ali, H., Kabir, M., Hameed, S. & Nawaz, M.A. (2014a). Being the underdog: an elusive small carnivore uses space with prey and time without enemies: Space and time use by Altai mountain weasel. J. Zool. 293, 40–48.

Bischof, R., Hameed, S., Ali, H., Kabir, M., Younas, M., Shah, K.A., Din, J.U. & Nawaz, M.A. (2014b). Using time-to-event analysis to complement hierarchical methods when assessing determinants of photographic detectability during camera trapping. Methods Ecol. Evol. 5, 44–53.

Bornand, C.N., Kéry, M., Bueche, L., Fischer, M. & Yoccoz, N. (2014). Hide-and-seek in vegetation: time-to-detection is an efficient design for estimating detectability and occurrence. Methods Ecol. Evol. 5, 433–442.

Bullard, R.W. (1982). Wild canid associations with fermentation products. Ind. Eng. Chem. Prod. Res. Dev. 21, 646–655.

Bullard, R.W., Turkowski, F.J. & Kilburn, S.R. (1983). Responses of free-ranging coyotes to lures and their modifications. J. Chem. Ecol. 9, 877–888.

Burki, S., Roth, T., Robin, K. & Weber, D. (2010). Lure sticks as a method to detect pine martens *Martes martes*. Acta Theriol. 55, 223–230.

Burton, A.C., Neilson, E., Moreira, D., Ladle, A., Steenweg, R., Fisher, J.T., Bayne, E. & Boutin, S. (2015). Wildlife camera trapping: a review and recommendations for linking surveys to ecological processes. J. Appl. Ecol. 52, 675–685.

Canu, A., Mattioli, L., Santini, A., Apollonio, M. & Scandura, M. (2017). 'Video-scats': combining camera trapping and non-invasive genotyping to assess individual identity and hybrid status in gray wolf. Wildlife Biol. 2017, wlb.00355.

Caravaggi, A., Banks, P.B., Burton, A.C., Finlay, C.M.V., Haswell, P.M., Hayward, M.W., Rowcliffe, M.J. & Wood, M.D. (2017). A review of camera trapping for conservation behaviour research. Remote Sens. Ecol. Conserv. 3, 109–122.

Carricondo-Sanchez, D., Odden, M., Linnell, J.D.C. & Odden, J. (2017). The range of the mange: Spatiotemporal patterns of sarcoptic mange in red foxes (*Vulpes vulpes*) as revealed by camera trapping. PLoS ONE 12, e0176200.

Clapham, M., Nevin, O.T., Ramsey, A.D. & Rosell, F. (2014). Scent-marking investment and motor patterns are affected by the age and sex of wild brown bears. Anim. Behav. 94, 107–116.

Dannevig, P. (2009). Østfold: Klima: Store norske leksikon. Available at: `https://snl.no/%C3%98stfold_-_klima` (accessed: 19.02.2018).

Dannevig, P. & Harstveit, K. (2013). Klima i Norge. I:. Stor norske leksikon. Available at: `https://snl.no/klima_i_Norge` (accessed: 30.01.2018).

Dorning, J. & Harris, S. (2019). The challenges of recognising individuals with few distinguishing features: Identifying red foxes *Vulpes vulpes* from camera-trap photos. PLoS ONE 14, e0216531.

Ferreras, P., Diaz-Ruiz, F. & Monterroso, P. (2018). Improving mesocarnivore detectability with lures in camera-trapping studies. Wildl. Res. 45, 505–517.

Garrard, G.E., Bekessy, S.A., McCarthy, M.A. & Wintle, B.A. (2008). When have we looked hard enough? A novel method for setting minimum survey effort protocols for flora surveys. Austral Ecol. 33, 986–998.

Garrote, G., Gil-Sanchez, J.M., McCain, E.B., de Lillo, S., Telleria, J.L. &

Simon, M.A. (2012). The effect of attractant lures in camera trapping: a case study of population estimates for the Iberian lynx (*Lynx pardinus*). Eur. J. Wildl. Res. 58, 881–884.

Garvey, P.M., Glen, A.S., Clout, M.N., Wyse, S.V., Nichols, M. & Pech, R.P. (2017). Exploiting interspecific olfactory communication to monitor predators. Ecol. Appl. 27, 389–402.

Gerber, B.D., Karpanty, S.M. & Kelly, M.J. (2012). Evaluating the potential biases in carnivore capture–recapture studies associated with the use of lure and varying density estimation techniques using photographic-sampling data of the Malagasy civet. Popul. Ecol. 54, 43–54.

van Ginkel, H.A.L., Smit, C. & Kuijper, D.P.J. (2019). Behavioral response of naïve and non-naïve deer to wolf urine. PLoS ONE 14, e0223248.

Glen, A.S., Cockburn, S., Nichols, M., Ekanayake, J. & Warburton, B. (2013). Optimising Camera Traps for Monitoring Small Mammals. PLoS ONE 8, e67940.

Guillera-Arroita, G., Lahoz-Monfort, J.J., MacKenzie, D.I., Wintle, B.A. & McCarthy, M.A. (2014). Ignoring Imperfect Detection in Biological Surveys Is Dangerous: A Response to 'Fitting and Interpreting Occupancy Models'. PLoS ONE 9, e99571.

Guthlin, D., Storch, I. & Kuchenhoff, H. (2014). Is it possible to individually identify red foxes from photographs? Wildl. Soc. Bull. 38, 205–2010.

Halstead, B.J., Kleeman, P.M. & Rose, J.P. (2018). Time-to-Detection Occupancy Modeling: An Efficient Method for Analyzing the Occurrence of Amphibians and Reptiles. J. Herpetol. 52, 415–424.

Hamel, S., Killengreen, S.T., Henden, J.-A., Eide, N.E., Roed-Eriksen, L., Ims, R.A. & Yoccoz, N.G. (2013). Towards good practice guidance in using camera-traps in ecology: influence of sampling design on validity of ecological inferences. Methods Ecol. Evol. 4, 105–113.

Harrington, L.A., Harrington, A.L. & Macdonald, D.W. (2009). The Smell of New Competitors: The Response of American Mink, *Mustela vison*, to the Odours of Otter, *Lutra lutra* and Polecat, *M. putorius*. Ethology 115, 421–428.

Hofmeester, T.R., Cromsigt, J.P.G.M., Odden, J., Andrén, H., Kindberg, J. & Linnell, J.D.C. (2019). Framing pictures: A conceptual framework to identify and correct for biases in detection probability of camera traps enabling multi-species comparison. Ecol. Evol. 9, 2320–2336.

Hughes, N.K., Price, C.J. & Banks, P.B. (2010). Predators Are Attracted to the Olfactory Signals of Prey. PLoS ONE 5, e13114.

Hunt, R.J., Dall, D.J. & Lapidge, S.J. (2007). Effect of a synthetic lure on site visitation and bait uptake by foxes (*Vulpes vulpes*) and wild dogs (*Canis lupus dingo*, *Canis lupus familiaris*). Wildl. Res. 34, 461.

Kartverket. (2017). Høyeste fjelltopp i hver kommune. Available at: `https://www.kartverket.no/kunnskap/Fakta-om-Norge/Hoyeste-fjelltopp-i-kommunen/hoyeste-fjelltopp-i-hver-kommune/` (accessed: 09.11.2017)

Kays, R., Arbogast, B.S., Baker-Whatton, M., Beirne, C., Boone, H.M., Bowler, M., Burneo, S.F., Cove, M.V., Ding, P., Espinosa, S., Luis Sousa Gonçalves, A., Hansen, C.P., Jansen, P.A., Kolowski, J.M., Knowles, T.W., Guimarães Moreira Lima, M., Millspaugh, J., McShea, W.J., Pacifici, K., Parsons, A.W., Pease, B.S., Rovero, F., Santos, F., Schuttler, S.G., Sheil, D., Si, X., Snider, M. & Spironello, W.R. (2020). An empirical evaluation of camera trap study design: how many, how long, and when? Methods Ecol. Evol. 2041–210X.13370.

Larrucea, E.S., Brussard, P.F., Jaeger, M.M. & Barrett, R.H. (2007). Cameras, Coyotes, and the Assumption of Equal Detectability. J. Wildl. Manag. 71, 1682–1689.

Lindström, E.R., Brainerd, S.M. & Overskaug, K. (1995). Pine marten-red fox interactions: a case of intraguild predation? Ann. Zool. Fenn. 32, 123-130.

Macdonald, D.W., Buesching, C.D., Stopka, P., Henderson, J., Ellwood, S.A. & Baker, S.E. (2004). Encounters between two sympatric carnivores: red foxes (*Vulpes vulpes*) and European badgers (*Meles meles*). J. Zool. 263, 385–392.

MacKenzie, D.I., Nichols, J.D., Royle, J.A., Pollock, K.H., Bailey, L. & Hines, J.E. (2017). Occupancy estimation and modeling: inferring patterns and dynamics of species occurrence. Elsevier.

McDaniel, G.W., McKelvey, K.S., Squires, J.R. & Ruggiero, L.F. (2000). Efficacy of lures and hair snares to detect lynx. Wildl. Soc. Bull. 28, 119–123.

McLean, W.R., Goldingay, R.L. & Westcott, D.A. (2017). Visual lures increase camera-trap detection of the southern cassowary (*Casuarius casuarius johnsonii*). Wildl. Res. 44, 230–237.

Meek, P., Ballard, G., Fleming, P. & Falzon, G. (2016). Are we getting the full picture? Animal responses to camera traps and implications for predator studies. Ecol. Evol. 6, 3216–3225.

Mills, D., Fattebert, J., Hunter, L. & Slotow, R. (2019). Maximising camera trap data: Using attractants to improve detection of elusive species in multi-species surveys. PLoS ONE 14, e0216447.

Moen, A. (1999). National Atlas of Norway: Vegetation. Hønefoss: Norwegian Mapping Authority.

Monterroso, P., Alves, P.C. & Ferreras, P. (2011). Evaluation of attractants for non-invasive studies of Iberian carnivore communities. Wildl. Res. 38, 446.

Monterroso, P., Díaz-Ruíz, F., Lukacs, P.M., Alves, P.C. & Ferreras, P. (2020). Ecological traits and the spatial structure of competitive coexistence among carnivores. Ecology ecy.3059.

Monterrubio-Rico, T.C., Charre-Medellin, J.F., Perez-Martinez, M.Z. & Mendoza, E. (2018). Use of remote cameras to evaluate ocelot (*Leopardus pardalis*) population parameters in seasonal tropical dry forests of central-western Mexico. Mammalia 82, 113–123.

Moriarty, K.M., Linnell, M.A., Thornton, J.E. & Watts, G.W. (2018). Seeking Efficiency With Carnivore Survey Methods: A Case Study With Elusive Martens. Wildl. Soc. Bull. 42, 403–413.

Neilson, E.W., Avgar, T., Burton, A.C., Broadley, K. & Boutin, S. (2018). Animal movement affects interpretation of occupancy models from camera-trap surveys of unmarked animals. Ecosphere 9.

Nielsen, B.L., Rampin, O., Meunier, N. & Bombail, V. (2015). Behavioral responses to odors from other species: introducing a complementary model of allelochemics involving vertebrates. Front. Neurosci. 9.

O'Connor, K.M., Nathan, L.R., Liberati, M.R., Tingley, M.W., Vokoun, J.C. & Rittenhouse, T.A.G. (2017). Camera trap arrays improve detection probability of wildlife: Investigating study design considerations using an empirical dataset. PLoS ONE 12, e0175684.

R Development Core Team (2018). R: a language and environment for statistical computing. R Foundation for Statistical Computing, Vienna, Austria. `https://www.r-project.org/`

Randler, C. & Kalb, N. (2018). Distance and size matters: A comparison of six wildlife camera traps and their usefulness for wild birds. Ecol. Evol. 8, 7151–7163.

Read, J.L., Bengsen, A.J., Meek, P.D. & Moseby, K.E. (2015). How to snap your cat: optimum lures and their placement for attracting mammalian predators

in arid Australia. Wildl. Res. 42, 1–12.

Rocha, D.G., Ramalho, E.E. & Magnusson, W.E. (2016). Baiting for carnivores might negatively affect capture rates of prey species in camera-trap studies. J. Zool. 300, 205–212.

Roughton, R.D. (1982). A Synthetic Alternative to Fermented Egg as a Canid Attractant. J. Wildl. Manag. 46, 230.

Rovero, F., Fridolin Zimmermann, Duccio Berzi & Paul Meek. (2013). "Which camera trap type and how many do I need?" A review of camera features and study designs for a range of wildlife research applications. Hystrix 24, 148–156.

Rowcliffe, J., Carbone, C., Jansen, P.A., Kays, R. & Kranstauber, B. (2011). Quantifying the sensitivity of camera traps: an adapted distance sampling approach. Methods Ecol. Evol. 2, 464–476.

Rowcliffe, J.M., Field, J., Turvey, S.T. & Carbone, C. (2008). Estimating animal density using camera traps without the need for individual recognition. J. Appl. Ecol. 45, 1228–1236.

Saunders, G. & Harris, S. (2000). Evaluation of attractants and bait preferences of captive red foxes (*Vulpes vulpes*). Wildl. Res. 27, 237.

Sollmann, R. (2018). A gentle introduction to camera-trap data analysis. Afr. J. Ecol. 56, 740–749.

Stratman, M.R. & Apker, J.A. (2014). Using infrared cameras and skunk lure to monitor swift fox (*Vulpes velox*). Southwest. Nat. 59, 502–510.

Suárez-Tangil, B.D. & Rodríguez, A. (2017). Detection of Iberian terrestrial mammals employing olfactory, visual and auditory attractants. Eur. J. Wildl. Res. 63, 93.

Tobler, M.W., Carrillo-Percastegui, S.E., Leite Pitman, R., Mares, R. & Powell, G. (2008). An evaluation of camera traps for inventorying large- and medium-sized terrestrial rainforest mammals. Anim. Conserv. 11, 169–178.

Trolle, M. & Kéry, M. (2003). Estimation of ocelot density in the Pantanal using capture-recapture analysis of camera-trapping data. J. Mammal. 84, 8.

Wikenros, C., Jarnemo, A., Frisén, M., Kuijper, D.P.J. & Schmidt, K. (2017). Mesopredator behavioral response to olfactory signals of an apex predator. J. Ethol. 35, 161–168.

Zhou, H., Hanson, T. & Zhang, J. (2018). spBayesSurv: Fitting Bayesian Spatial Survival Models Using R. arXiv:1705.04584 [stat].

Supporting information

Appendix S1: Time to first detection
Appendix S2: Distance to the focal point
Appendix S3: Duration of exposure

Supporting Information. Tourani, M., Brøste, E.N., Bakken, S., Odden, J. & Bischof, R. Sooner, closer, or longer: detectability of mesocarnivores at camera traps. *Journal of Zoology*.

Appendix S1: Time to first detection

R code with the JAGS (Plummer, 2003) model definition for the occupancy model with detection modeled as a time-to-detection process following Bornand et al. (2014):

```
sink("ttdocc.txt")
cat("

    model{

    ###--- ECOLOGICAL PROCESS ---###
    # True state model for the partially observed true state
    # True occupancy z at site i

    psi ~ dunif(0,1)

    for(i in 1:M){ ##--loop over sites
    z[i] ~ dbern(psi)
    }

    ###--- OBSERVATION PROCESS ---###
    for(l in 1:5){ ##--loop over lure types
        lambda[l] ~ dgamma(0.001,0.001)
        }

    for(i in 1:M){
        ##--Exponential time to detection
        y[i] ~ dexp(lambda[lure[i]])
        }#M:site

    for(i in 1:M){
        d[i] ~ dbern(theta[i])##--model for censoring indicator
        theta[i] <- z[i] * step(y[i]-Tmax) + (1-z[i])
        }#M:site

    }#model
    ",fill=TRUE)
sink()
```

References

Bornand, C.N., Kéry, M., Bueche, L., Fischer, M. & Yoccoz, N. (2014). Hide-and-seek in vegetation: time-to-detection is an efficient design for estimating detectability and occurrence. Methods Ecol. Evol. 5, 433–442.

Plummer, M. (2003). JAGS: a program for analysis of Bayesian graphical models using Gibbs sampling. In Proceedings of the 3rd International Workshop on Distributed Statistical Computing (DSC 2003), March 20–22. Vienna, Austria.

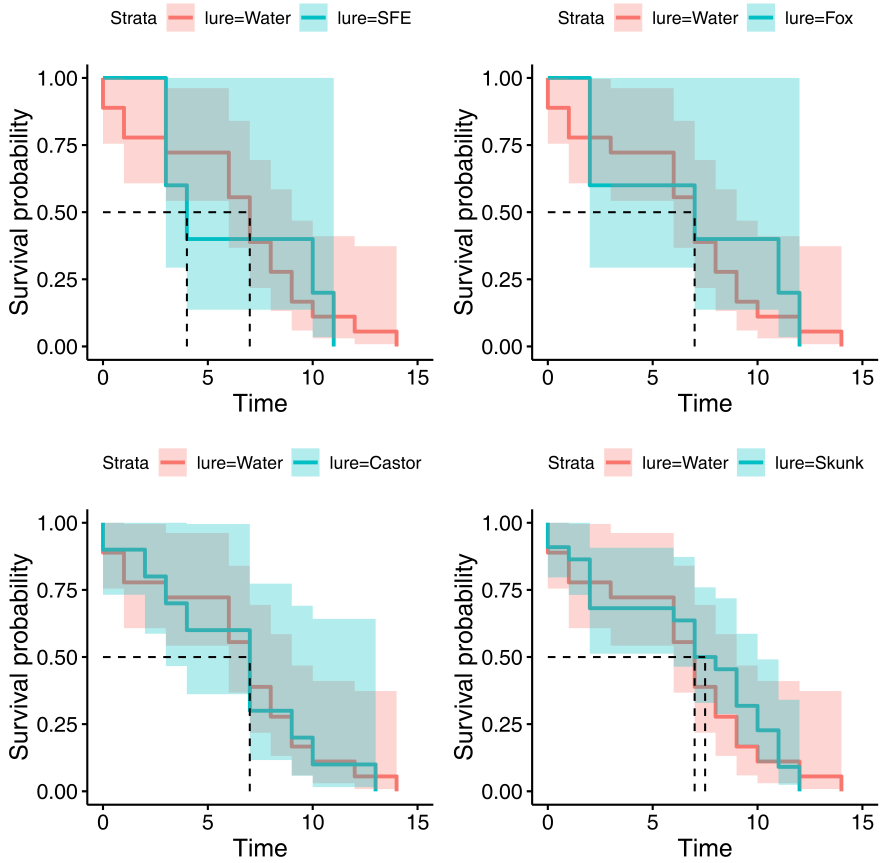

Figure S1: Time-to-event plots for European badger (*Meles meles*). The four plots contrast the four lure treatments against water (control). Survival probability refers to probability of no detection. The median time to first detection (days) is visualized with dashed lines.

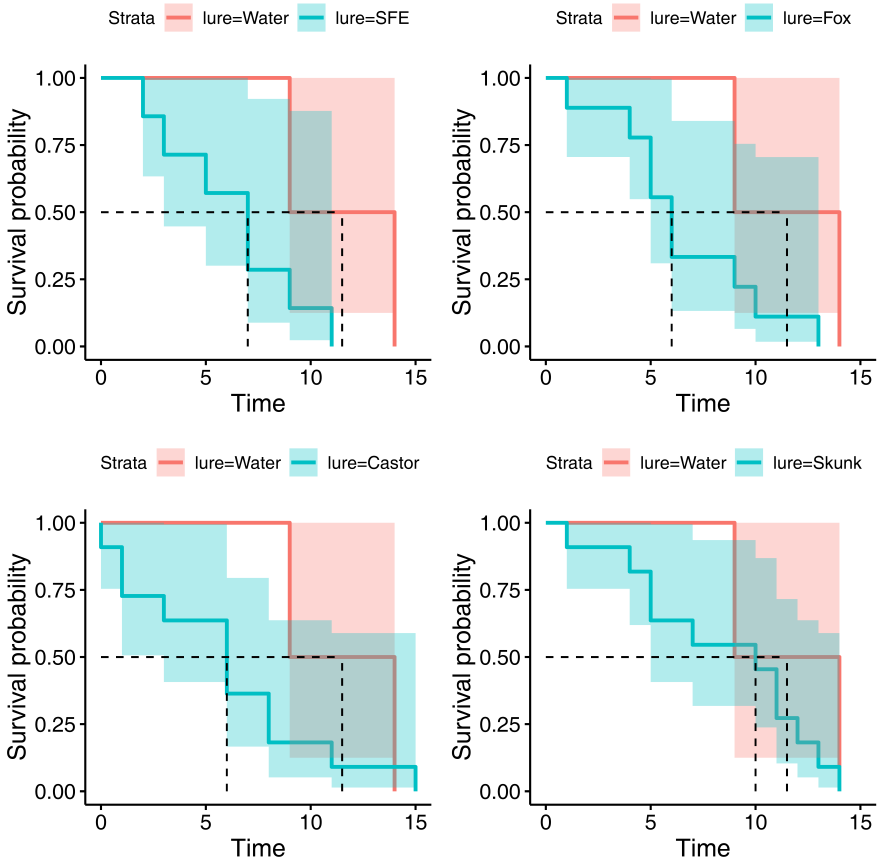

Figure S2: Time-to-event plots for domestic cat (*Felis catus*). The four plots contrast the four lure treatments against water (control). Survival probability refers to probability of no detection. The median time to first detection (days) is visualized with dashed lines.

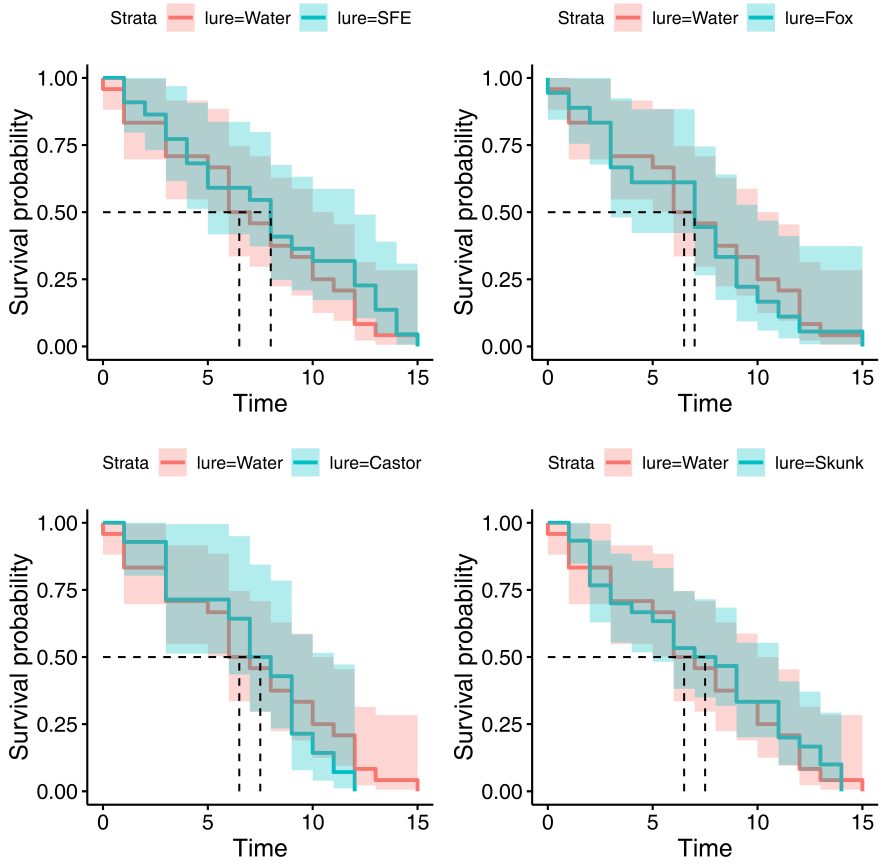

Figure S3: Time-to-event plots for red fox (*Vulpes vulpes*). The four plots contrast the four lure treatments against water (control). Survival probability refers to probability of no detection. The median time to first detection (days) is visualized with dashed lines.

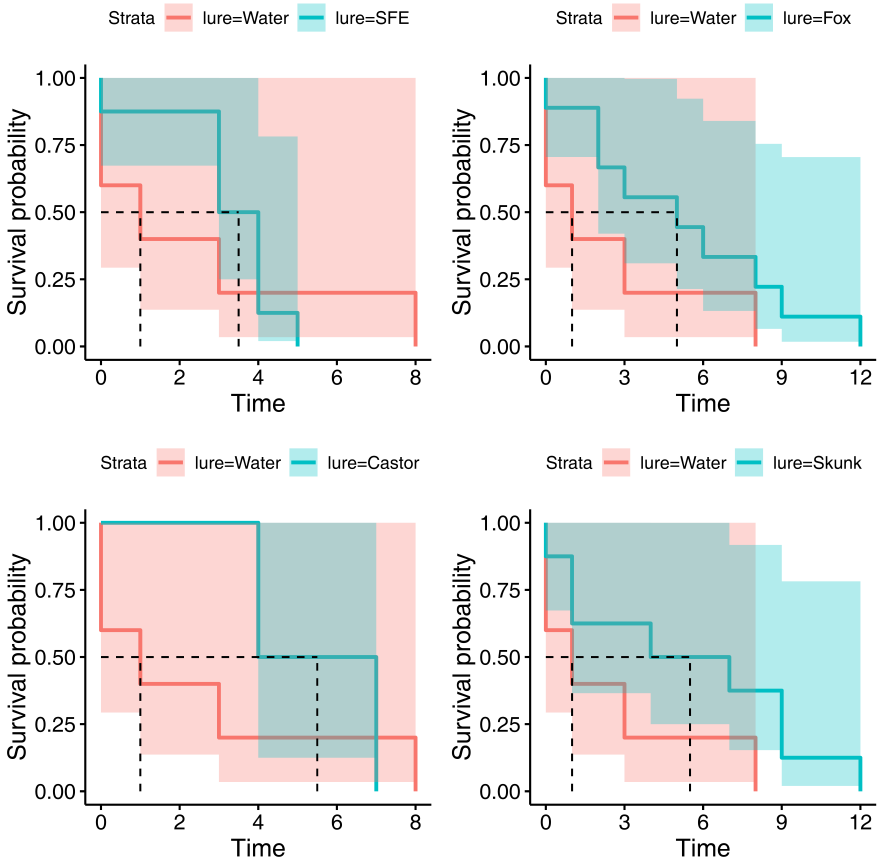

Figure S4: Time-to-event plots for pine marten (*Martes martes*). The four plots contrast the four lure treatments against water (control). Survival probability refers to probability of no detection. The median time to first detection (days) is visualized with dashed lines.

Supporting Information. Tourani, M., Brøste, E.N., Bakken, S., Odden, J. & Bischof, R. Sooner, closer, or longer: detectability of mesocarnivores at camera traps. *Journal of Zoology.*

Appendix 2: Distance to the focal point

Table S1: The summary output of species-specific mixed model for the effect of lure treatments on the log of distance of European badger (*Meles meles*) to the lure stick (camera's focal point). Estimates show β coefficients. The 95% credible interval (CI) for the effects that did not overlap zero are shown in bold.

Predictors	log(Distance)	
	Estimates	CI (95%)
Intercept	0.03	–1.35 - 1.44
Lure.Type: SFE	0.14	–2.18 - 2.57
Lure.Type: Castor	–1.34	–3.21 - 0.70
Lure.Type: Fox	–1.46	–3.69 - 0.93
Lure.Type: Skunk	**–2.04**	**–3.47 - –0.58**
Random Effects		
σ^2	0.77	
τ_{00}	5.33	
ICC	0.13	
$N_{Camera.ID}$	14	
Observations	60	
Marginal R^2/Conditional R^2	0.195 / 0.331	

Table S2: The summary output of species-specific mixed model for the effect of lure treatments on the log of distance of domestic cat (*Felis catus*) to the lure stick (camera's focal point). Estimates show β coefficients.

Predictors	log(Distance)	
	Estimates	CI (95%)
Intercept	0.11	–3.01 - 2.85
Lure.Type: SFE	–0.32	–3.21 - 2.57
Lure.Type: Castor	–0.05	–2.99 - 2.85
Lure.Type: Fox	–0.34	–3.30 - 2.54
Lure.Type: Skunk	–1.55	–4.27 - 1.18
Random Effects		
σ^2	1.59	
τ_{00}	1.99	
ICC	0.45	
$N_{Camera.ID}$	10	
Observations	40	
Marginal R^2/Conditional R^2	0.159 / 0.621	

Table S3: The summary output of species-specific mixed model for the effect of lure treatments on the log of distance of red fox (*Vulpes vulpes*) to the lure stick (camera's focal point). Estimates show β coefficients.

Predictors	log(Distance)	
	Estimates	CI (95%)
Intercept	–0.34	–1.25 - 0.56
Lure.Type: SFE	0.40	–0.69 - 1.48
Lure.Type: Castor	0.24	–1.11 - 1.55
Lure.Type: Fox	0.07	–1.09 - 1.28
Lure.Type: Skunk	–0.32	–1.38 - 0.75
Random Effects		
σ^2	1.00	
τ_{00}	3.20	
ICC	0.24	
$N_{Camera.ID}$	27	
Observations	108	
Marginal R^2/Conditional R^2	0.044 / 0.288	

Table S4: The summary output of species-specific mixed model for the effect of lure treatments on the log of distance of pine marten (*Martes martes*) to the lure stick (camera's focal point). Estimates show β coefficients. The 95% credible interval (CI) for the effects that did not overlap zero are shown in bold.

Predictors	log(Distance)	
	Estimates	CI (95%)
Intercept	–4.38	–6.28 - –2.41
Lure.Type: SFE	2.33	–0.19 - 4.77
Lure.Type: Castor	**3.99**	**0.64 - 7.43**
Lure.Type: Fox	**4.02**	**1.71 - 6.32**
Lure.Type: Skunk	**3.15**	**0.67 - 5.50**
Random Effects		
σ^2	0.53	
τ_{00}	5.69	
ICC	0.09	
$N_{Camera.ID}$	12	
Observations	32	
Marginal R^2/Conditional R^2	0.402 / 0.473	

Supporting Information. Tourani, M., Brøste, E.N., Bakken, S., Odden, J. & Bischof, R. Sooner, closer, or longer: detectability of mesocarnivores at camera traps. *Journal of Zoology.*

Appendix 3: Duration of exposure

Table S1: The summary output of species-specific model of proportional hazard for the effect of lure treatments on the duration of European badger (*Meles meles*) stay in front of camera. Estimates show coefficients, CI: Credible Interval.

Predictors	Duration	
	Estimates (mean)	CI (95%)
Lure.Type: SFE	–0.03	–1.5 - 1.2
Lure.Type: Castor	–0.43	–1.52 - 0.52
Lure.Type: Fox	–0.3	–1.73 - 0.98
Lure.Type: Skunk	–0.26	–0.99 - 0.5
Random Effects Variance		
Mean	0.5	
Standard deviation	0.54	
95% CI	0.13	
Observations	60	
$N_{Camera.ID}$	14	
Log pseudo marginal likelihood	–220.41	

Table S2: The summary output of species-specific model of proportional hazard for the effect of lure treatments on the duration of domestic cat (*Felis catus*) stay in front of camera. Estimates show coefficients, CI: Credible Interval.

Predictors	Duration	
	Estimates (mean)	CI (95%)
Lure.Type: SFE	0.52	–1.1 - 2.7
Lure.Type: Castor	0.87	–0.83 - 2.9
Lure.Type: Fox	0.13	–1.66 - 2.2
Lure.Type: Skunk	–0.08	–1.8 - 2
Random Effects Variance		
Mean	0.16	
Standard deviation	0.43	
95% CI	0.0008 - 1.1	
Observations	40	
$N_{Camera.ID}$	10	
Log pseudo marginal likelihood	–102.578	

Table S3: The summary output of species-specific model of proportional hazard for the effect of lure treatments on the duration of red fox (*Vulpes vulpes*) stay in front of camera. Estimates show coefficients, CI: Credible Interval. The 95% CI for the effects that did not overlap zero are shown in bold.

Predictors	Duration	
	Estimates (mean)	CI (95%)
Lure.Type: SFE	–0.24	–0.86 - 0.4
Lure.Type: Castor	0.09	-0.7 - 0.8
Lure.Type: Fox	**–0.84**	**–1.5 - –0.2**
Lure.Type: Skunk	**–0.77**	**–1.4 - –0.2**
Random Effects Variance		
Mean	0.11	
Standard deviation	0.12	
95% CI	0.0008 - 0.43	
Observations	108	
$N_{Camera.ID}$	27	
Log pseudo marginal likelihood	–300.06	

Table S4: The summary output of species-specific model of proportional hazard for the effect of lure treatments on the duration of pine marten (*Martes martes*) stay in front of camera. Estimates show coefficients, CI: Credible Interval.

Predictors	Duration	
	Estimates (mean)	CI (95%)
Lure.Type: SFE	–0.41	–2 - 1.4
Lure.Type: Castor	0.65	–1.4 - 2.5
Lure.Type: Fox	0.58	–0.8 - 2.2
Lure.Type: Skunk	0.61	–0.7 - 2.1
Random Effects Variance		
Mean	0.4	
Standard deviation	0.8	
95% CI	0.0009 – 2.7	
Observations	32	
$N_{Camera.ID}$	12	
Log pseudo marginal likelihood	–104.26	

Article II

Statistical Reports

Ecology, 101(7), 2020, e03030

Multiple observation processes in spatial capture–recapture models: How much do we gain?

Mahdieh Tourani,[1,4] Pierre Dupont,[1] Muhammad Ali Nawaz,[2,3] and Richard Bischof[1]

[1]*Faculty of Environmental Sciences and Natural Resource Management, Norwegian University of Life Sciences, P.O. Box 5003,1432Ås, Norway*
[2]*Department of Animal Sciences, Quaid-i-Azam University, Islamabad 44000 Pakistan*
[3]*Snow Leopard Trust, Islamabad 44000 Pakistan*

Citation: Tourani, M., P. Dupont, M. A. Nawaz, and R. Bischof. 2020. Multiple observation processes in spatial capture–recapture models: How much do we gain? Ecology 101(7):e03030. 10.1002/ecy.3030

Abstract. Population monitoring data may originate from multiple methods and are often sparse and fraught with incomplete information due to practical and economic constraints. Models that can integrate multiple survey methods and are able to cope with incomplete data may help investigators exploit available information more thoroughly. Here, we developed an integrated spatial capture–recapture (SCR) model to incorporate multiple data sources with imperfect individual identification. We contrast inferences drawn from this model with alternate models incorporating only subsets of the data available. Using extensive simulations and an empirical example of multi-method brown bear (*Ursus arctos*) monitoring data from northern Pakistan, we quantified the benefits of including multiple sources of information in SCR models in terms of parameter precision and bias. Our multiple observation processes SCR model (MOP) yielded a more complete picture of the underlying processes, reduced bias, and led to more precise parameter estimates. Our results suggest that the greatest gains from integrated SCR models can be expected in situations where detection probability is low, a large proportion of detections is not attributable to individuals, and the degree of overlap between individual home ranges is low.

Key words: camera trap; data integration; large carnivore; multiple observation process; noninvasive monitoring; simulation; spatial capture–recapture.

Introduction

Wildlife monitoring is an integral part of applied ecology, providing valuable information about populations in order to assess their status and inform recovery or control. One of the primary challenges in wildlife monitoring arises from the failure to detect all individuals in a population. For decades, capture–recapture (CR) methods were used to deal with this challenge by estimating detection probability and accounting for it during the estimation of ecological parameters such as abundance and vital rates (Lukacs and Burnham 2005). A comparatively recent development, spatial capture–recapture (SCR; Efford 2004, Royle et al. 2018) additionally uses the information in the spatial configuration of individual detections to directly estimate density when data are available only for a subset of the population.

Sparse data sets are common in SCR studies, because this framework is particularly popular for inventory and monitoring of rare or elusive species, to estimate density with data obtained noninvasively over large areas (e.g., Sollmann et al. 2013*b*). This poses a challenge, because SCR models, like non-spatial CR models (Gerber et al. 2014), are known to return biased and imprecise estimates when fit to sparse data (Marques et al. 2011, Sollmann et al. 2012). Moreover, noninvasive monitoring methods often yield detections that are not attributable to specific individuals (e.g., incomplete genotype information in genetic capture–recapture studies or camera trap data with inconclusive individual designation). Discarding these unidentified detections further reduces the amount of data used for estimation (Augustine et al. 2019).

Nowadays, many species inventories combine multiple survey methods, such as noninvasive DNA sampling,

Manuscript received 12 July 2019; revised 27 December 2019; accepted 29 January 2020. Corresponding Editor: José M. Ponciano.
[4] E-mail: mahdieh.tourani@gmail.com

camera trapping, sign surveys, or physical mark–recapture to maximize the amount of data (Blanc et al. 2014, Clare et al. 2017, Burgar et al. 2018, Murphy et al. 2018). One way to better exploit the available information is integrated modeling, the joint analysis of multiple data sets traditionally analyzed separately (Besbeas et al. 2002). This trend has also found its way into the SCR framework (Gopalaswamy et al. 2012, Sollmann et al. 2013*b*). The idea of integrated modeling is to combine into one analysis different data sets that contain (potentially partial) information about the same underlying ecological processes of interest. The different data sets do not necessarily originate from different survey methods (e.g., individual detections from DNA-sampling and camera trapping; Sollmann et al. 2013*b*) but they can also represent different data types collected using the same survey method. For example, this is the case of spatial mark–resight models (SMR) that combine detections of the marked, identified, and unmarked, always unidentified, parts of a population collected using camera traps (Rich et al. 2014). Traditionally, unidentified detections are discarded further reducing available data for analysis. Recently, generalized SMR proposed to deal with this situation (Whittington et al. 2018). However, these models still rely on the assumption that marked individuals are always recognized as marked if detected (Royle et al. 2013). This assumption is violated when the marking status is not observable with certainty. For example, in case of tag loss an individual may be misclassified as unmarked when it belongs to the marked part of the population. Poor quality pictures in camera trapping are another example for uncertain mark status for a detection usually leading to that detection being discarded.

Here we describe an integrated SCR model that combines data sets originating from different survey types, each with potentially varying degree of completeness in terms of the proportion of individually identified detections. In addition, this model relaxes the assumption that marked individuals are always recognized as marked. We then ask to what extent the integrated analysis of multiple sources of information boosts our ability to draw inferences from monitoring data by comparing the precision and bias of parameter estimates from four models using different subsets of the available data.

- Model 1: classic SCR, uses only identified detections from a single survey method.
- Model 2: integrates identified and unidentified detections from a single survey method.
- Model 3: integrates identified detections from one survey method and unidentified detections from a second independent survey method.
- Model 4: the multiple observation processes (MOP) SCR model that combines all data sets.

Finally, we showcase our modeling approach by applying it to a sparse multi-method survey data set on brown bear (*Ursus arctos*) from the western Himalayas in Pakistan.

Methods

Model specification

We developed an integrated Bayesian SCR model composed of two hierarchical levels. The first one describes the underlying ecological process of interest (i.e., density) and the second one describes the associated observation processes (Fig. 1).

Ecological process.—The ecological process describes population density, which arises from the distribution of individuals in space. Following a homogeneous point process (Royle et al. 2018), the positions of individual activity centers s_i are uniformly distributed across the habitat S, the spatial extent within which individual activity centers can be placed:

$$s_i \sim \text{Uniform}(S) \tag{1}$$

To account for the fact that some individuals in the population may never be detected, we used a data-augmentation approach (Royle et al. 2007). For all M individuals (M much larger than the unknown true population size), we modeled inclusion in the population through a latent state variable z_i, governed by the inclusion probability Ψ:

$$z_i \sim \text{Bernoulli}(\Psi) \tag{2}$$

Population size N is then the sum of individuals included in the population:

$$N = \sum_{i=1}^{M} z_i \tag{3}$$

Observation processes.—In SCR, the classic observation model describes the probability of detecting individual i at discrete locations (i.e., detectors) conditional on its s_i location. In our integrated model, we considered K different survey types deployed simultaneously corresponding to K independent sets of detectors, each composed of J^k detectors. Considering the commonly used half-normal detection function (Borchers and Efford 2008), we expressed probability p_{ij}^k of detecting individual i at the jth detector of the detector set k as:

$$p_{ij}^k = p_0^k \times e^{-\frac{\left(d_{ij}^k\right)^2}{2\sigma^2}} \times z_i, \tag{4}$$

where d_{ij}^k is the distance between the individual's activity center s_i and detector j^k; p_0^k is the magnitude parameter for survey type k; and σ is the scale parameter. While

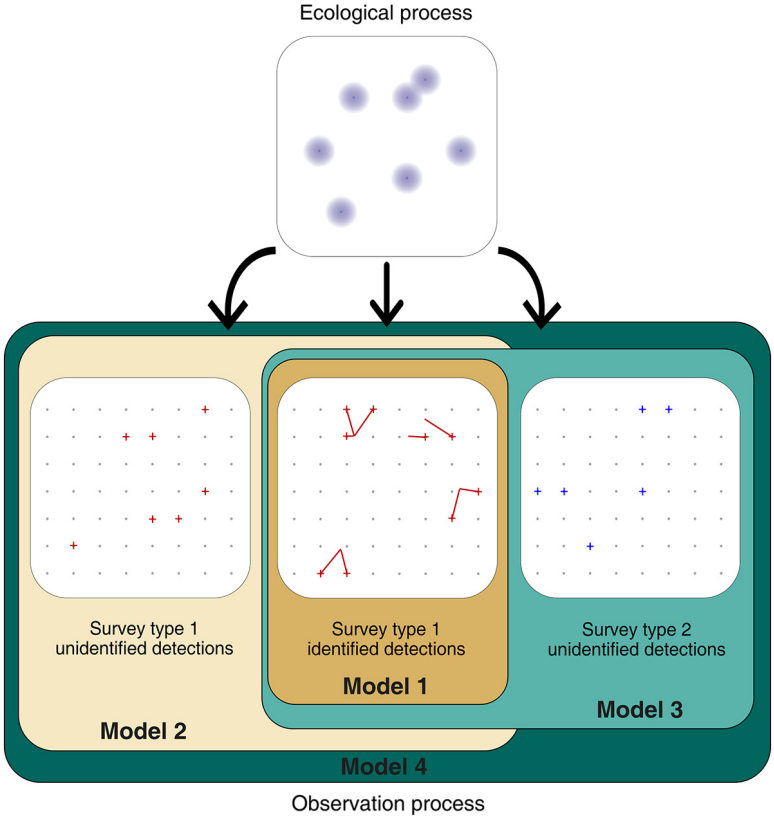

FIG. 1. Hierarchical structure of the four spatial capture–recapture (SCR) models integrating different combinations of data. The top box shows the distribution of latent individual activity centers, with associated detection probability indicated as gradual shading. Lower boxes show detections of those individuals at detectors (gray points). Survey type 1 yields detections both with (red plus signs, left panel) and without individual identity (lines connecting detections to individual activity centers, middle panel). Survey type 2 yields detections without individual identity indicated by blue crosses.

the baseline detection probability is specific to each survey type, the scale parameter is shared as we assume it arises from the ecological process (e.g., space use). Alternatively, σ could be survey type-specific if it is linked with the detection process rather than animal space use (e.g., acoustic methods; Efford et al. 2009), as long as each survey type contributes detections of identified individuals at multiple detectors.

In many situations, detections cannot be linked to an individual with certainty, yet the spatial information of unidentified detections can be used in an integrated SCR framework by modeling the probability of obtaining unidentified detections conditional on the latent activity centers of individuals in the population. Individual detections might not be independent (e.g., temporal correlation of fecal samples), which results in violation of Poisson assumptions (Royle et al. 2013). This is the case of our bear study where the sampling process did not allow us to consider the number of detections as real counts. We therefore considered binary detector-level detections, instead of counts of unidentified detections, and expressed the probability to collect at least one unidentified detection at detector j from survey type k as:

$$\dot{p}_J^k = 1 - \prod_{i=1}^{M} \left(1 - p_{ij}^k \times \left(1 - \alpha^k\right)\right), \tag{5}$$

where α^k is the probability that any sample from survey type k be identified. Following this formulation, the K matrices of individually identified detections y_{ij}^k for the M individuals at J^k detectors are the outcome of a Bernoulli process with probability of detection p_{ij}^k :

$$y_{ij}^k \sim \text{Bernoulli}\left(p_{ij}^k \cdot \alpha^k\right) \tag{6}$$

Detections without individual ID are compiled as K vectors of zeros and ones of length J^k, where $\dot{y}_j^k$

represents the presence/absence of at least one unidentified detection at detector j^k:

$$\dot{y}_J^k \sim \text{Bernoulli}\left(\dot{p}_J^k\right) \quad (7)$$

Under this formulation, identified and unidentified components of a given survey type k share parameters p_0^k and α^k, while σ and N (or density; z_i: individual inclusion) are shared by all observation processes. When all observation models are combined in a joint likelihood in the MOP model, both identified and unidentified detections from multiple survey types inform about the same ecological parameters (σ and N), thus potentially improving inferences.

Simulation study

We used simulations to quantify and compare the performance of models with different levels of data integration. Specifically, we were interested in the consequences of data integration on the precision and bias of two key parameters, N and σ, under different scenarios of population size, individual home range overlap, proportion of identified detections, and overall detectability.

Although SCR studies often use multiple occasions, this is not necessary (Efford et al. 2009) and we simulated a population surveyed with $k = 2$ survey types during a single occasion. Method 1 yields both identified and unidentified detections with variable levels of identification ($\alpha = 0.25$, 0.50, and 0.75). This is, for example, the case in most DNA-based studies where some DNA samples fail to produce definite identification. We considered that method 2 could only generate unidentified detections ($\alpha = 0$), as would be the case in a camera-trap study of a species without unique external markings. In a square habitat of 50 × 50 arbitrary distance units without a surrounding unsampled buffer area, we randomly drew either 30 or 50 individuals' s_i positions, following Eq. 1. Although many SCR studies incorporate an unsampled buffer into their state space, not doing so allowed us to use the same state-space for all scenarios, instead of dealing with variable buffer sizes for each σ scenario, which would have made comparisons between simulations difficult (forcing either variable densities or variable population sizes). We defined two independent detector grids, placed 1.0 and 1.2 distance units apart, leading to $J^1 = 2{,}500$ and $J^2 = 1{,}764$ detectors, respectively. We then simulated individual detections for three levels of σ (1, 2, or 3 distance units) to generate increasing levels of overlap between individual home ranges (Efford and Hunter 2018). To avoid any confounding effect of higher detectability associated with higher σ, we parameterized our simulations using a constant effective sampling area A_0 (Borchers and Efford 2008). This allowed us to calculate a different value of p_0 for each σ while keeping the overall individual detectability constant

$$p_0 = 1 - \exp - \left(A_0 / 2\pi\sigma^2\right) \quad (8)$$

Detection parameters were chosen so that approximately 65% or 85% of the population was detected by the two survey types combined, corresponding to levels of detections of approximately 50% or 70% detected by survey method 1, and 30% or 50% by method 2, respectively. We generated individual detection histories y_{ij}^1 and y_{ij}^2 (Eq. 6), using the detection probabilities defined in Eq. 4. As survey type 1 yields both identified and unidentified detections, we randomly retained individual detection histories with three levels of identification probability ($\alpha = 0.25$, 0.50, and 0.75). For example, considering high detections, if 85% of the population was detected, given the identification probability of 0.75, we only detected and identified 64% of the population in the best-case scenario, and only 21% in the worst-case scenario (low detection: 65%, $\alpha = 0.25$). We then created the unidentified data set $\dot{y}_J^1$ by aggregating unidentified detections into one vector of length J^1 composed of one when at least one detection was collected, and zero if no detection occurred at detector j.

We generated 50 data sets for each set of parameters before fitting all four models (Appendix S1) to each. We fitted all models to the simulated data using NIMBLE (version 0.6-9, de Valpine et al. 2017) and R (version 3.5.2, R Development Core Team 2018). We drew from three chains, 15,000 MCMC samples each, and the initial 5,000 samples were discarded as burn-in. We assessed convergence using the potential scale reduction value for all parameters and by inspecting the mixing of the chains using trace-plots (Brooks and Gelman 1998). We performed a frequentist validation of our Bayesian model and evaluated its performance by checking the relative bias (RB) of the mode of the posterior distribution, the coefficient of variation (CV) and the coverage of the 95% credible intervals of N and σ (Walter and Moore 2005).

Himalayan brown bear in northern Pakistan

The development of the MOP SCR model was originally motivated by our intent to estimate abundance of Himalayan brown bears in northern Pakistan's Deosai National Park. The bear population of Deosai was monitored across an area of 2,262 km^2 through both noninvasive DNA-sampling (survey type 1; consisting of both identified and unidentified observations) and camera trapping (survey type 2; only unidentified observations) from 23 September to 9 November 2012. This data set is a good example of the different challenges faced by surveys of rare and elusive species, due to remoteness, high elevation, and imposing logistic challenges. To highlight the benefits of data integration for a case study, we fitted the same four models to the bear data and compared estimates of parameters N and σ (see Appendix S2 for a detailed description of the data collection and analysis).

Results

Simulations

Of the 7,200 simulation runs, 6,478 converged: 1,487 for model 1, 1,561 model 2, 1,686 model 3 and 1,744 model 4. We considered only these runs in all further analyses (Appendix S3: Table S1). Coverage for both N and σ was nominal in all models (Appendix S3: Table S2). In all simulation scenarios, data integration led to conspicuous improvements in precision and reduced bias in estimates of parameters N and σ (Fig. 2). Gains in precision from data integration increased with decreasing overall detection probability, decreasing proportion of identified detections, and decreasing overlap between individual home ranges. In the situation where data were the most sparse (and gains greatest), i.e., when detectability, identification probability and overlap were low ($\alpha = 0.25$ and $\sigma = 1$), we obtained an 80% CV reduction for N with model 4 (CV(N) = 0.25), compared to model 1 (CV(N) = 1.2). By comparison, the reduction in CV was only 20% (CV$(N)_{\text{Model 4}} = 0.24$ and CV$(N)_{\text{Model 1}} = 0.29$), when detection was high, $\alpha = 0.75$, and $\sigma = 3$. The pattern was similar for σ with up to a 90% CV reduction (CV$(\sigma)_{\text{Model 4}} = 0.2$ and CV$(\sigma)_{\text{Model 1}} = 1.6$) at low detectability, identification probability and overlap to only 30% (CV$(\sigma)_{\text{Model 4}} = 0.16$ and CV$(\sigma)_{\text{Model 1}} = 0.24$) at high detectability, identification probability and overlap.

Similarly, data integration led to a reduction in bias in all scenarios. This effect was greater with decreasing overall detectability, decreasing identification probability, and decreasing overlap between individual home ranges (Fig. 2). For example, the mean relative bias in N obtained with model 4 was 90% smaller (RB$(N)_{\text{Model 4}} = -0.03$) than that of model 1 (RB$(N)_{\text{Model 1}} = -0.4$) when detectability was low, $\alpha = 0.25$, and $\sigma = 1$. By comparison, when detectability was high, $\alpha = 0.75$, and $\sigma = 3$, the reduction in RB was only 20% (RB$(N)_{\text{Model 4}} = -0.04$ and RB$(N)_{\text{Model 1}} = -0.05$). Again, the pattern was similar for σ: 80% reduction in RB (RB$(\sigma)_{\text{Model 4}} = -0.09$ and RB $(\sigma)_{\text{Model 1}} = -0.6$) versus 20% (RB$(\sigma)_{\text{Model 4}} = -0.07$ and RB$(\sigma)_{\text{Model 1}} = -0.09$) at low and high detectability, identification probability and overlap, respectively.

Empirical example: Himalayan brown bear in northern Pakistan

The identified part of the data contained 22 DNA samples from 14 individual bears collected at 19 different locations. Of these, only four individuals were detected more than once (one detected four times; two detected three times, and one detected two times). Our data set included an additional 21 bear DNA samples lacking individual identification. The camera trap data contributed an additional eight camera trap locations where bears were detected at least once. Using the MOP model (model 4), we estimated the mode of brown bear density at 22 bear/1,000 km^2 (95% CI = 14–30) and the spatial scale parameter σ at 3.2 km (95% CI = 2.1–5). The point estimates produced by the four models were similar (Fig. 3, Table S2). However, data integration in the model 4 led to pronounced improvements in the precision of bear population size (up to 30% reduction in standard deviation [SD]) and space-use parameter estimates (up to 40% reduction in SD), compared to model 1 (Appendix S2).

Discussion

In both simulations and empirical analyses, data integration led to more reliable estimates, i.e., increased precision and reduced bias. We used a frequentist validation of our Bayesian modeling approach, and our simulation study confirmed that the MOP model reliably and precisely estimated density and space-use when using additional information from unidentified observations and multiple survey types. This has direct implications for inferences in real-life, where the integration of auxiliary data, if available, can mitigate the problems associated with data sparsity. We were also able to identify under which conditions the benefits of integration were most substantial.

1.. Low detectability; the lower the proportion of individuals detected, the higher the relative importance of any additional information. When very few individuals are detected, even a single unidentified detection far away from all other detections contains valuable information as it most likely originated from a previously undetected individual.
2.. Minimal home range overlap; the certainty with which the integrated model associates an unidentified detection to a given individual (and therefore the precision of N) increases as the overlap between individual home ranges decreases (Efford and Hunter 2018). When individual detections are well segregated, an unidentified sample will be assigned with a high level of certainty to the closest individual, or, if no individuals were detected in proximity, to a new individual. This should prove particularly useful for territorial species or low-density populations where individual detections minimally overlap, i.e., many of the species commonly studied using SCR models (e.g., Gopalaswamy et al. 2012, Sollmann et al. 2013*b*).
3.. High proportion of unidentified detections; SCR models that ignore unidentified detections risk ignoring a substantial source of information. Although less informative, unidentified detections can still inform about the spatial configuration of individuals, i.e., density, thus reducing the bias and uncertainty around both the scale parameter and population size. This is particularly pronounced under simulated scenarios where only a small percentage of the detections can be assigned to individuals. Conversely, when overall detection and

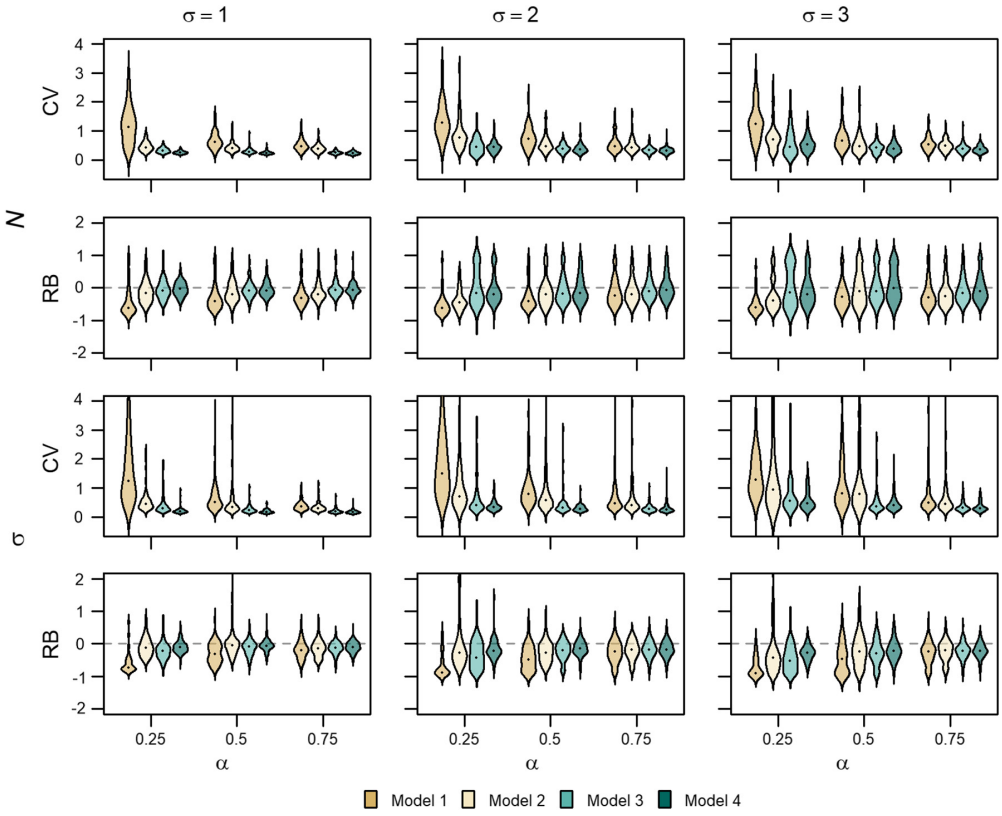

FIG. 2. Violin plots show coefficient of variation (CV) and relative bias (RB) of population size (*N*) and spatial scale parameter of the detection function (σ), under the low detectability scenario for different levels of home-ranges overlap (higher σ = higher overlap) and identification (α). Points indicate medians.

identification is high, the gains from integration of additional data from unidentified detections are minimal. In such cases, the benefits of data integration are likely outweighed by its cost, namely increased model complexity and computation time.

Despite employing both camera trapping and noninvasive DNA sampling, monitoring data of brown bears in our study area remained sparse. Furthermore, only 50% of DNA samples were attributable to individuals and none of the camera trap photos. Integration (including DNA samples without individual identity and camera trap photos), led to improvements in the precision of bear population size and space-use parameter estimates, compared to solely using identified DNA samples. Furthermore, data integration increased the spatial coverage of detectors and detections, which boosted the spatial detail and extent of the model-derived realized density surface (Appendix S2: Fig. S1).

The MOP model is an SCR model that integrates any number of additional survey methods that produce spatially explicit observation data, regardless of whether these methods yield individually identifiable observations or not. Unmarked SCR models that use only unidentified detections are known to have identifiability issues unless an informative prior is used (e.g., Chandler and Royle 2013, Ramsey et al. 2015) or additional data contribute information about individual space-use (e.g., telemetry data in Sollmann et al. 2013*a*). Informative priors can also be used in the MOP model, but even without them, the space-use parameter becomes directly estimable by integrating a proportion of data with identified detections. The MOP model can also allocate undesignated detections to marked or unmarked individuals. This is particularly important when survey method yields observations within which mark status is independent of identification status (e.g., noninvasive DNA sampling).

The observation model of the MOP could also be reformulated as a Poisson counting process (Borchers and Fewster 2016). In this situation, estimates are likely to be even more precise due to increased information in count

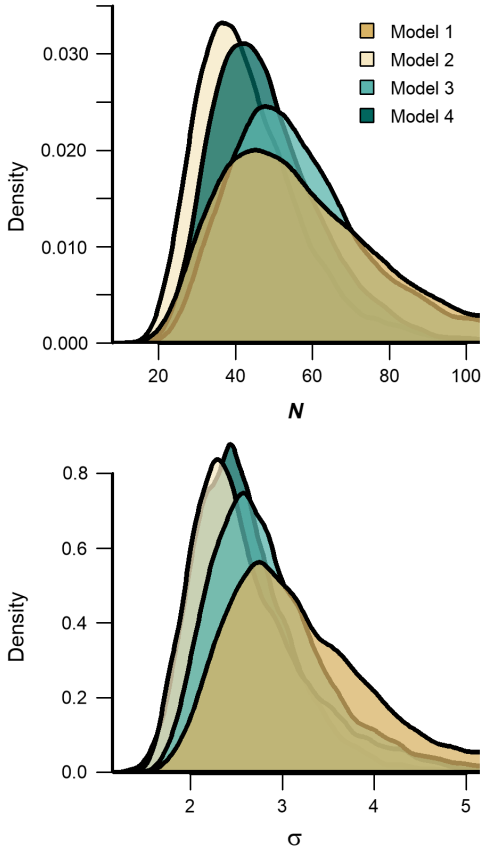

FIG. 3. Posterior densities of the population size (N) and spatial scale (σ) estimates from the four models for the brown bear population in Deosai National Park, Pakistan (see also Fig. 1).

data compared to binary data. Here, we used a Bernoulli observation model because the data collection procedure did not allow us to consider multiple samples collected at the same location as independent. This is also true of many studies that use hair-snares to collect DNA samples without a way to designate samples to separate visits of an individual at a given detector. Each observation process in our model can be re-formulated to include partial/uncertain identification (Augustine et al. 2019) upon availability of such data.

Of the models tested here, the MOP model makes the best use of noninvasive monitoring data. By informing model parameters that are shared between observation processes, it may help fitting SCR models that otherwise would have failed to converge and return reliable estimates. The assumption of a shared σ between detection processes always holds for identified and unidentified detections coming from the same data collection scheme. In cases of survey type-specific σ, the link between detection processes is broken and the CR data can only be integrated with unidentified detections as in integration of CR and occupancy (Blanc et al. 2014).

Although it is often assumed that reducing sample size will lead to decreased precision without introducing bias, this is clearly not the case when using sparse data, as we have shown here, where negative bias in parameter estimates was typical when true population size was small. By discarding detections with uncertain individual identity, investigators may inadvertently risk obtaining biased estimates. In addition, our observation of negative bias in estimates of N in all models when the σ estimate was biased upwards should be investigated rigorously. This pattern could be associated with identifiability issues (Lele et al. 2010, Ponciano et al. 2012) and further research on this topic for SCR models is greatly needed.

The MOP model can also be adjusted to accommodate other extensions of the SCR framework, such as covariates on focal parameters (Borchers and Fewster 2016), non-Euclidean distances (Royle et al. 2018), or it can be re-formulated as an open population SCR model to incorporate population dynamics (Bischof et al. 2016). Finally, we emphasize that, while the incorporation of multiple observation processes can help mitigate the challenges brought on by data sparsity, this does not diminish the necessity for appropriate survey design, lest investigators are to draw erroneous inferences.

Acknowledgments

The study in Deosai National Park was funded by the Norwegian Research Council grants 204202/F20 and 286886 (project WildMap). We thank Snow Leopard Foundation biologists, field staff, and national park rangers for assisting in data collection and E. Bellemain for genetic analysis. We thank C. Milleret, E. Moqanaki, and J. D. Chipperfield for fruitful discussions. We thank the subject matter editor and four anonymous reviewers for their comments on the previous draft of this article. The authors declare no conflicts of interest. R. Bischof conceived the idea of integrating multiple sources of information in SCR framework. M. Tourani and R. Bischof developed the concept and methodology. R. Bischof and M. A. Nawaz coordinated and implemented field data collections. M. Tourani led the analysis and wrote the manuscript with contributions from R. Bischof and P. Dupont. All authors provided revisions to scientific content of the manuscript and gave final approval for publication.

Literature Cited

Augustine, B. C., J. A. Royle, S. M. Murphy, R. B. Chandler, J. J. Cox, and M. J. Kelly. 2019. Spatial capture–recapture for categorically marked populations with an application to genetic capture–recapture. Ecosphere 10:e02627.

Besbeas, P., S. N. Freeman, B. J. T. Morgan, and E. A. Catchpole. 2002. Integrating mark-recapture-recovery and census data to estimate animal abundance and demographic parameters. Biometrics 58:540–547.

Bischof, R., H. Brøseth, and O. Gimenez. 2016. Wildlife in a politically divided world: Insularism inflates estimates of brown bear abundance. Conservation Letters 9:122–130.

Blanc, L., E. Marboutin, S. Gatti, F. Zimmermann, O. Gimenez, and H. McCallum. 2014. Improving abundance estimation by combining capture-recapture and occupancy data: example with a large carnivore. Journal of Applied Ecology 51:1733–1739.

Borchers, D. L., and M. G. Efford. 2008. Spatially explicit maximum likelihood methods for capture-recapture studies. Biometrics 64:377–385.

Borchers, D. L., and R. M. Fewster. 2016. Spatial capture–recapture models. Statistical Science 31:219–232.

Brooks, S. P., and A. Gelman. 1998. General methods for monitoring convergence of iterative simulations. Journal of Computational and Graphical Statistics 7:434–455.

Burgar, J. M., F. E. C. Stewart, J. P. Volpe, J. T. Fisher, and A. C. Burton. 2018. Estimating density for species conservation: Comparing camera trap spatial count models to genetic spatial capture-recapture models. Global Ecology and Conservation 15:e00411.

Chandler, R. B., and J. A. Royle. 2013. Spatially explicit models for inference about density in unmarked or partially marked populations. Annals of Applied Statistics 7:936–954.

Clare, J., S. T. Mckinney, J. E. Depue, and C. S. Loftin. 2017. Pairing field methods to improve inference in wildlife surveys. Ecological Applications 27:2031–2047.

de Valpine, P., D. Turek, C. J. Paciorek, C. Anderson-Bergman, D. T. Lang, and R. Bodik. 2017. Programming with models: writing statistical algorithms for general model structures with NIMBLE. Journal of Computational and Graphical Statistics 26:403–413.

Efford, M. G. 2004. Density estimation in live-trapping studies. Oikos 106:598–610.

Efford, M. G., D. K. Dawson, and D. L. Borchers. 2009. Population density estimated from locations of individuals on a passive detector array. Ecology 90:2676–2682.

Efford, M. G., and C. M. Hunter. 2018. Spatial capture-mark-resight estimation of animal population density. Biometrics 74:411–420.

Gerber, B. D., J. S. Ivan, and K. P. Burnham. 2014. Estimating the abundance of rare and elusive carnivores from photographic-sampling data when the population size is very small. Population Ecology 56:463–470.

Gopalaswamy, A. M., J. A. Royle, M. Delampady, J. D. Nichols, K. U. Karanth, and D. W. W. Macdonald. 2012. Density estimation in tiger populations: combining information for strong inference. Ecology 93:1741–1751.

Lele, S., R. K. Nadeem, and B. Schmuland. 2010. Estimability and likelihood inference for generalized linear mixed models using data cloning. Journal of the American Statistical Association 105:1617–1625.

Lukacs, P. M., and K. P. Burnham. 2005. Review of capture-recapture methods applicable to noninvasive genetic sampling: review of DNA-based capture-recapture. Molecular Ecology 14:3909–3919.

Marques, T. A., L. Thomas, and J. A. Royle. 2011. A hierarchical model for spatial capture-recapture data: comment. Ecology 92:526–528.

Murphy, S., B. Augustine, J. R. Adams, L. P. Waits, and J. J. Cox. 2018. Integrating multiple genetic detection methods to estimate population density of social and territorial carnivores. Ecosphere 9:e02479.

Ponciano, J. M., J. G. Burleigh, E. L. Braun, and M. L. Taper. 2012. Assessing parameter identifiability in phylogenetic models using data cloning. Systematic Biology 61:955–972.

R Development Core Team. 2018. R: a language and environment for statistical computing. R Foundation for Statistical Computing, Vienna, Austria. https://www.R-project.org/

Ramsey, D. S. L., P. A. Caley, and A. Robley. 2015. Estimating population density from presence-absence data using a spatially explicit model. Journal of Wildlife Management 79:491–499.

Rich, L., M. J. Kelly, R. Sollmann, A. J. Noss, L. Maffei, R. L. Arispe, A. Paviolo, C. D. De Angelo, Y. E. Di Blanco, and M. S. Di Bitetti. 2014. Comparing capture-recapture, mark-resight, and spatial mark-resight models for estimating puma densities via camera traps. Journal of Mammalogy 95:382–391.

Royle, J. A., R. B. Chandler, R. Sollmann, and B. Gardner.2013. Spatial capture-recapture. Academic Press, Cambridge, Massachusetts, USA.

Royle, J. A., R. M. Dorazio, and W. A. Link. 2007. Analysis of multinomial models with unknown index using data augmentation. Journal of Computational and Graphical Statistics 16:67–85.

Royle, J. A., A. K. Fuller, and C. Sutherland. 2018. Unifying population and landscape ecology with spatial capture-recapture. Ecography 41:444–456.

Sollmann, R., B. Gardner, and J. L. Belant. 2012. How does spatial study design influence density estimates from spatial capture-recapture models? PLoS ONE 7:e34575.

Sollmann, R., B. Gardner, A. W. Parsons, J. J. Stocking, B. T. McClintock, T. R. Simons, K. H. Pollock, and A. F. O'Connell. 2013*a*. A spatial mark–resight model augmented with telemetry data. Ecology 94:553–559.

Sollmann, R., N. M. Tôrres, M. M. Furtado, A. T. de Almeida Jácomo, F. Palomares, S. Roques, and L. Silveira. 2013*b*. Combining camera-trapping and noninvasive genetic data in a spatial capture–recapture framework improves density estimates for the jaguar. Biological Conservation 167:242–247.

Walter, B. A., and J. L. Moore. 2005. The concepts of bias, precision and accuracy, and their use in testing the performance of species richness estimators, with a literature review of estimator performance. Ecography 28:815–829.

Whittington, J., M. Hebblewhite, and R. B. Chandler. 2018. Generalized spatial mark–resight models with an application to grizzly bears. Journal of Applied Ecology 55:157–168.

Supporting Information

Additional supporting information may be found in the online version of this article at http://onlinelibrary.wiley.com/doi/10.1002/ecy.3030/suppinfo

Data Availability

An associated R script is available on Zenodo: http://doi.org/10.5281/zenodo.3647866.

Appendix S1: Model definitions in NIMBLE

Model 1 is the basic SCR using identified detections e.g., DNA samples with individual genotypes. Model 2 integrates identified and unidentified detections of the same detector type. Model 3 integrates identified detections of one detector type, with unidentified detections of the second detector type and model 4 integrates all available data including identified detections of one detector type with unidentified detections of two survey methods. An example R script is available: `https://zenodo.org/badge/latestdoi/192947256` to go through the model fitting process on simulated data sets.

```
Model_1 <- nimbleCode({

    ## AC LOCATIONS
    for (i in 1:M) {
        sxy[i, 1] ~ dunif(0, x.max)                ##equation(1)
        sxy[i, 2] ~ dunif(0, y.max)
    }

    ## INDIVIDUAL INCLUSION
    psi ~ dunif(0, 1)
    for (i in 1:M) {
        z[i] ~ dbern(psi)                          ##equation(2)
    }

N <- sum(z[1:M])                                   ##equation(3)

    sigma ~ dunif(0, 100)
    p0_1 ~ dunif(0, 1)

    ## IDENTIFIED DETECTIONS, SURVEY TYPE 1
    for (i in 1:M) {
d_squared_1[i, 1:J_1] <-
(sxy[i, 1] - detector.xy_1[1:J_1,1])^2
+ (sxy[i, 2] - detector.xy_1[1:J_1,2])^2

p_1[i, 1:J_1] <-
p0_1 * exp(-d_squared_1[i,1:J_1])/(2*sigma*sigma)) ##equation(4)
##p_1 in model 1 and 3 is equivalent to
##p_1*alpha in model 2 and 4

y_1[i, 1:J_1] ~ dbern_vector(p_1[i, 1:J_1], z[i])  ##equation(6)
    }#i
})
```

```
Model_2 <- nimbleCode({

    ## AC LOCATIONS
    for (i in 1:M) {
        sxy[i, 1] ~ dunif(0, x.max)                ## equation(1)
        sxy[i, 2] ~ dunif(0, y.max)
    }

    ## INDIVIDUAL INCLUSION
    psi ~ dunif(0, 1)
    for (i in 1:M) {
        z[i] ~ dbern(psi)                          ## equation(2)
    }

   N <- sum(z[1:M])                                ## equation(3)
    sigma ~ dunif(0, 100)
    p0_1 ~ dunif(0, 1)
    alpha_1 ~ dunif(0, 1)

    ## SURVEY TYPE 1: IDENTIFIED + UNIDENTIFIED
    for (i in 1:M) {
d_squared_1[i, 1:J_1] <-
(sxy[i, 1] - detector.xy_1[1:J_1,1])^2
+ (sxy[i, 2] - detector.xy_1[1:J_1,2])^2

p_1[i, 1:J_1] <-
p0_1 * exp(-d_squared_1[i,1:J_1])/(2*sigma*sigma))## equation(4)
##p_1 in model 1 and 3 is equivalent to
##p_1*alpha in model 2 and 4

                                                   ## equation(6)
y_1[i, 1:J_1] ~ dbern_vector(p_1[i, 1:J_1] * alpha_1, z[i])

punid_1[i, 1:J_1] <-
p_1[i, 1:J_1] * (1 - alpha_1) * z[i]
    }

    for (j in 1:J_1) {
        pdot_1[j] <-
        1 - prod((1 - punid_1[1:M, j]))            ## equation(5)

    }
    ydot_1[1:J_1] ~ dbern_vector(pdot_1[1:J_1], 1)## equation(7)
   })
```

```
Model_3 <- nimbleCode({

    ## INDIVIDUAL INCLUSION
    ## AC LOCATIONS
    for (i in 1:M) {
        sxy[i, 1] ~ dunif(0, x.max)                ## equation(1)
        sxy[i, 2] ~ dunif(0, y.max)
    }

    psi ~ dunif(0, 1)
    for (i in 1:M) {
         z[i] ~ dbern(psi)                         ## equation(2)
    }

    N <- sum(z[1:M])                               ## equation(3)

    sigma ~ dunif(0, 100)
    p0_1 ~ dunif(0, 1)
    p0_2 ~ dunif(0, 1)

    ## IDENTIFIED DETECTIONS, SURVEY TYPE 1
    for (i in 1:M) {
d_squared_1[i, 1:J_1] <- (sxy[i, 1] - detector.xy_1[1:J_1,1])^2
+ (sxy[i, 2] - detector.xy_1[1:J_1,2])^2

p_1[i, 1:J_1] <-                                   ## equation(4)
p0_1 * exp(-d_squared_1[i,1:J_1])/(2*sigma*sigma))
##p_1 in model 1 and 3 is equivalent to
##p_1*alpha in model 2 and 4

y_1[i, 1:J_1] ~ dbern_vector(p_1[i, 1:J_1], z[i]) ## equation(6)
    }

    ## UNIDENTIFIED DETECTIONS, SURVEY TYPE 2
    for (i in 1:M) {
d_squared_2[i, 1:J_2] <-
(sxy[i, 1] - detector.xy_2[1:J_2,1])^2 + (sxy[i, 2]
- detector.xy_2[1:J_2,2])^2

p_2[i, 1:J_2] <-                                   ## equation(4)
p0_2 * exp(-d_squared_2[i,1:J_2])/(2*sigma*sigma)) * z[i]
    }
```

```
for (j in 1:J_2) {
pdot_2[j] <- 1 - prod((1 - p_2[1:M, j]))          ## equation(5)
    }
    ydot_2[1:J_2] ~ dbern_vector(pdot_2[1:J_2], 1)## equation(7)
 })
```

```
Model_4 <- nimbleCode({

    ## AC LOCATIONS
    for (i in 1:M) {                                    ## equation(1)
        sxy[i, 1] ~ dunif(0, x.max)
        sxy[i, 2] ~ dunif(0, y.max)
    }

    ## INDIVIDUAL INCLUSION
    psi ~ dunif(0, 1)
    for (i in 1:M) {
        z[i] ~ dbern(psi)                               ## equation(2)
    }

    N <- sum(z[1:M])                                    ## equation(3)

    sigma ~ dunif(0, 100)
    p0_1 ~ dunif(0, 1)
    p0_2 ~ dunif(0, 1)
    alpha_1 ~ dunif(0, 1)

    ## SURVEY TYPE 1: IDENTIFIED + UNIDENTIFIED DETECTIONS
    for (i in 1:M) {
d_squared_1[i, 1:J_1] <- (sxy[i, 1] - detector.xy_1[1:J_1,1])^2
+ (sxy[i, 2] - detector.xy_1[1:J_1,2])^2

p_1[i, 1:J_1] <-                                        ## equation(4)
p0_1 * exp(-d_squared_1[i,1:J_1])/(2*sigma*sigma))
##p_1 in model 1 and 3 is equivalent to
##p_1*alpha in model 2 and 4

y_1[i, 1:J_1] ~
dbern_vector(p_1[i, 1:J_1] * alpha_1 , z[i])        ## equation(6)
         punid_1[i, 1:J_1] <-
         p_1[i, 1:J_1] * (1 - alpha_1) * z[i]
    }
    for (j in 1:J_1) {
        pdot_1[j] <-
        1 - prod((1 - punid_1[1:M, j]))                 ## equation(5)
    }
    ydot_1[1:J_1] ~
    dbern_vector(pdot_1[1:J_1], 1)                      ## equation(7)

    ## SUVERY TYPE 2: UNIDENTIFIED DETECTIONS
    for (i in 1:M) {
```

```
d_squared_2[i, 1:J_2] <- (sxy[i, 1] - detector.xy_2[1:J_2,1])^2
+ (sxy[i, 2] - detector.xy_2[1:J_2,2])^2

p_2[i, 1:J_2] <-
p0_2 * exp(-d_squared_2[i, 1:J_2]/
(2*sigma*sigma)) * z[i]                              ## equation(4)
    }
    for (j in 1:J_2) {
     pdot_2[j] <- 1 - prod((1 - p_2[1:M, j]))        ## equation(5)
    }
    ydot_2[1:J_2] ~ dbern_vector(pdot_2[1:J_2], 1)## equation(7)
})
```

Appendix 2: Empirical example - Himalayan brown bear in northern Pakistan

Study system

Himalayan brown bear (*Ursus arctos isabellinus*) has experienced a shrink of its historical range during the past decades (McLellan et al. 2016). Extant populations persist in small and isolated patches, of which the population in Deosai National Park is likely the largest and the only stable one in the western Himalayas (Bellemain et al. 2007, Nawaz et al. 2008). Our 2,262-km^2 study area is an alpine plateau, located between the Himalayan and Karakoram Mountains in northern Pakistan. Details about the study area has been provided elsewhere (Bellemain et al. 2007, Nawaz et al. 2014).

Data collection

Between 23 September and 9 November 2012, non-invasive surveys were conducted by dividing the national park into survey blocks based on watershed boundaries. Search transects followed mainly along trails in each block to collect and store fresh bear feces in 95% ethanol as described in Bellemain et al. (2007). Spatial locations of all fecal samples were recorded by handheld GPS. Camera trapping was conducted simultaneously at 116 stations along the same trails. The procedure is described in detail in Bischof et al. (2014).

DNA analysis

Eleven newly developed tetranucleotide microsatellite loci were used for individual identification (UA03, UA06, UA17, UA25, UA51, UA57, UA63, UA64, UA65, UA67, UA68, De Barba et al. 2017, product size $\leq$117bp) and a sex marker ZFX/Y (Pagès et al. 2009, product size 104bp). Details on lab procedure and error checking is described in De Barba et al. (2017).

Data processing

We overlaid a grid over the sampling area with 2 km spacing between detectors of DNA samples, and considered the centers of grid cells that intersected a search trail as detectors of DNA samples (337 detectors). We then assigned DNA samples

to the nearest detector. We created two detection histories based on this data: (1) detections of individually identified bears by DNA samples, and (2) bear DNA samples without individual ID.

In addition we created a third vector of detection histories composed of detections of any bears at the different camera trap locations (Efford et al. 2009, Borchers and Fewster 2016). Since individual detections might not be independent (e.g. temporal correlation of fecal samples), we avoided accumulating detections of an individual at a given detector in the identified DNA samples data set, but also detections of any bears at detector locations in the unidentified data set, hence detection histories consist of zeros and ones.

We fitted the same four models to the bear data by drawing 30,000 MCMC samples from 3 chains and discarded the initial 5,000 samples from each chain as burn-in. We checked R-hat and mixing of the chains in trace-plots to assess convergence. We compared the precision in estimates of N and σ using standard deviation. Since the true value is unknown, we compared the mode estimates from the four models to evaluate the model performances, and visualized the realized density maps estimated by the four models. To do so, we discretized the habitat and counted the number of individual activity centers falling within each cell for each iteration of the MCMC sampling, thus obtaining a posterior distribution of density for each habitat cell.

The dataset available for model 1 consisted of 22 DNA samples from 14 individual bears, detected at 19 different locations, with 4 individuals captured more than once. When considering DNA samples lacking individual ID, 21 additional bear detections were available for incorporation in models (2) and (4). Of these 21 detections, 5 were collected at locations where an identified individual was also detected and 16 were collected at "new" locations. Including the camera trap data led to an additional 8 locations where a bear was detected at least once for incorporation in models (3) and (4) (out of 116 camera trap locations).

Results

All 4 models converged and yielded estimates of the parameters of interest. Using the MOP model, we estimated brown bear density at 22 bear/1000 km^2 (CI = 14, 30) and the spatial scale parameter σ = 3.2 km (CI = 2.1, 5), which translates into 193 km2 mean home range size for brown bears.

Integrating unidentified detections in all three models yielded more precise N estimates (SD Model 4 = 18.1, Model 3 = 20.6, Model 2 = 20.2), compared to

the model 1 (SD = 25.1). This corresponds to increases in precision of 28%, 18% and 20% respectively. The gain is also pronounced in estimation of parameter σ (Model 4 SD = 0.1, Model 3 = 0.1, Model 2 = 1.1, Model 1 = 1.1). Results are summarized in Table S1.

The maps of realized density from the four models (Fig. S1) provide information about heterogeneity in density across space, and can be useful to direct management efforts. Moreover, the addition of detections from camera trapping allowed to identify a hotspot of bear density in the northern part of the study area, which would have been missed otherwise (Fig. S1).

Table S1: *Parameter estimates (Param) from the four models for brown bear in Deosai National Park. Population size (N), spatial scale parameter (σ; in km), probability of detection by the two survey methods (P_{DNA} and P_{CAM}). Numbers in parentheses indicates 95% CI boundaries of the mode.*

Param	**Model 1**	**Model 2**	**Model 3**	**Model 4**
N	43 (26 - 124)	36 (23 - 102)	47 (30 - 108)	42 (26 - 97)
σ	2.8 (2.0 - 6.2)	2.9 (2.0 - 6.2)	2.5 (1.9 - 4.4)	2.9 (2.1 - 5.0)
P_{DNA}	.03 (.01 - 0.1)	.07 (.03 - 0.2)	.04 (.02 - 0.1)	.09 (.04 - .2)
P_{CAM}	-	-	.06 (.02 - .2)	.06 (.02 - .17)

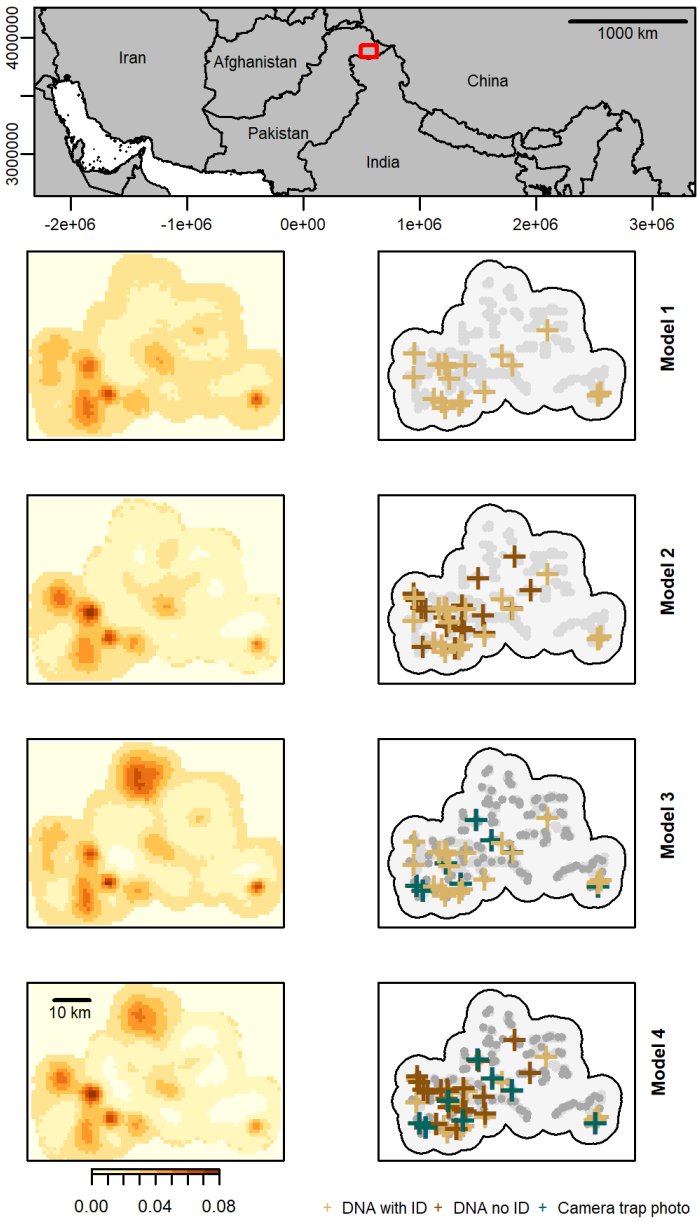

Figure S1: *The upper plot shows the location of Deosai National Park in Pakistan (red square). Plots on the left hand side show maps of estimated density for brown bears in the study area by the four models. Plots on the right show non-invasive monitoring data of brown bears in the study area. Grey dots indicate the location of detectors (light: DNA sampling, dark: camera trapping), yellow, brown and green crosses indicate the locations of identified DNA samples, unidentified DNA samples and unidentified camera trap picture respectively.*

References

Bellemain, E., M. Nawaz, A. Valentini, J. Swenson, and P. Taberlet. 2007. Genetic tracking of the brown bear in northern Pakistan and implications for conservation. Biological Conservation 134: 537-547.

Bischof, R., H. Ali, M. Kabir, S. Hameed, and M. A. Nawaz. 2014. Being the underdog: an elusive small carnivore uses space with prey and time without enemies. Journal of Zoology 293: 40-48.

Borchers, D. L., and R. M. Fewster. 2016. Spatial Capture-Recapture Models. Statistical Science 31: 219-232.

De Barba, M., C. Miquel, S. Lobréaux, P. Y. Quenette, J. E. Swenson, and P. Taberlet. 2017. High-throughput microsatellite genotyping in ecology: Improved accuracy, efficiency, standardization and success with low-quantity and degraded DNA. Molecular Ecology Resources 17(3): 492-507.

Efford, M. G., D. K. Dawson, and D. L. Borchers. 2009. Population density estimated from locations of individuals on a passive detector array. Ecology 90: 2676–2682.

McLellan, B. N., M. F. Proctor, D. Huber, S. and Michel, and I. S. B. S. Group. 2016. Brown Bear (*Ursus arctos*) Isolated Populations (Supplementary Material to *Ursus arctos* Redlisting account). The IUCN Red List of Threatened Species 2016.

Nawaz, M. A., J. Martin, and J. E. Swenson. 2014. Identifying key habitats to conserve the threatened brown bear in the Himalaya. Biological Conservation 170: 198-206.

Nawaz, M. A., J. E. Swenson, and V. Zakaria. 2008. Pragmatic management increases a flagship species, the Himalayan brown bears, in Pakistan's Deosai National Park. Biological Conservation 141: 2230-2241.

Pagès, M., C. Maudet, E. Bellemain, P. Taberlet, S. Hughes, and C. Hänni. 2009. A system for sex determination from degraded DNA: a useful tool for palaeogenetics and conservation genetics of ursids. Conservation Genetics 10: 897-907.

Appendix 3: Simulation results

Table S1: *Number of converged simulation runs under simulated scenarios of detections, individual home range overlap (represented by the scale parameter σ of the detection function) and population size.*

Model	σ	Detectability	Pop. size	#Converged	%Converged
mod1	1	Low	30	113	75
mod2	1	Low	30	134	89
mod3	1	Low	30	143	95
mod4	1	Low	30	149	99
mod1	1	High	30	132	88
mod2	1	High	30	146	97
mod3	1	High	30	149	99
mod4	1	High	30	150	100
mod1	2	Low	30	111	74
mod2	2	Low	30	110	73
mod3	2	Low	30	130	86
mod4	2	Low	30	140	93
mod1	2	High	30	133	89
mod2	2	High	30	141	94
mod3	2	High	30	150	100
mod4	2	High	30	149	99
mod1	3	Low	30	88	59
mod2	3	Low	30	89	59
mod3	3	Low	30	115	76
mod4	3	Low	30	127	85
mod1	3	High	30	130	86
mod2	3	High	30	134	89
mod3	3	High	30	146	97
mod4	3	High	30	149	99
mod1	1	Low	50	130	86
mod2	1	Low	50	141	94
mod3	1	Low	50	146	97
mod4	1	Low	50	150	100
mod1	1	High	50	147	98
mod2	1	High	50	147	98
mod3	1	High	50	150	100
mod4	1	High	50	150	100
mod1	2	Low	50	110	73
mod2	2	Low	50	114	76
mod3	2	Low	50	139	93
mod4	2	Low	50	144	96
mod1	2	High	50	141	94
mod2	2	High	50	146	97
mod3	2	High	50	150	100
mod4	2	High	50	150	100
mod1	3	Low	50	114	76
mod2	3	Low	50	120	80
mod3	3	Low	50	119	79
mod4	3	Low	50	137	91
mod1	3	High	50	138	92
mod2	3	High	50	139	93
mod3	3	High	50	149	99
mod4	3	High	50	149	99

Table S2: *Coverage properties of the 95% credible interval of N and σ across the parameter set. Three levels of overlap are calculated based on density and the scale parameter σ of the detection function, following Efford et al. (2016).*

Sim. set	Model	σ	Overlap	Pop. size	N Coverage	σ Coverage
1	mod1	1	0.14	30	0.9836735	0.9551020
2	mod2	1	0.14	30	0.9928571	0.9571429
3	mod3	1	0.14	30	0.9520548	0.9349315
4	mod4	1	0.14	30	0.9431438	0.9431438
5	mod1	2	0.23	30	0.9918033	0.8032787
6	mod2	2	0.23	30	0.9800797	0.9561753
7	mod3	2	0.23	30	0.9535714	0.9035714
8	mod4	2	0.23	30	0.9619377	0.9377163
9	mod1	3	0.33	30	0.9724771	0.7385321
10	mod2	3	0.33	30	0.9730942	0.8878924
11	mod3	3	0.33	30	0.9463602	0.8237548
12	mod4	3	0.33	30	0.9601449	0.9202899
13	mod1	1	0.11	50	0.9927798	0.9314079
14	mod2	1	0.11	50	0.9895833	0.9479167
15	mod3	1	0.11	50	0.9527027	0.9155405
16	mod4	1	0.11	50	0.9633333	0.9600000
17	mod1	2	0.28	50	0.9840637	0.8286853
18	mod2	2	0.28	50	0.9807692	0.9307692
19	mod3	2	0.28	50	0.9377163	0.8823529
20	mod4	2	0.28	50	0.9591837	0.9285714
21	mod1	3	0.42	50	0.9801587	0.8015873
22	mod2	3	0.42	50	0.9845560	0.9382239
23	mod3	3	0.42	50	0.9701493	0.9067164
24	mod4	3	0.42	50	0.9755245	0.9230769

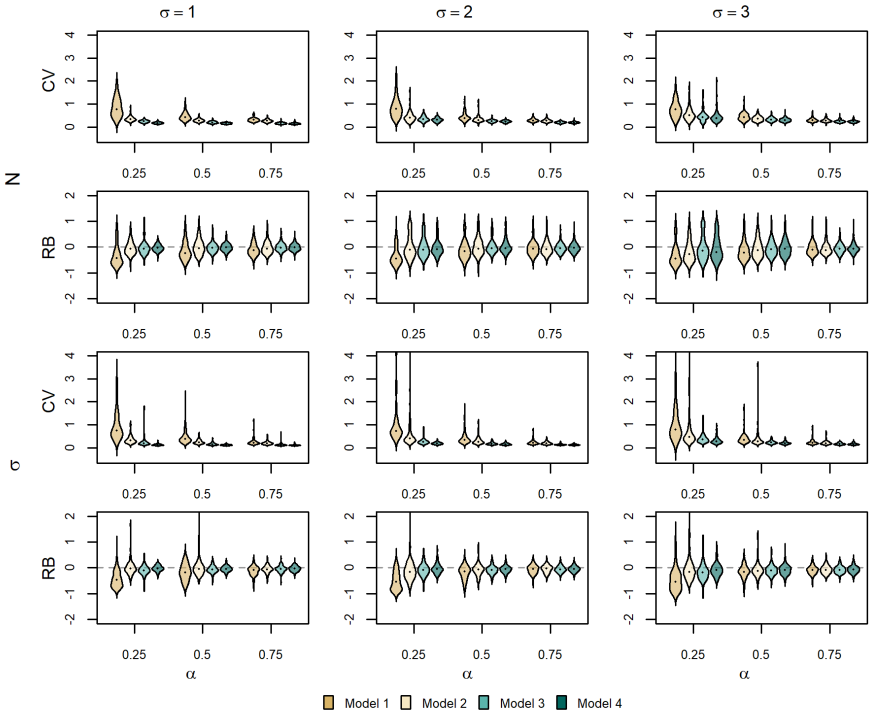

Figure S1: *Coefficient of variation (CV) and relative bias (RB) of population size (N) and spatial scale parameter of the detection function (σ), under the high detectability scenario for different levels of home-ranges overlap (higher σ = higher overlap) and identification (α). The results are shown for both true population sizes of 30 and 50 combined.*

References

Efford M., D. K. Dawson, Y. V. Jhala, and Q. Qureshi. 2016. Density-dependent home-range size revealed by spatially explicit capture–recapture. Ecography 39(7): 676-688.

Article III

Non-invasive genetic sampling reveals landscape-level patterns in wolverine home range size

Mahdieh Tourani[1,*], Pierre Dupont[1], Cyril Milleret[1], Henrik Brøseth[2], and Richard Bischof[1]

1. *Faculty of Environmental Sciences and Natural Resource Management, Norwegian University of Life Sciences, P.O. Box 5003, 1432 Ås, Norway*
2. *Department of Terrestrial Ecology, Norwegian Institute for Nature Research, PB 5685 Torgarden, NO-7485 Trondheim, Norway*

∗ Email: mahdieh.tourani@gmail.com

Abstract. Of perennial interest in ecology is the study of the home range, the area within which an individual does its routine foraging, mating and parenting while avoiding risks. Identifying large-scale correlates of home range size has usually been performed using a patchwork of telemetry studies. Animal welfare, as well as logistic and economic considerations limit the scale at which telemetry studies can be implemented, both in terms of spatial extent and the proportion of the population tracked. Non-invasive monitoring methods, such as genetic sampling, offer opportunities to obtain information about animal space-use at the scale of populations and landscapes. In this study, we analyse non-invasive genetic monitoring data of wolverine (*Gulo gulo*) in Norway using spatial capture-recapture models. We fit sex-specific models and quantify the population-level effects of latitude and elevation on home range size variation at an unprecedented spatial extent (∼266,000 km^2). Male wolverines had on average larger home ranges than females. Our results revealed an interaction between latitude and elevation leading to larger home ranges in both regions of high latitude and low elevation or low

latitude but high elevation. Our model also predicted that this effect was more pronounced for females, leading to larger variation in home range sizes amongst females than males. The biological (population) and spatial (landscape) scale at which non-invasive monitoring allows investigators to operate, could in many cases compensate for the reduced spatiotemporal detail (observations per individual) when compared with contemporary GPS-based telemetry.

Keywords: *Home range, Non-invasive monitoring, Space-use, Spatial capture-recapture, Wolverine*

Introduction

Home range, the area within which an individual does its routine foraging, mating and parenting while avoiding risks (Burt 1943, Börger et al. 2008, Powell and Mitchell 2012), is a fundamental concept in wildlife ecology. It conditions the extent to which individuals of the same species interact with each other, and with their environment (Giuggioli and Kenkre 2014), thus affecting population density and directing conservation or management actions (Doherty and Driscoll 2018, Kennerley et al. 2019).

Telemetry studies yield the crux of our knowledge about the size, configuration, and dynamics of home ranges, and insights have received a drastic boost since the advent of GPS-telemetry (Fuller and Fuller 2012). The latter can provide detailed, fine-grained data on instrumented individuals (Kie et al. 2010). However, although the combined number of animals ever tagged is staggering, resource limitations force most investigations to instrument only a small proportion of animals in any given population or species (Hebblewhite and Haydon 2010). Furthermore, instrumentation relies on physical capture, which can raise concerns about animal welfare (Arnemo et al. 2006, Lindsjö et al. 2019), and make it difficult to obtain a random sample of the population (Hebblewhite and Haydon 2010). Typically, small sample sizes and questionable representativeness pose a challenge to scaling up inferences to populations, landscapes and thus identifying and explaining general patterns (Hebblewhite and Haydon 2010, Morales et al. 2010, Owen-Smith et al. 2010). To circumvent this issue, meta-analyses or reviews based on a patchwork of studies using different monitoring methods, grains, locations and temporal extents have generally been used to yield more fundamental and general insights (Börger et al. 2006, van Beest et al. 2011, Morellet et al. 2013, Ofstad et al. 2016). Such meta-analyses are still limited by the different challenges listed above and our

understanding of animal space-use would greatly benefit from methods that can yield data for population-level exploration.

Non-invasive population monitoring methods are increasingly used in conjunction with hierarchical models to draw population-level inferences about various aspects of populations. Camera trapping, sign surveys, and non-invasive genetic sampling (NGS) have been increasingly employed to collect data over large spatial extents at comparatively low costs (Beja-Pereira et al. 2009, Rodgers and Janečka 2013, Burton et al. 2015). The data are then used to answer questions about population abundance and dynamics (Gardner et al. 2010), spatial processes such as dispersal (Ergon and Gardner 2014, Schaub and Royle 2014) or landscape connectivity (Sutherland et al. 2015, Bischof et al. 2017) among others.

Spatial capture-recapture (SCR) models have emerged as a particularly efficient and popular tool for studying spatial ecological processes using non-invasively collected data (Royle et al. 2018). These models were originally developed to exploit the spatial information contained in repeated detections of individuals at different locations to estimate density and abundance (Efford 2004, Borchers and Efford 2008). However, the SCR-specific observation model explicitly links the probability to detect an individual in space to the distance to its activity centre. In other words, SCR implicitly assumes a model of animal movement around a centre of activity (e.g. home range centre) and can yield information about individual space-use (Efford et al. 2016).

Here, we use non-invasive genetic sampling data in combination with SCR to estimate home range size and its determinants at an unprecedented spatial extent for an elusive large carnivore, the wolverine (*Gulo gulo*). Using the national monitoring data from the entire wolverine range in Norway, we obtain estimates of home range size and corresponding estimates of the magnitude of the effect of extrinsic and intrinsic determinants thereof. Finally, we discuss the novelty and limitations of our results in light of previous telemetry studies that have reported home range size estimates for wolverines from spatially, temporally and demographically disjoint samples from different continents and populations.

Methods

Data

The Scandinavian large carnivore monitoring database (Rovbase 3.0, `http://rovbase.se/` or `http://rovbase.no/`) compiles long-term monitoring data, including NGS data on brown bear *Ursus arctos*, wolf *Canis lupus* and wolverine

across Norway and Sweden. Wolverine NGS data used in this study were collected throughout the Norwegian range of the species by field staff between February and May 2015 (Figs 1-2). Observers conducted structured search-encounter sampling on snow and GPS-recorded the search-tracks and location of samples. A total trail length of 98,779 km was searched during this sampling effort. Genetic analysis was performed on all collected samples. DNA was extracted, and individuals identified using microsatellite genotyping (for a complete description of the genetic analysis see Flagstad et al. (2004) and Bischof et al. (2016b)). As a result, the data consisted of individual identity, sex and location associated with non-invasive wolverine detections.

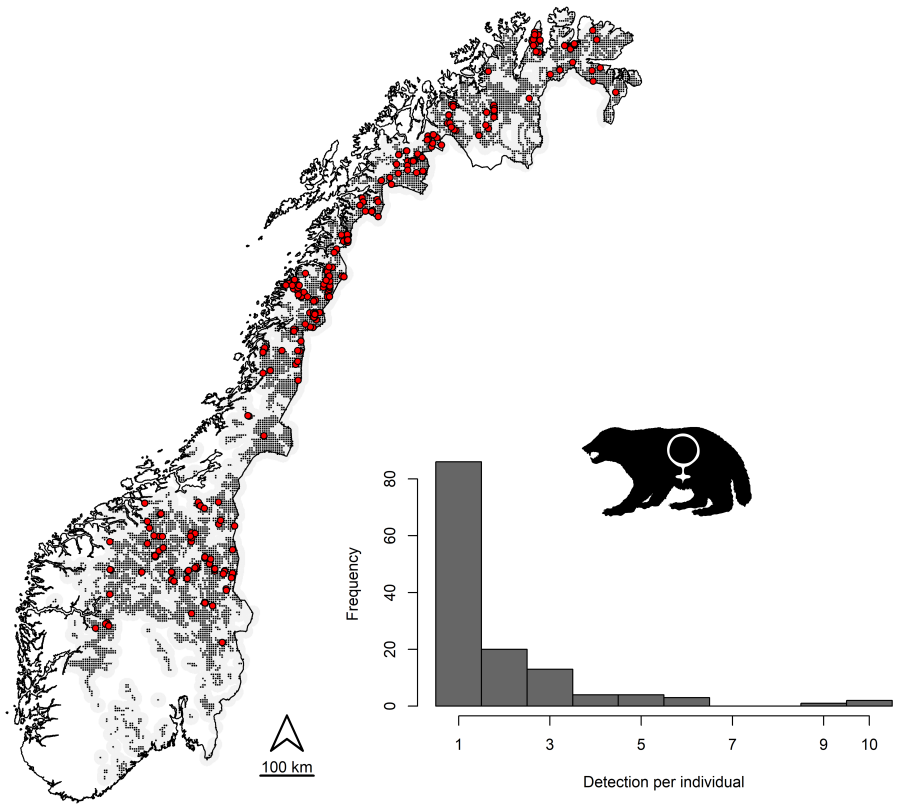

Figure 1: *DNA samples of female wolverines (red circles) collected in Norway (winter 2015). The black dots and grey background outline detectors and the spatial extent included in the analysis (buffer = 13 km), respectively. Only samples included in the analysis are shown. Histogram shows number of detections per individual.*

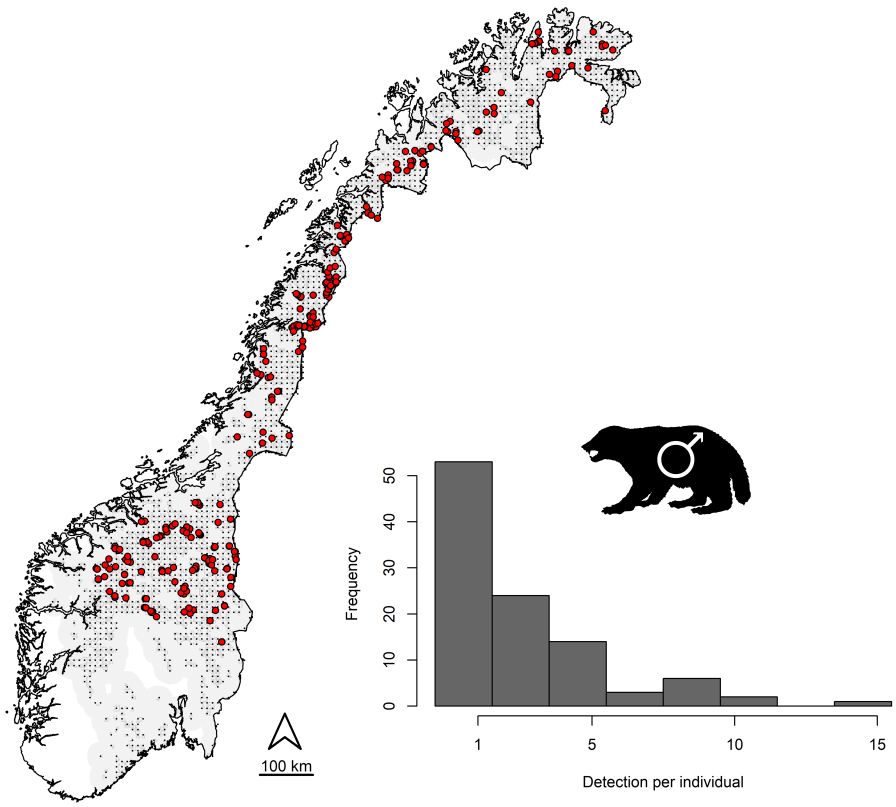

Figure 2: *DNA samples of male wolverines (red circles) collected in Norway (winter 2015). The black dots and grey background outline detectors and the spatial extent included in the analysis (buffer = 25 km), respectively. Only samples included in the analysis are shown. Histogram shows number of detections per individual.*

Analysis

We built an SCR model in a Bayesian framework (Royle et al. 2009) with two hierarchical levels distinguishing the observation process from the ecological process (see Appendix S1 for model script).

i) Ecological process. In SCR models, the location of individuals is defined by their centre of activity or home range centre (s_i). Abundance is then defined as the number of individual activity centres within the region of interest or habitat. Here, we defined the habitat as the area searched for wolverine DNA samples surrounded

by a sex-specific buffer (25 km for males and 13 km for females; Figs 1-2) to account for the possibility to detect individuals that had their activity centre outside of the searched area (Efford 2004). Based on preliminary analysis, we decided to use different buffer sizes for females and males since the choice of buffer depends on space-use (Efford 2011). After removing contiguous non-land and urban areas, the habitat polygon was 251,875 km^2 for females and 266,655 km^2 for males. We subdivided that region into 262,319 and 331,187 1 x 1 km grid cells for females and males, respectively, to define the available habitat used in the analysis (Figs. 1-2). To account for potential variation in wolverine density across the habitat, we modelled the distribution of activity centres as an inhomogeneous Poisson point process (Illian et al. 2008) whose intensity surface was related to the observed wolverine den counts in each habitat grid cell h:

$$log(I_h) = \beta_{dens}.DenCounts_h \tag{1}$$

Where I_h is the point process intensity in habitat grid cell h and β_{dens} is the effect of the number of dens in a given habitat cell on the probability that an individual has its activity centre located in this same cell. We constructed the den counts covariate by applying a smoothing kernel to locations of known dens for wolverines (Fig. 3), which was a multi-year aggregate of yearly counts conducted by authorities in Norway between 2013 and 2018 (May et al. 2012).

To account for the fact that some individuals in the population may never be detected, we used a data-augmentation approach (Royle et al. 2007). We derived estimates of population size N by summing the number of individuals included in the population, where M is an arbitrary value, larger than the true population size.

$$N = \Sigma_{i=1}^{M} z_i \tag{2}$$

We modelled individual inclusion in the population through a latent state variable z_i, governed by the inclusion parameter Ψ for all individuals i in 1:M as:

$$z_i \sim Bernoulli(\Psi) \tag{3}$$

ii) Observation process. The SCR observation component models how individual detection probability varies over a set of detectors. Detectors can stand for fixed devices, such as camera traps, hair snares and physical traps, or they can be search transects (Efford et al. 2009, Royle et al. 2011). Here, we generated detector locations by discretizing the search area into 6,975 grid cells of size 4 x 4 km for females and 1,783 cells of size 10 x 10 km for males (Figs 1-2). We

differentiated between the female and male setup based on preliminary analysis to make sure several detectors were available within home ranges of both female and male wolverines. To retain as much information from the collected NGS data as possible, we used the partially aggregated binomial model (Milleret et al. 2018) and further divided each detector grid cell into 16 sub-cells (or less if some sub-cells did not overlap the suitable habitat). We then generated individual spatial detection histories by retrieving the frequency of sub-cells with at least one NGS sample from the focal individual for each detector main grid cell.

The SCR detection process is closely linked with the home-range concept as the probability of detecting an individual at a given detector is modelled as a decreasing function of the distance between this individual's centre of activity and the detector considered (Fig. 4). Implicit in this model of detection probability in space is the idea that an individual's detection pattern reflects its underlying space-use pattern across its home range. Hence, it becomes possible to use the SCR framework to study individual space-use and home ranges. The most common detection function used in SCR models is the half-normal (Royle et al. 2014; Fig. 4), which implies an isotropic normal home-range shape:

$$p_{ij} = p_0.e^{-d_{ij}^2/2\sigma^2} \tag{4}$$

Where p_{ij} is the detection probability of individual i at detector j, p_0 is the baseline detection probability, d_{ij} is the distance between the individual's activity centre and detector j and σ is the scale parameter which dictates how fast the detection probability decays with distance (i.e. related to home range size; Fig. 4). It is then possible to calculate the 95% kernel home range size based on σ:

$$HR_{0.95} = \pi(\sigma\sqrt{5.99})^2 \tag{5}$$

The value 5.99 comes from the 95% quantile value of a Chi-square distribution with 2 degrees of freedom (Royle et al. 2014). To study the variation in wolverine home range sizes across Norway, we considered effects of elevation and latitude (Fig. 3) and their interaction on σ in a log-linear model:

$$log(\sigma_i) = \sigma_0 + \beta_{elev}.Elevation_{s_i} + \beta_{lat}.Latitude_{s_i} + \beta_{int}.Elevation_{s_i}.Latitude_{s_i} \tag{6}$$

We created elevation and latitude covariates using Shuttle Radar Topographic Mission (SRTM) maps downloaded at 1 x 1-km resolution. All spatial covariates were resampled, smoothed using a smoothing kernel as depicted in Fig. 3, and standardised before being used in the analyses.

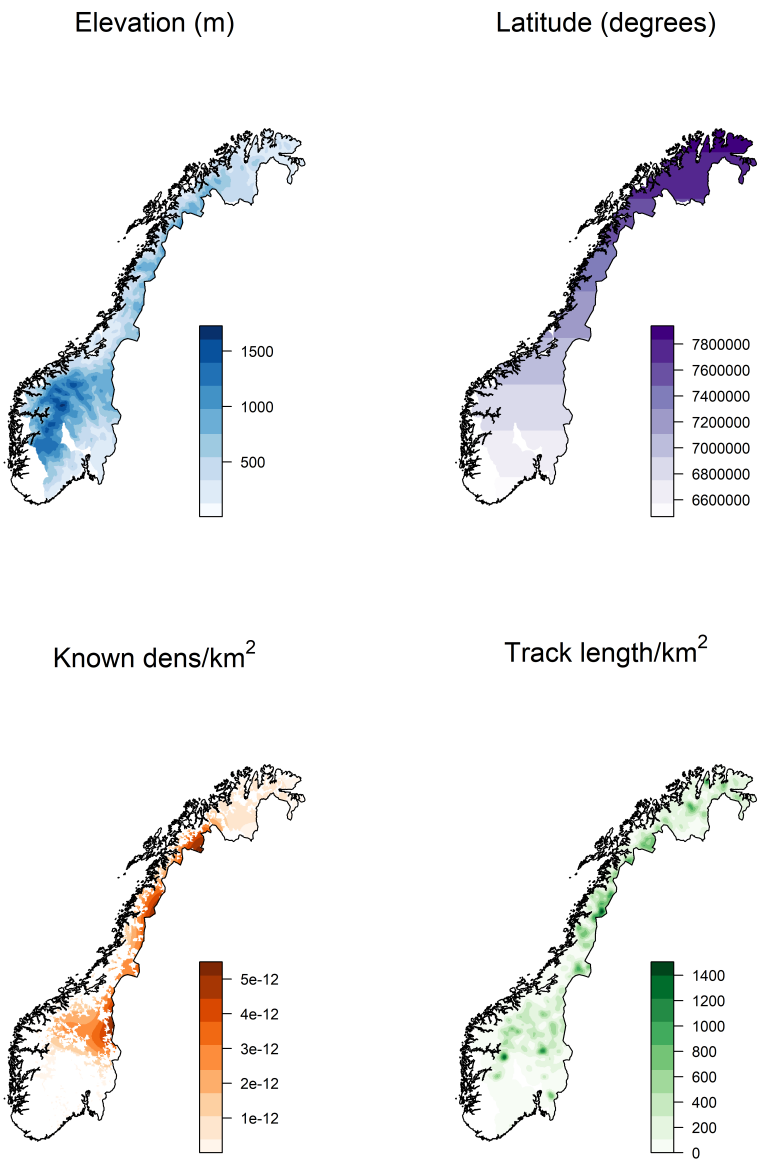

Figure 3: *Spatial covariates included to model variation in wolverine home range size (scale parameter of detection function, σ; elevation and latitude), placement of activity centres (den counts per habitat pixel as derived by applying smoothing kernel to location of known dens for wolverines), and detection probability (p; lengths of search tracks) in Norway.*

The novelty of this model is that the latent location of an individual's activity centre s_i is used to extract the value of the corresponding spatial covariates (Fig. 3) thus producing a spatially explicit model of wolverine home range sizes across the entire habitat used in the analysis.

We considered a negative covariance structure between p_0 and σ, so that their reciprocal variation results in a constant effective sampling area A_0 (Borchers and Efford 2008, Efford and Mowat 2014).

$$p_{0i} = 1 - exp(-(A_0/2\pi\sigma_i^2)) \tag{7}$$

This formulation implies a negative covariance between p_0 and σ, whereby the expected number of detections does not change for varying levels of σ.

In addition, we included the length of search tracks (Fig. 3) within each detector grid cell as a logit linear covariate on p_0 to account for the variation in detectability related to the variation in search intensity. $P_{0_{ij}}$ is the baseline detection probability for a given individual i and detector j.

$$logit(P_{0_{ij}}) = p_{0_i} + \beta_{tracks}.Tracks_j \tag{8}$$

iii) Model fitting. We fitted separate models for males and females to minimize computational challenges associated with the analysis of such large datasets, with large spatial extent and at high resolution. In addition, we used a local evaluation approach (Milleret et al. 2019) to enable the fitting of our SCR models at the country scale. This method reduces the number of calculations performed by the Markov chain Monte Carlo (MCMC) algorithm by removing unnecessary evaluations of the likelihood whenever the distance between a detector and a predicted individual home range centre is larger than an arbitrary distance threshold (37 km for females and 30 km for males). The distance threshold is decided based on maximum distance of individual detections in the data

We fitted the two models using NIMBLE version 0.6-9 (de Valpine et al. 2017) and R (version 3.5.2, R Development Core Team 2018). We ran four chains of 15,500 iterations each and discarded the first 1,000 samples as burn-in, leading to a total of 58,000 MCMC samples per model to draw inferences from. We assessed convergence by looking at the potential scale reduction value for all parameters and mixing of the chains using trace-plots (Brooks and Gelman 1998).

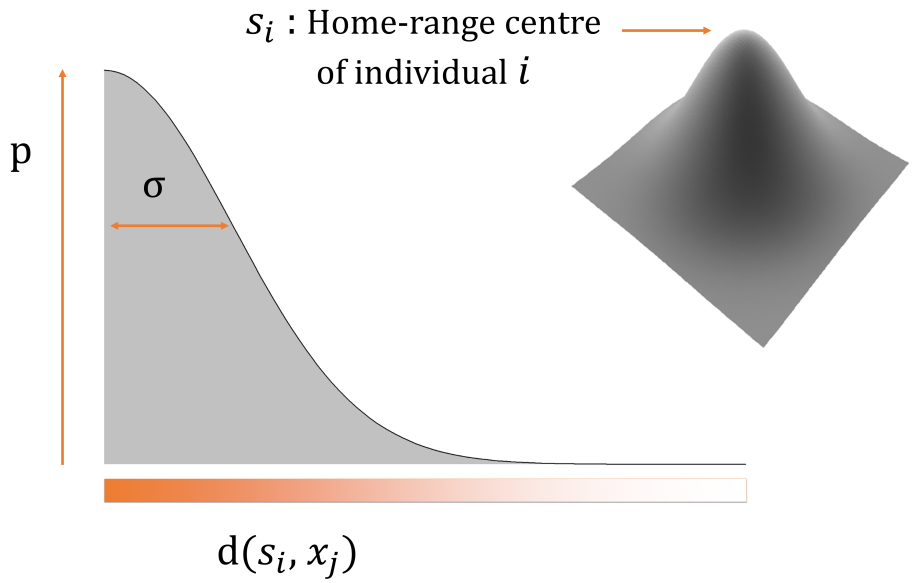

Figure 4: *Half-normal detection function describing the decrease in detection probability (p) with increasing distance (d) between the activity centre location (s_i) and detector location (x_j). σ is the spatial scale parameter of the detection function.*

Results

The data consisted of 325 detections of 103 males and 317 detections of 128 female wolverines across Norway (mean number of detections per individual = 2 for females and 3 for males). The Norwegian wolverine population size was estimated at 523 (322 females, 95% Credible intervals = 270 to 382 and 201 males, 95% CI = 170 to 236) for the winter of 2015 (Table 1). Wolverine abundance in Norway was positively associated with the number of dens reported both for females ($\varphi\beta_{dens}$ = 0.4, 95% CI = 0.2 to 0.6) and for males ($\sigma\beta_{dens}$ = 0.4, 95% CI = 0.25 to 0.65). The baseline detection probability was positively associated with the length of GPS tracks recorded ($\varphi\beta_{tracks}$ = 0.4, 95% CI = 0.3 to 0.5, $\sigma\beta_{dens}$ = 0.36, 95% CI = 0.24 to 0.48).

The average scale parameter of the detection function σ_0 differed between males and females, with male σ_0 being twice as large as that of females ($\varphi\sigma_0$ = 4.1, 95% CI = 3.4 to 4.8 and $\sigma\sigma_0$ = 7.8, 95% CI = 6.5 to 9.5). These σ_0 values translate to average home range sizes of 316 km^2 (95% CI = 218 to 434) and 1,145 km^2 (95% CI = 795 to 1,699) for females and males, respectively.

We detected an interaction between the effects of latitude and elevation. At average elevation, latitude had a positive effect on σ_0 and thus home range size for both females and males ($\varphi\beta_{Latitude}$ = 0.4, 95% CI = 0.2 to 0.6, $\sigma^{\male}\beta_{Latitude}$ = 0.2, 95% CI = 0.1 to 0.4). At below-average elevation the positive effect of latitude on home range size becomes more pronounced (Fig. 5, Table 1). This pattern reversed at above-average elevation; home range size decreases with latitude for sites at high elevation (Fig. 5, Table 1). The pattern is qualitatively similar, although less pronounced for males.

Table 1: *Posterior estimates of model parameters from spatial capture-recapture models for female and male wolverines. N: abundance; A_0: effective sampling area; Ψ: the inclusion parameter; and β coefficients show effects of elevation (β_{elev}), latitude (β_{lat}), and their interaction (β_{int}) on the scale parameter (σ), effect of length of search tracks (β_{tracks}) on detection probability, and effect of known den counts of wolverine (β_{dens}) on placement of individual activity centres. The 95% credible interval (CI) for the effects that did not overlap zero are shown in bold.*

Parameters	**Female**		**Male**	
	mean	**95%CI**	**mean**	**95%CI**
N	322	270 - 382	201	170 - 236
A_0	3.0	2.5 - 3.7	21.2	17.3 - 25.8
β_{elev}	0.04	–0.1 - 0.2	0.2	–0.02 - 0.3
β_{int}	–0.6	**–0.7 - –0.5**	–0.1	–0.3 - 0
β_{dens}	0.4	**0.2 - 0.6**	0.5	**0.3 - 0.7**
β_{lat}	0.4	**0.2 - 0.6**	0.2	**0.05 - 0.4**
β_{tracks}	0.3	**0.3 - 0.5**	0.4	**0.3 - 0.5**
Ψ	0.5	0.4 - 0.6	0.4	0.3 - 0.5
σ_0	4.1	3.4 - 4.9	7.8	6.5 - 9.5

Discussion

Using solely NGS data, we were able to quantify the variation in wolverine home range size and revealed patterns related to sex, latitude and elevation across the entire species' range in Norway. Our results confirmed that on average, male wolverines had substantially larger home ranges than females. Under average conditions of latitude and elevation, home range size was estimated at 301 km^2 for females and 1,116 km^2 for males. This sex-difference in home range size is consistent with previous studies on wolverines (Hedmark et al. 2007), and carnivores in general. In solitary carnivores, males are not involved in parental care, hence their reproductive success is mostly defined by their access to mates, rather than

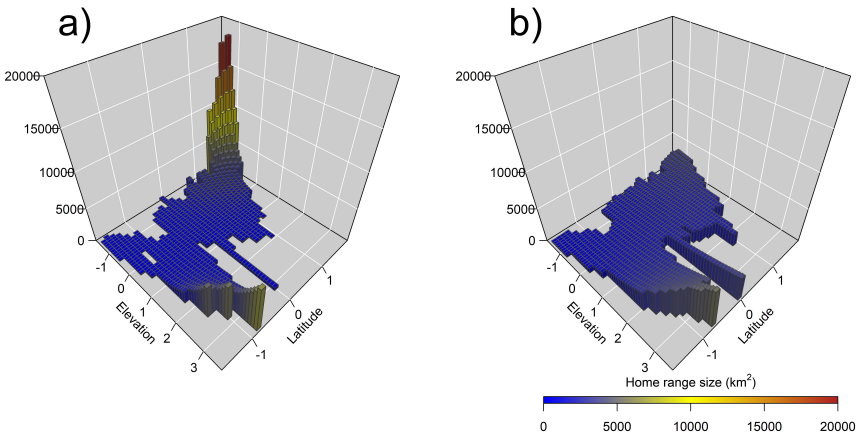

Figure 5: *Sex-specific predictions of home range size for wolverines in Norway (February-May 2015) based on the posterior estimates of parameters σ (the scale parameter of half-normal detection function) and interaction effect of latitude and elevation in the spatial capture-recapture analysis. Note the substantial variation in female home range (a) compared to males (b). Inferences for extreme combination of elevation and latitude should proceed with caution, as indicated by unrealistically high values of home range size (especially for females). These are likely a result of low sample size for these predictor combinations and overly simplistic assumption of linearity of effects.*

food acquisition (Aronsson and Persson 2018, Graw et al. 2019). Males generally have larger home ranges that overlap with one or more of females (Landa et al. 1998, Persson et al. 2010, Inman et al. 2012, Bischof et al. 2016b).

Although larger home range sizes have been reported in North America (Copeland 1996: female 384 km^2, male 1582 km^2; Dawson et al. 2010: female 428 km^2, male 2,563 km^2), the absolute values of home range sizes estimated in our study are larger than previously reported in Scandinavia (Landa et al. 1998: female 274 km^2, male 663 km^2; Persson et al. 2010: female 170 km^2, male 669 km^2; Mattisson et al. 2011: female 195 km^2 and male 733 km^2) and other North American studies (e.g. Inman et al. 2012: female 303 km^2; male 797 km^2). There are several potential explanations for the discrepancy between our estimates and smaller home ranges estimated elsewhere. First, the DNA-based data accessible for this study did not allow us to distinguish between age classes and our estimates are based on the overall population. Sub-adult wolverines have larger home ranges compared to resident adults (Inman et al. 2012). Second, we assumed a bivariate normal distribution in the detection probability model that results in circular home ranges. This assumption might be an over-simplification of movement of individuals in

structured landscapes (Sutherland et al. 2015).

Population parameters estimated in this study (i.e. N and σ) are different from the ones reported by Bischof et al. (2019b). First, because of the type of data used; the present study only includes faecal DNA from structured searches, whereas Bischof et al. (2019b) incorporated dead recoveries and opportunistic samples. In addition, the spatial extent of the two studies varies, as we limited the models to one country, and reported estimates for total spatial extent including the buffer area, but Bischof et al. (2019b) provide estimates for the transboundary population in Norway and Sweden. Second, because of the model type; Bischof et al. (2019b) used an open-population SCR, with covariates on detection probability but no covariate on the scale parameter, whereas the present study is a model of closed-population SCR with den counts covariate on population size and covariates on sigma (see Table 1).

Using the latent location of individual activity centres, we extracted the values of the spatial covariates and were able to describe the spatial variation in wolverine home range size with latitude and elevation at the population level. At this scale, observed patterns in home range size result from processes occurring over relatively long ecological time periods, over generations (e.g. density) or geological time (e.g. climate). Both latitude and elevation can be considered as proxies for climate and as such, were expected to influence home-range size. Climate can be an indirect determinant of home range size through its influence on primary productivity, and seasonality (Nilsen et al. 2005, Saïd et al. 2009). For example, red foxes (*Vulpes vulpes*) residing in the northern boreal vegetation zone have home ranges four times larger than foxes in the more productive landscape of the south of Scandinavia (Walton et al. 2017). Wolf home range sizes increase with latitude, elevation and lower prey density (Mattisson et al. 2013) or independent of prey density (Jedrzejewski et al. 2007).

Consistent with this, we detected a positive effect of latitude on home range size in our study, at least for wolverines occupying sites at average and below-average elevation (Fig. 5). However, with increasing elevation the effect of latitude diminished and eventually reversed. We were able to detect this interaction between elevation and latitude due to the immense spatial extent and population-level inferences made possible by the combination of NGS and SCR. Similarly, the landscape and population-level analysis revealed that home range size variation across the landscape was greater for females than males. This lower variability in male home range size may be indicative of lower flexibility.

Home range size may be affected by several additional factors not accounted for

in this study. Chief among these is density. Several studies have revealed density dependence in home range size (e.g. Dahle and Swenson 2003, Saïd et al. 2009, Efford et al. 2016), with territorial exclusion, competition or facilitation as drivers. Wolverines are known to exhibit intrasex territoriality (Bischof et al. 2016b) and higher densities can thus be expected to lead to smaller home range sizes. The combination of NGS and SCR offers an opportunity to further explore and quantify density-dependent effects on home range size at the landscape and population level. Other possible confounders include age, reproductive status and landscape structure, such as roads and terrain.

Logistic and economic constraints, as well as concerns for animal welfare, cause an inherent trade-off between the level of detail and the scope of studies on animal space-use. Telemetry is challenging and the cost per individual is high (Hebblewhite and Haydon 2010). This limits the total sample size in terms of number of instrumented individuals. However, once an animal is tagged or collared, the number of observations obtained per individual, and consequently the level of detail, can be substantial (Bischof et al. 2019a). By contrast, non-invasive sampling combined with SCR, yielded inferences based on a large proportion of the population across the entire national range. This large scope comes at the price of obtaining only a limited number of observations per individual.

While numerous telemetry studies have focused on parts of populations, there is a dearth of empirical studies that have yielded population or species-level information about animal space use. To fill this gap, general large-scale inferences are sometimes drawn by scaling-up from local studies or combining the results from multiple studies. However, scaling-up can be risky (Hebblewhite and Haydon 2010, Morales et al. 2010, Owen-Smith et al. 2010) especially for telemetry studies, which typically suffer not only from sample size limitations but also from being a non-representative sample of the population, at least in carnivores. Without a truly random sample of instrumented animals across the entire population, population-level inferences are questionable, yet needed for management and conservation of populations. The extent to which meta-analyses yield generalizable and large-scale results is further influenced by the similarity of approaches used and temporal consistency in the constituent studies and remains subject to biases inherent to them.

Combining NGS with SCR, we were not only able to collect observations across the wolverine population's entire range within Norway, but also accounted for imperfect detection. As such, the approach has practical potential to yield truly population-level inferences. Ultimately, investigators must weigh the benefits of greater detail vs scope based on their research objectives. Modern survey methods

and advances in hierarchical modelling have helped broaden the options available for making that choice. There are several developments that could further enhance the utility of non-invasive SCR for quantifying wildlife space-use and its drivers. The SCR framework can be integrated with resource selection, as already shown by Linden et al. (2018). Similarly, non-Euclidean distance SCR models (Sutherland et al. 2015) take the influence of landscape characteristics on home range configuration into account and can model non-circular home ranges. Both developments would also allow investigators to quantify inter and intra-species interactions in terms of home range size or configuration. One particularly promising extension of SCR, open-population SCR, allows for the simultaneous analysis of multiple sampling seasons by incorporating a population dynamic component (Bischof et al. 2016a). Open-population SCR can not only estimate vital rates and changes in abundance over time but also home range dynamics, such as shifts in position and changes in size (Ergon and Gardner 2014). These developments would not eliminate the need for tracking animals directly but could provide further non-invasive and population-level access to inferences about movement and habitat use that have so far been the domain of telemetry applications.

Acknowledgment

This work was funded by the Norwegian Environment Agency (Miljødirektoratet), the Swedish Environmental Protection Agency (Naturvårdsverket), and the Research Council of Norway (NFR 286886; project WildMap). We thank the field staff and members of the public that collected the data compiled in the Scandinavian large carnivore database Rovbase. We thank Daniel Turek and J. Andrew Royle for fruitful discussions.

References

Arnemo, J. M., P. Ahlqvist, R. Andersen, F. Berntsen, G. Ericsson, J. Odden, S. Brunberg, P. Segerström, and J. E. Swenson. 2006. Risk of capture-related mortality in large free-ranging mammals: experiences from Scandinavia. Wildlife Biology 12:109–113.

Aronsson, M., and J. Persson. 2018. Female breeding dispersal in wolverines, a solitary carnivore with high territorial fidelity. European Journal of Wildlife Research 64:7.

van Beest, F. M., I. M. Rivrud, L. E. Loe, J. M. Milner, and A. Mysterud. 2011. What determines variation in home range size across spatiotemporal scales in a

large browsing herbivore? Journal of Animal Ecology 80:771–785.

Beja-Pereira, A., R. Oliveira, P. C. Alves, M. K. Schwartz, and G. Luikart. 2009. Advancing ecological understandings through technological transformations in noninvasive genetics. Molecular Ecology Resources 9:1279–1301.

Bischof, R., H. Brøseth, and O. Gimenez. 2016a. Wildlife in a Politically Divided World: Insularism Inflates Estimates of Brown Bear Abundance. Conservation Letters 9:122–130.

Bischof, R., J. G. O. Gjevestad, A. Ordiz, K. Eldegard, and C. Milleret. 2019a. High frequency GPS bursts and path-level analysis reveal linear feature tracking by red foxes. Scientific Reports 9:8849.

Bischof, R., E. R. Gregersen, H. Brøseth, H. Ellegren, and Ø. Flagstad. 2016b. Noninvasive genetic sampling reveals intrasex territoriality in wolverines. Ecology and Evolution 6:1527–1536.

Bischof, R., C. Milleret, P. Dupont, J. Chipperfield, H. Brøseth, and J. Kindberg. 2019b. RovQuant: Estimating density, abundance and population dynamics of bears, wolverines and wolves in Scandinavia. MINA fagrapport 63. 79 pp.

Bischof, R., S. M. J. G. Steyaert, and J. Kindberg. 2017. Caught in the mesh: roads and their network-scale impediment to animal movement. Ecography 40:1369–1380.

Borchers, D. L., and M. G. Efford. 2008. Spatially Explicit Maximum Likelihood Methods for Capture-Recapture Studies. Biometrics 64:377–385.

Börger, L., B. D. Dalziel, and J. M. Fryxell. 2008. Are there general mechanisms of animal home range behaviour? A review and prospects for future research. Ecology Letters 11:637–650.

Börger, L., N. Franconi, F. Ferretti, F. Meschi, G. D. Michele, A. Gantz, and T. Coulson. 2006. An Integrated Approach to Identify Spatiotemporal and Individual-Level Determinants of Animal Home Range Size. The American Naturalist 168:471–485.

Burt, W. H. 1943. Territoriality and home range concepts as applied to mammals. Journal of Mammalogy 24:346–352.

Burton, A. C., E. Neilson, D. Moreira, A. Ladle, R. Steenweg, J. T. Fisher, E. Bayne, and S. Boutin. 2015. Wildlife camera trapping: a review and recommendations for linking surveys to ecological processes. Journal of Applied Ecology 52:675–685.

Copeland, J. P. 1996. Biology of the wolverine in central Idaho. MS thesis, University of Idaho, USA. 152 pp.

Dahle, B., and J. E. Swenson. 2003. Seasonal range size in relation to reproductive strategies in brown bears *Ursus arctos*. Journal of Animal Ecology 72:660–667.

Dawson, F. N., A. J. Magoun, J. Bowman, and J. C. Ray. 2010. Wolverine, *Gulo gulo*, Home Range Size and Denning Habitat in Lowland Boreal Forest in Ontario. The Canadian Field-Naturalist 124:139.

Doherty, T. S., and D. A. Driscoll. 2018. Coupling movement and landscape ecology for animal conservation in production landscapes. Proceedings of the Royal Society B: Biological Sciences 285:20172272.

Efford, M. 2004. Density estimation in live-trapping studies. Oikos 106:598–610.

Efford, M. G. 2011. Estimation of population density by spatially explicit capture–recapture analysis of data from area searches. Ecology 92:2202–2207.

Efford, M. G., D. K. Dawson, and D. L. Borchers. 2009. Population density estimated from locations of individuals on a passive detector array. Ecology 90:2676–2682.

Efford, M. G., D. K. Dawson, Y. V. Jhala, and Q. Qureshi. 2016. Density-dependent home-range size revealed by spatially explicit capture-recapture. Ecography 39:676–688.

Efford, M. G., and G. Mowat. 2014. Compensatory heterogeneity in spatially explicit capture–recapture data. Ecology 95:1341–1348.

Ergon, T., and B. Gardner. 2014. Separating mortality and emigration: modelling space use, dispersal and survival with robust-design spatial capture-recapture data. Methods in Ecology and Evolution 5:1327–1336.

Flagstad, Ø., E. Hedmark, A. Landa, H. Brøseth, J. Persson, R. Andersen, P. Segerström, and H. Ellegren. 2004. Colonization History and Noninvasive Monitoring of a Reestablished Wolverine Population. Conservation Biology 18:676–688.

Fuller, M. R., and T. K. Fuller. 2012. Radio-telemetry equipment and applications for carnivores. in L. Boitani and R. A. Powell, editors. Carnivore ecology and conservation: a handbook of techniques. Oxford University Press, Oxford, UK.

Gardner, B., J. Reppucci, M. Lucherini, and J. A. Royle. 2010. Spatially explicit inference for open populations: estimating demographic parameters from camera-trap studies. Ecology 91:3376–3383.

Giuggioli, L., and V. M. Kenkre. 2014. Consequences of animal interactions on their dynamics: emergence of home ranges and territoriality. Movement Ecology 2:20.

Graw, B., B. Kranstauber, and M. B. Manser. 2019. Social organization of a solitary carnivore: spatial behaviour, interactions and relatedness in the slender mongoose. Royal Society Open Science 6:182160.

Hebblewhite, M., and D. T. Haydon. 2010. Distinguishing technology from biology: a critical review of the use of GPS telemetry data in ecology. Philosophical Transactions of the Royal Society B: Biological Sciences 365:2303–2312.

Hedmark, E., J. Persson, P. Segerström, A. Landa, and H. Ellegren. 2007. Paternity and mating system in wolverines *Gulo gulo*. Wildlife Biology 13:13–30.

Illian, J., A. Penttinen, H. Stoyan, and D. Stoyan. 2008. Statistical Analysis and Modelling of Spatial Point Patterns. John Wiley & Sons.

Inman, R. M., M. L. Packila, K. H. Inman, A. J. Mccue, G. C. White, J. Persson, B. C. Aber, M. L. Orme, K. L. Alt, S. L. Cain, J. A. Fredrick, B. J. Oakleaf, and S. S. Sartorius. 2012. Spatial ecology of wolverines at the southern periphery of distribution. The Journal of Wildlife Management 76:778–792.

Jedrzejewski, W., K. Schmidt, J. Theuerkauf, B. Jedrzejewska, and R. Kowalczyk. 2007. Territory size of wolves *Canis lupus*: linking local (Białowieża Primeval Forest, Poland) and Holarctic-scale patterns. Ecography 30:66–76.

Kennerley, R. J., M. A. C. Nicoll, S. J. Butler, R. P. Young, J. M. Nuñez-Miño, J. L. Brocca, and S. T. Turvey. 2019. Home range and habitat data for Hispaniolan mammals challenge assumptions for conservation management. Global Ecology and Conservation 18:e00640.

Kie, J. G., J. Matthiopoulos, J. Fieberg, R. A. Powell, F. Cagnacci, M. S. Mitchell, J.-M. Gaillard, and P. R. Moorcroft. 2010. The home-range concept: are traditional estimators still relevant with modern telemetry technology? Philosophical Transactions of the Royal Society B: Biological Sciences 365:2221–2231.

Landa, A., O. Strand, J. D. Linnell, and T. Skogland. 1998. Home-range sizes and altitude selection for arctic foxes and wolverines in an alpine environment. Canadian Journal of Zoology 76:448–457.

Linden, D. W., A. P. K. Sirén, and P. J. Pekins. 2018. Integrating telemetry data into spatial capture–recapture modifies inferences on multi-scale resource selection. Ecosphere 9.

Lindsjö, J., K. Cvek, E. M. F. Spangenberg, J. N. G. Olsson, and M. Stéen. 2019. The Dividing Line Between Wildlife Research and Management—Implications for Animal Welfare. Frontiers in Veterinary Science 6:13.

Mattisson, J., H. Andrén, J. Persson, and P. Segerström. 2011. Influence of intraguild interactions on resource use by wolverines and Eurasian lynx. Journal of Mammalogy 92:1321–1330.

Mattisson, J., H. Sand, P. Wabakken, V. Gervasi, O. Liberg, J. D. C. Linnell, G. R. Rauset, and H. C. Pedersen. 2013. Home range size variation in a recovering wolf population: evaluating the effect of environmental, demographic, and social factors. Oecologia 173:813–825.

May, R., L. Gorini, J. Van Dijk, H. Brøseth, J. D. C. Linnell, and A. Landa. 2012. Habitat characteristics associated with wolverine den sites in Norwegian multiple-use landscapes. Journal of Zoology 287(3):195-204.

Milleret, C., P. Dupont, C. Bonenfant, H. Brøseth, Ø. Flagstad, C. Sutherland, and R. Bischof. 2019. A local evaluation of the individual state-space to scale up Bayesian spatial capture-recapture. Ecology and Evolution 9:352–363.

Milleret, C., P. Dupont, H. Brøseth, J. Kindberg, J. A. Royle, and R. Bischof. 2018. Using partial aggregation in spatial capture recapture. Methods in Ecology and Evolution 9:1896–1907.

Morales, J. M., P. R. Moorcroft, J. Matthiopoulos, J. L. Frair, J. G. Kie, R. A. Powell, E. H. Merrill, and D. T. Haydon. 2010. Building the bridge between animal movement and population dynamics. Philosophical Transactions of the Royal Society B: Biological Sciences 365:2289–2301.

Morellet, N., C. Bonenfant, L. Börger, F. Ossi, F. Cagnacci, M. Heurich, P. Kjellander, J. D. C. Linnell, S. Nicoloso, P. Sustr, F. Urbano, and A. Mysterud. 2013. Seasonality, weather and climate affect home range size in roe deer across a wide latitudinal gradient within Europe. Journal of Animal Ecology 82:1326–1339.

Nilsen, E. B., I. Herfindal, and J. D. C. Linnell. 2005. Can intra-specific variation in carnivore home-range size be explained using remote-sensing estimates of environmental productivity? Écoscience 12:68–75.

Ofstad, E. G., I. Herfindal, E. J. Solberg, and B.-E. Sæther. 2016. Home ranges, habitat and body mass: simple correlates of home range size in ungulates. Proceedings of the Royal Society B: Biological Sciences 283:20161234.

Owen-Smith, N., J. M. Fryxell, and E. H. Merrill. 2010. Foraging theory upscaled: the behavioural ecology of herbivore movement. Philosophical Transactions

of the Royal Society B: Biological Sciences 365:2267–2278.

Persson, J., P. Wedholm, and P. Segerström. 2010. Space use and territoriality of wolverines (*Gulo gulo*) in northern Scandinavia. European Journal of Wildlife Research 56:49–57.

Powell, R. A., and M. S. Mitchell. 2012. What is a home range? Journal of Mammalogy 93:948–958.

R Development Core Team. 2018. R: a language and environment for statistical computing. R Foundation for Statistical Computing, Vienna, Austria. https://www.R-project.org/

Rodgers, T. W., and J. E. Janečka. 2013. Applications and techniques for non-invasive faecal genetics research in felid conservation. European Journal of Wildlife Research 59:1–16.

Royle, J. A., R. B. Chandler, R. Sollmann, and B. Gardner. 2014. Spatial capture-recapture. Elsevier, Amsterdam.

Royle, J. A., R. M. Dorazio, and W. A. Link. 2007. Analysis of Multinomial Models With Unknown Index Using Data Augmentation. Journal of Computational and Graphical Statistics 16:67–85.

Royle, J. A., A. K. Fuller, and C. Sutherland. 2018. Unifying population and landscape ecology with spatial capture-recapture. Ecography 41:444–456.

Royle, J. A., M. Kéry, and J. Guélat. 2011. Spatial capture-recapture models for search-encounter data. Methods in Ecology and Evolution 2:602–611.

Royle, J. A., J. D. Nichols, K. U. Karanth, and A. M. Gopalaswamy. 2009. A hierarchical model for estimating density in camera-trap studies. Journal of Applied Ecology 46:118–127.

Saïd, S., J.-M. Gaillard, O. Widmer, F. Débias, G. Bourgoin, D. Delorme, and C. Roux. 2009. What shapes intra-specific variation in home range size? A case study of female roe deer. Oikos 118:1299–1306.

Schaub, M., and J. A. Royle. 2014. Estimating true instead of apparent survival using spatial Cormack-Jolly-Seber models. Methods in Ecology and Evolution 5:1316–1326.

Sutherland, C., A. K. Fuller, and J. A. Royle. 2015. Modelling non-Euclidean movement and landscape connectivity in highly structured ecological networks. Methods in Ecology and Evolution 6:169–177.

de Valpine, P., D. Turek, C. J. Paciorek, C. Anderson-Bergman, D. T. Lang, and

R. Bodik. 2017. Programming With Models: Writing Statistical Algorithms for General Model Structures With NIMBLE. Journal of Computational and Graphical Statistics 26:403–413.

Walton, Z., G. Samelius, M. Odden, and T. Willebrand. 2017. Variation in home range size of red foxes *Vulpes vulpes* along a gradient of productivity and human landscape alteration. PloS ONE 12:e0175291.

Appendix S1: Model definition in NIMBLE

```
nimModel <- nimbleCode({
  ##---------- SPATIAL PROCESS ----------##
  I[1:n.cells] <- exp(betaDENS * DEN[1:n.cells]) ##equation 1
  betaDENS ~ dnorm(0,0.0001)

    for(i in 1:M){
    sxy[i,1:2] ~ dbinomPPSingle(lowerHabCoords[1:n.cells,1:2],
                                upperHabCoords[1:n.cells,1:2],
                                I[1:n.cells],
                                1, n.cells) }#i

  ##---------- DEMOGRAPHIC PROCESS ----------##
  psi ~ dunif(0,1)                                  ##equation 3
  for(i in 1:M){
    z[i] ~ dbern(psi) }#i

  N <- sum(z[1:M])                                  ##equation 2

  ##---------- OBSERVATION PROCESS ----------##
  a0 ~ dgamma(0.01,0.01)
  sigma0 ~ dgamma(0.01,0.01)
  betaTRACKS ~ dnorm(0,0.0001)
  betaELEV ~ dnorm(0,0.0001)
  betaLAT ~ dnorm(0,0.0001)
  betaINT ~ dnorm(0,0.0001)

  for(i in 1:M){
    sigma[i] <- exp(log(sigma0)                     ##equation 6
                    + betaELEV * ELEVATION[sxy[i,2],sxy[i,1]]
                    + betaLAT * LATITUDE[sxy[i,2],sxy[i,1]]
                    + betaINT * ELEVATION[sxy[i,2],sxy[i,1]]
                              *LATITUDE[sxy[i,2],sxy[i,1]])

                                          ##equations 7,4,8
     p[i, 1:J] <- calculateDetProb_a0( sxy = sxy[i, 1:2]
                                     , detector.xy =
                                       detector.xy[1:J, 1:2]
                                     , aZero = a0
                                     , sigma = sigma[i]
                                     , maxDist = maxDist)

     y[i,1:J] ~ dbin_vector(p[i,1:J], z[i], trials[1:J])
  }#i
})
```

Article IV

Integrating dead recoveries in spatial capture-recapture models

Pierre Dupont[1,*], Cyril Milleret[1], Mahdieh Tourani[1], Henrik Brøseth[2], and Richard Bischof[1]

1. *Faculty of Environmental Sciences and Natural Resource Management, Norwegian University of Life Sciences, P.O. Box 5003, 1432 Ås, Norway*
2. *Department of Terrestrial Ecology, Norwegian Institute for Nature Research, PB 5685 Torgarden, NO-7485 Trondheim, Norway*

∗ Email: pierre.dupont@nmbu.no

Abstract. Integrating dead recoveries into capture-recapture models can improve inference on demographic parameters. But dead recovery data do not only inform on individual fates; they may also contain information about individual locations. Open-population spatial capture-recapture (OPSCR) has the potential to fully exploit such data. Here, we present an open-population spatial capture-recapture-recovery model integrating the spatial information associated with dead recoveries. We investigate the conditions under which this extension of the OPSCR model improves inference with simulations and illustrate the approach with the analysis of a wolverine (*Gulo gulo*) dataset collected in Norway. Our results highlight how leveraging the demographic and spatial information contained in dead recovery data in a spatial capture-recapture framework can greatly improve population parameter estimation with little to no additional cost of sampling. Not only can it enable analyses when data are sparse, it also markedly improves the precision of both demographic and spatial parameters and may help overcome some limitations of the study design.

Keywords: *Integrated modelling; Mortality; Population Dynamics; Known Fate; Spatial Capture-Recapture; Capture-Recapture-Recovery*

Introduction

Ecologists often struggle to obtain reliable estimates of population parameters. Imperfect detection poses the main challenge as it is close to impossible to detect all members and their fates in wild populations (Gimenez et al. 2008). Thus, observations usually pertain to a subset of the population only and statistical analyses are required to draw inferences about the entire population.

Historically, some of the first data used by demographers were census data, i.e. numbers of animals harvested by hunters (Elton 1924). These dead-recovery (or ring-recovery) models have long been used to study survival in natural populations but their scope remains limited by the type of data itself (Anderson et al. 1985). By contrast, capture-recapture (CR) data contain multiple live detections of the same individuals, which allow discriminating an individual that was not detected because it was missed, from an individual that could not be detected because it was dead or not present in the population. The CR framework also enables more complex models with survival and detection probabilities varying among years, sites, sex and age classes (Lebreton et al. 1992). Live detections and dead-recoveries can be combined in so-called capture-recapture-recovery models (Lebreton et al. 1995). The integration of known deaths further helps discriminating between a true absence and a missed individual, thus improving the precision of survival, detection probabilities, and ultimately population size estimates (Catchpole et al. 1998).

Spatial capture-recapture (SCR) models extend classical CR analysis by accounting for heterogeneity in detection probability among individuals arising from their distribution in space relative to trap locations (Royle and Young 2008, Borchers and Efford 2008). SCR also uses multiple detections of the same individuals, but at different locations, to infer the position of their activity centers (AC) and model individual detection probability in the landscape as a function of the distance to these ACs. As a consequence, and contrary to classical CR, SCR explicitly links population size to a given geographic area (i.e. density). One promising extension of SCR is the incorporation of several years (or seasons) of data, to build open-population spatial capture-recapture (OPSCR) models (Gardner et al. 2018). Just like open-population CR models, OPSCR models generate estimates of demographic parameters such as survival and recruitment, but they also model individual movements between years, thus providing a more complete picture of the spatiotemporal dynamics of the population under study (Ergon and Gardner 2014, Schaub and Royle 2014, Bischof et al. 2016, Gardner et al. 2018). It stands to reason that, like CR models, OPSCR would benefit from the integration of dead recovery data. Moreover, dead recovery data are often accompanied by the recovery

location and leveraging this information should further constrain the places an individual could have been, thus reducing uncertainty about the distribution and movements of individuals.

We present an Open-Population Spatial Capture-Recapture-Recovery model (OPSC-2R), that integrates spatial dead-recovery data, and test it with simulations against an OPSCR model without dead-recovery data and an OPSCR including dead-recovery data without spatial information (OPSCR+DR). Specifically, we test the predictions that gains from dead recovery integration will be higher when i) overall detectability is low, ii) population size (and thus sample size) is low, and iii) a large proportion of the population is recovered dead. We then demonstrate use of the OPSC2R model with a case study on long-term non-invasive genetic monitoring of wolverines (*Gulo gulo*) in Norway (Flagstad et al. 2004, Brøseth et al. 2010).

Material & Methods

1. Open-population spatial capture-recapture-recovery

The OPSC2R model consists of four sub-models: i) a demographic model describing when individuals are recruited into the population and when they die, ii) a spatial model describing the distribution of individual ACs at each detection occasion, as well as their movement between occasions (i.e. years), iii) a detection model, describing when and where individuals are detected alive, and iv) a recovery model, describing when and where dead individuals are recovered.

The demographic model. To describe the recruitment and survival processes, we opted for a multi-state formulation (Lebreton and Pradel 2002) and considered four states described by the random categorical variable $\mathbf{Z}$. The state of individual i at time t, z_{it}, can take the value 1 if the individual is "available", i.e. before it is recruited into the population; 2 if the individual is alive and present in the habitat considered (S); 3 if it died between $t-1$ and t and was recovered, and 4 if it was already dead at $t-1$ or if it died between $t-1$ and t but was not recovered. At the first occasion, individuals can only be designated as "available" or "alive" so that z_{i1} follows a categorical distribution with the probability vector describing probabilities to be in each of the four states considered: $z_{i1} \sim Categorical(1-\psi,\psi,0,0)$, where ψ is the probability to be alive at $t = 1$. Individual states at all subsequent occasions follow a Markov process as they depend on the previous individual state z_{it-1}. If $z_{it-1} = 1$, individual i can either stay in state 1 or be recruited into the population (transition to state 2): $z_{it} \sim Categorical(1-\gamma_{t-1},\gamma_{t-1},0,0)$, where γ_{t-1} is

the probability to be recruited into the population between $t-1$ and t from the pool of individuals available at $t-1$. If $z_{it-1} = 2$, individual i can either survive and stay in state 2, die and be recovered (transition to state 3), or die without being recovered (transition to state 4), so that $z_{it} \sim Categorical(0,\phi,(1–\phi)r,(1–\phi)(1–r))$ where ϕ is the survival probability and r the recovery probability. If $z_{it-1} = 3$ or 4, the only possibility is a transition to 4, the absorbent dead state.

The spatial model. Individual locations at each time step are described by the distribution of their ACs in the available habitat S. At the first occasion, ACs are assumed to follow a uniform distribution:

$$s_{i1} \sim Uniform(S) \tag{1}$$

where s_{i1} is the vector of x- and y-coordinates for the AC of individual i at time 1. In subsequent years, we modelled between-year movements using a Gaussian random-walk (Gardner et al. 2018), whereby the AC location of individual i at time t, s_{it}, follows a bivariate normal distribution (defined over S) centered on the previous location s_{it-1}, with standard deviation τ:

$$s_{it} \sim Normal(s_{it-1}, \tau) \tag{2}$$

The detection model. This sub-model describes how the detection probability of an individual varies in space depending on its AC location relative to the set of J possible detection locations (i.e. detectors). Here, we used the half-normal detection model (Royle et al. 2013) which assumes that p_{ijt}, the probability of detecting individual i at detector j at occasion t, decreases with the distance d_{ijt} between detector j and the individual AC location:

$$p_{ijt} = p_0.e^{-\frac{d_{ijt}^2}{2\sigma^2}} \tag{3}$$

where p_0 is the baseline detection probability and σ is the scale parameter of the half-normal detection function. The detection data is then modelled as:

$$y.alive_{ijt} \sim Bernoulli(p_{ijt}.I(z_{it} = 2)) \tag{4}$$

where $I(z_{it} = 2)$ is an indicator function used to condition the detection process on the individual being alive and thus available for detection.

The recovery model. The spatially explicit recovery model estimates the proba-

bility to recover a dead individual at a given location conditional on its AC location. This process resembles the "single-catch traps" situation (Borchers and Efford 2008) whereby the probability to recover an individual at a specific location is:

$$\mu_{ijt} = \frac{\dot{p}_{ijt}}{\Sigma_{k=1}^{J}\dot{p}_{ikt}} \text{ where } \dot{p}_{ikt} = e^{-\frac{d_{ijt}^2}{2\sigma^2}} \tag{5}$$

It follows that the ID of the detector where individual i was recovered at time t ($y.dead_{it}$), is categorically distributed with probability vector $K_{it} = (\mu_{i1t}, ..., \mu_{iJt})$:

$$y.dead_{it} \sim Categorical(K_{it}) \tag{6}$$

Note that the number and configuration of detectors for dead recoveries and live detections may differ. Dead recovery detectors may refer to specific locations if recovery is limited to certain sites or to gridded discrete locations across the entire habitat S if no spatial restriction applies to where individuals can be recovered (Milleret et al. 2018).

Data augmentation. We used a data augmentation approach (Royle and Dorazio 2012) and derived estimates of population size at each time step by summing the number of individuals alive $N_t = \Sigma_{i=1}^{M} I(z_{it} = 2)$ where M is the augmented population size ($M >> N_t$).

2. Alternative models

We compared the OPSC2R model with two reduced models; i) a traditional OPSCR ignoring dead-recovery data, and ii) an OPSCR integrating non-spatial dead-recovery data (OPSCR+DR). In the OPSCR, the demographic sub-model reduces to three states only (corresponding to states 1, 2 and 4) as dead recoveries are not considered and the r parameter is absent from the model. Then, if $z_{it-1} = 2$, individual i can only survive and stay in state 2 or die without being recovered, so that $z_{it} \sim Categorical(0, \phi, 1 - \phi)$. The recovery model is completely absent from the OPSCR model, whereas in the OPSCR+DR, dead recovery data are reduced to binary detections, i.e. $y.dead_{it} = 1$ if individual i was recovered at time t and 0 otherwise and $y.dead_{it} \sim Bernoulli(I(z_{it} = 3))$. See Appendix S1 for the different model scripts.

3. Simulations

To evaluate how the different models performed, we created a habitat grid of 35x35 distance units (du) in which we centered a regular square grid of 400 detectors, with one every 1.5 du. We simulated populations over a 5-year period by sampling survival, reproduction and recovery events for either 40 (small population) or 120 (large population) individuals present at the first occasion ($t = 1$). We simulated data for five different recovery probabilities (0, 0.25, 0.5, 0.75, and 1), whilst the other demographic parameters were chosen to generate a stable population (survival $\Phi = 0.6$; per-capita recruitment rate $\rho = 0.4$). Individual ACs were uniformly distributed in space at the first occasion (equation 1). Subsequent AC locations were generated using equation 2 with a standard deviation $\tau = 3$ du. Finally, the detection and dead recovery data were generated conditional on the individual states and locations using equations 3 to 6 with a scale parameter $\sigma = 1.2$ du. We used either a low ($p_0 = 0.1$) or high ($p_0 = 0.5$) baseline detection probability leading to approximately 25% and 75% of the population detected each year, respectively. We repeated the simulation process 100 times for each combination of parameters, for a total of 2000 simulated datasets. We evaluated the performance of the models based on accuracy and precision of the Bayesian estimator of the model parameters. As a measure of accuracy, we used relative bias $RB = \frac{\hat{\theta}-\theta}{\theta}$, where $\hat{\theta}$ is the posterior mean and θ is the true value of the parameter. As a measure of precision, we used the coefficient of variation $CV = \frac{sd(\theta)}{\hat{\theta}}$ (Walther and Moore 2005). R scripts for data simulation and model fitting are provided in Appendix S1.

4. Wolverine case study

For a real-life illustration of the benefits of integrating dead recovery data in SCR, we applied the OPSCR and OPSC2R models to a subset of the long-term non-invasive genetic dataset collected as part of the national monitoring program of wolverines in Norway (Flagstad et al. 2004, Brøseth et al. 2010). We used seven years of data collected during winters 2012/2013 to 2018/2019 in eastern Norway (Hedmark, Oppland and parts of Sør-Trøndelag counties), composed of 1011 alive detections and 70 dead recoveries from 232 individually identified female wolverines and 1635 alive detections and 80 dead recoveries from 250 individually identified male wolverines (Appendix S3: Fig. S1). More details about the data and models can be found in Appendix S3.

5. Model fitting

We fitted all models using Markov chain Monte Carlo (MCMC) simulations with NIMBLE (de Valpine et al. 2017) in R version 3.5.2 (R core team, 2017). To reduce computation time, we implemented the LESS approach (Milleret et al. 2019a) and built custom NIMBLE distributions (Appendix S1). We ran three chains of 40,000 iterations including an initial burn-in phase of 10,000 iterations for simulations, and four chains of 20,000 iterations including an initial burn-in phase of 5,000 iterations for the models fitted to wolverine data. We only retained models that reached convergence, i.e. all R-hat values were $\leq$1.1 and visual inspections of trace plots from a subset of the simulations showed good mixing of the chains (Brooks and Gelman 1998).

Results

Convergence. The number of models that reached convergence in the simulation study increased with the recovery and baseline detection probabilities and, to a lesser extent, with population size (Appendix S2: Fig. S1). The OPSC2R reached convergence consistently more often than the OPSCR and OPSCR+DR (in that order). Convergence failure was almost always due to high R-hat values of the movement parameter (R-hat $>$ 1.1). This was most apparent in the small population – low detectability scenario where only 18% of the OPSCR runs reached convergence, compared with 33% ($r = 0.25$) to 52% ($r = 1$) for the OPSCR+DR, and 43% ($r = 0.25$) to 84% ($r = 1$) for the OPSC2R (Fig. 1b).

Bias. All parameter estimates returned by the three models were virtually unbiased (RB $<$ 1%) except for the small population – low detectability scenario. In this situation, the lack of data led to an average positive bias of up to 58% for the baseline detection probability parameter with all three models with the small population – low detectability scenario (Appendix S2: Fig. S10a).

Precision. On average, the coefficients of variation of the population size estimates were 33% lower for both the OPSCR+DR and OPSC2R compared to the OPSCR (Appendix S2: Fig. S2-S6). Despite similar relative gains amongst scenarios, the absolute gain in CV was much higher for the small population – low detectability scenario. For example, the average CV of the population size estimates was as high as 22% of the estimated population size with the OPSCR compared with 14% for the two other models ($r = 1$; Fig. 2a), whereas it decreased from 4.3% to 2.9% in the large population – high detectability scenario (Fig. 2b).

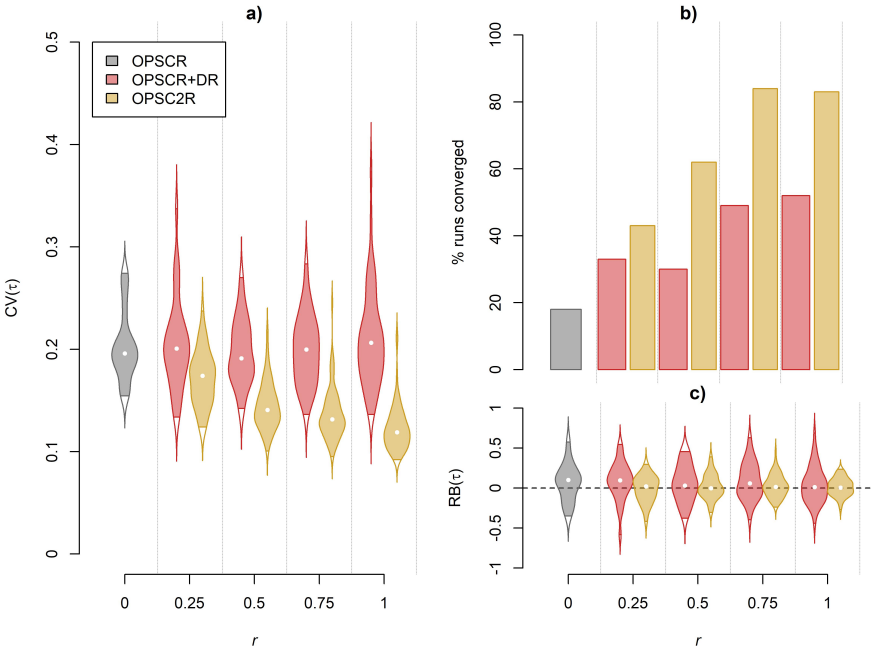

Figure 1: *a) Coefficient of variation of the movement parameter CV(τ), b) proportion of converged simulations, and c) relative bias of the movement parameter RB(τ) with increasing proportion of dead individuals recovered (r) for the OPSCR model without dead recoveries (OPSCR), the model integrating non-spatial dead recovery (OPSCR +DR), and the model integrating spatial dead recovery (OPSC2R) for the small population – low detectability scenario ($N = 40$; $p_0 = 0.1$). Violins present the distribution of values over 100 repeated simulations. White dots represent median values and colored areas the 95% credible intervals.*

Movement. The main difference between the OPSC2R and the OPSCR+DR relates to the movement parameter τ. Whilst relative bias and coefficient of variation of all other parameters were similar between the OPSC2R and OPSCR+DR, explicitly modelling the spatial aspect of the dead recovery process led to a significant improvement in the precision of τ. CV(τ) steadily decreased with increasing proportion of dead recoveries to reach an average value of 0.12 for the OPSC2R compared with approximately 0.22 for the OPSCR and OPSCR+DR (Fig. 1a).

Wolverine case study. Yearly population size estimates did not significantly differ between models with (OPSC2R) and without (OPSCR) dead recoveries (Fig. 3a, b). Associated coefficients of variation displayed a similar temporal trend for both models, but CVs from the OP2SCR were always lower than those from the

OPSCR model (with the exception of the final year). CVs for the survival estimates were also slightly lower for the OPSC2R compared with the OPSCR (Appendix S3: Tables S1 and S2). The OPSC2R mean estimates of the movement parameter were 12% and 30% larger than the OPSCR estimates for males and females respectively (Fig. 3c). The associated coefficients of variation were slightly smaller with the OPSC2R (Fig. 3d). Other parameters did not significantly differ between the two models (Appendix S3: Tables S2 and S3).

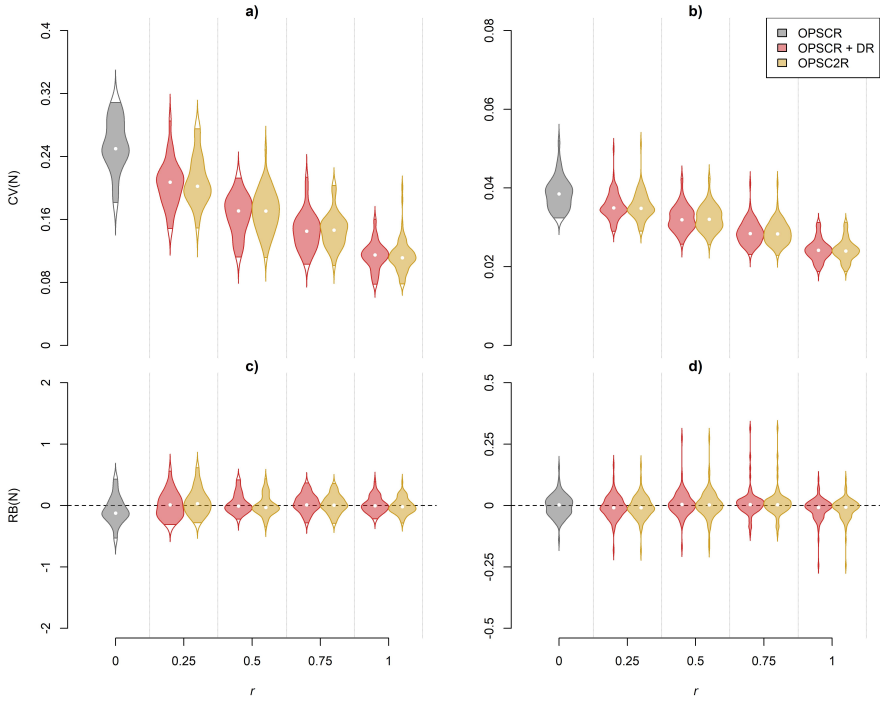

Figure 2: *Coefficient of variation (CV) and relative bias (RB) of population size estimates for the third capture occasion (see Fig. S2-S6 for other occasions) with increasing proportion of dead individuals recovered (r) for the OPSCR model without dead recoveries (OPSCR), the model integrating non-spatial dead recovery (OPSCR +DR), and the model integrating spatial dead recovery (OPSC2R). Presented are the results for, (a, c) the small population – low detectability scenario ($N = 40; p_0 = 0.1$) and, (b, d) the large population – high detectability scenario ($N = 120; p_0 = 0.5$). Violins present the distribution of values over 100 repeated simulations. White dots represent median values and colored areas the 95% credible intervals.*

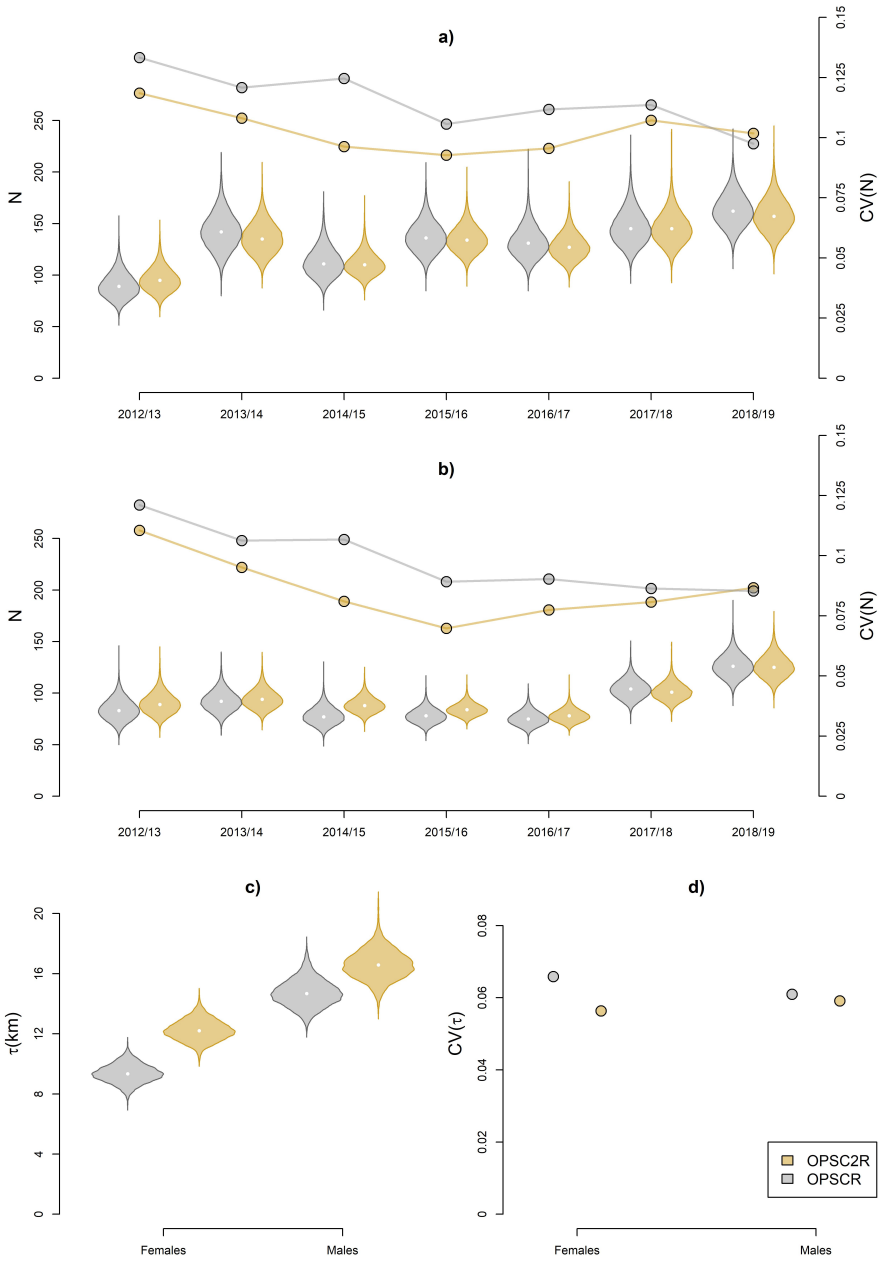

Figure 3: *a) Female and b) male posterior distributions of population size estimates (N) and associated coefficients of variation (CV) for the wolverine population in eastern Norway (Appendix 3, Fig S1) estimated using a model integrating spatial dead recovery information (OPSC2R) and a traditional OPSCR model. c) posterior distribution and d) coefficients of variation of the movement parameter (τ) for female and male wolverines. White dots represent the posterior means.*

Discussion

Our results show that combining spatial live detections and spatial dead recoveries into an open-population spatial capture-recapture-recovery model can greatly improve population estimates and mitigate detrimental effects of data sparsity. In both our simulations and empirical analysis, models incorporating dead recoveries led to more precise estimates of the main demographic parameters, without causing additional bias. The benefits of integration of dead recoveries in terms of increased precision were most substantial for small populations with low detectability and high recovery probabilities.

Incorporating dead recoveries, regardless of whether the associated spatial information is taken into account, increased the precision of both survival and recruitment estimates, and consequently population size. This is consistent with previous CR studies where integration of known-fate data led to greater precision of survival estimates (Catchpole et al. 1998). We additionally show that when more individuals are recovered, the uncertainty about individual states at each occasion declines, thus reducing the uncertainty of demographic parameters. Modelling the dead recovery process in a spatially explicit fashion significantly improves convergence and precision of movement parameter estimates, which has proved difficult to study (Fujiwara et al. 2006, Schaub and Royle 2014). In the small population – low detectability scenario, the standard deviation of the bivariate normal distribution (i.e. the movement parameter) was twice as precise when 50% of the dead individuals were recovered with the OPSC2R compared with the OPSCR and OPSCR+DR models (Fig. 1a). Convergence of the movement parameter in OPSCR is known to be slow and occasionally unattainable due to a lack of repeated recaptures across successive years and consequently little available information on shifts of individual ACs between years (Milleret et al. 2019b). The spatial information associated with dead recovery data informs individual trajectories when live recaptures are sparse, in some cases making model fitting possible in the first place.

In the wolverine study, precision gains were not as large as in the simulation study, despite detectability levels of live individuals in the range of values tested in the simulation study ($53 \pm 6\%$ of the population detected alive each year for males and $39 \pm 4\%$ for females). This might be explained by the fact that yearly wolverine recovery rates (between 8 and 20% of the population for males and between 7 and 18% for females; Appendix S3: Tables S1 and S2) are at the lower end of the gradient we tested in the simulation study. Nonetheless, the pattern in parameter precision generally followed the simulation results, albeit less conspicuous, with slightly lower coefficients of variation for most parameters with the OPSC2R model

compared to the OPSCR model. Interestingly, the largest gain in population size precision was for the year 2014 where the recovery rate was highest for both sexes (Fig. 3; Appendix S3: Tables S1 and S2). Contrary to the simulation results, we observed an increase in the movement parameter estimate for both male and female wolverines with the OPSC2R compared to the OPSCR. This may be explained by the inclusion of dead recoveries of all individuals that were detected alive at least once, even if the recovery occurred outside the detector grid area (inside the buffer, see Appendix S3: Fig. S1). In OPSCR studies, the definition of the habitat and especially the buffer around the detector area is crucial; it must be large enough to allow for multi-year movements of individuals outside the detector area. In other words, it must be large enough so as not to truncate the movement distance distribution, otherwise survival and movement estimates are negatively biased (Ergon and Gardner 2014, Gardner et al. 2018). Furthermore, if the area covered by detectors is too small relative to the distance travelled by some individuals in the population, the range of "observed" AC movements within the study area will be skewed towards short distances irrespective of the buffer specification, leading to under-estimation of movement and survival parameters (Dupont 2017). This is most likely the case in the wolverine example where long-distance movements are missed by the OPSCR. By incorporating dead recoveries outside the detector area, the OPSC2R may overcome this limitation of the non-invasive genetic dataset and provide more realistic values of the movement distribution.

In capture-recapture studies, high recapture probabilities are pivotal to estimate population parameters with satisfactory precision, but the effort required to collect adequate data is often a critical limitation (Williams et al. 2002). Dead recovery data, on the other hand, are readily available for a wide array of taxa studied with CR methods. Leveraging the demographic and spatial information contained in such data in an open population spatial capture-recapture framework can greatly improve population parameter estimation with little to no additional cost of sampling. Not only can it enable analyses when data are sparse, it can also improve the precision of the parameter estimates and help overcome limitations of the study design.

Acknowledgments

P.D., C.M., and R.B. conceived and designed the study. P.D. implemented the analysis with contributions from C.M., M.T, and R.B. All authors contributed to writing the manuscript and gave final approval for publication. This work was funded by the Norwegian Environment Agency (Miljødirektoratet), the Swedish Environmental Protection Agency (Naturvårdsverket) and the Research Council of

Norway (NFR 286886). We thank the field staff and members of the public that collected the large carnivore database Rovbase3.0 (rovbase.no). Model fitting was performed on NMBU's computing cluster "Orion", administered by the Centre for Integrative Genetics.

Supplementary information

Appendix S1: Open-Population Spatial Capture-Recapture models R and NIMBLE scripts
Appendix S2: Supplementary information for the simulation study
Appendix S3: Supplementary information for the wolverine case study

References

Anderson, D. R., K. P. Burnham, and G. C. White. 1985. Problems in Estimating Age-Specific Survival Rates from Recovery Data of Birds Ringed as Young. Journal of Animal Ecology 54:89–98.

Bischof, R., H. Brøseth, and O. Gimenez. 2016. Wildlife in a Politically Divided World: Insularism Inflates Estimates of Brown Bear Abundance: Transboundary wildlife populations. Conservation Letters 9:122–130.

Borchers, D. L., and M. G. Efford. 2008. Spatially Explicit Maximum Likelihood Methods for Capture-Recapture Studies. Biometrics 64:377–385.

Brooks, S. P., and A. Gelman. 1998. General Methods for Monitoring Convergence of Iterative Simulations. Journal of Computational and Graphical Statistics 7:434–455.

Brøseth, H., Ø. Flagstad, C. Wärdig, M. Johansson, and H. Ellegren. 2010. Large-scale noninvasive genetic monitoring of wolverines using scats reveals density dependent adult survival. Biological Conservation 143:113–120.

Catchpole, E. A., S. N. Freeman, B. J. T. Morgan, and M. P. Harris. 1998. Integrated Recovery/Recapture Data Analysis. Biometrics 54:33–46.

Dupont, P. 2017, January 26. The Influence of sociality on population dynamics in the Alpine Marmot. phdthesis, Université de Lyon.

Elton, C. S. 1924. Periodic fluctuations in the numbers of animals: their causes and effects. Journal of Experimental Biology 2:119–163.

Ergon, T., and B. Gardner. 2014. Separating mortality and emigration: mod-

elling space use, dispersal and survival with robust-design spatial capture–recapture data. Methods in Ecology and Evolution 5:1327–1336.

Flagstad, Ø., E. Hedmark, A. Landa, H. Brøseth, J. Persson, R. Andersen, P. Segerström, and H. Ellegren. 2004. Colonization History and Noninvasive Monitoring of a Reestablished Wolverine Population. Conservation Biology 18:676–688.

Fujiwara, M., K. E. Anderson, M. G. Neubert, and H. Caswell. 2006. On the Estimation of Dispersal Kernels from Individual Mark-Recapture Data. Environmental and Ecological Statistics 13:183–197.

Gardner, B., R. Sollmann, N. S. Kumar, D. Jathanna, and K. U. Karanth. 2018. State space and movement specification in open population spatial capture–recapture models. Ecology and Evolution 8:10336–10344.

Gimenez, O., A. Viallefont, A. Charmantier, R. Pradel, E. Cam, C. R. Brown, M. D. Anderson, M. B. Brown, R. Covas, and J. Gaillard. 2008. The Risk of Flawed Inference in Evolutionary Studies When Detectability Is Less than One. The American Naturalist 172:441–448.

Lebreton, J. D., and R. Pradel. 2002. Multistate recapture models: Modelling incomplete individual histories. Journal of Applied Statistics 29:353–369.

Lebreton, J.-D., K. P. Burnham, J. Clobert, and D. R. Anderson. 1992. Modeling Survival and Testing Biological Hypotheses Using Marked Animals: A Unified Approach with Case Studies. Ecological Monographs 62:67–118.

Lebreton, J.-D., B. J. T. Morgan, R. Pradel, and S. N. Freeman. 1995. A Simultaneous Survival Rate Analysis of Dead Recovery and Live Recapture Data. Biometrics 51:1418-1428.

Milleret, C., P. Dupont, C. Bonenfant, H. Brøseth, Ø. Flagstad, C. Sutherland, and R. Bischof. 2019a. A local evaluation of the individual state-space to scale up Bayesian spatial capture–recapture. Ecology and Evolution 9:352–363.

Milleret, C., P. Dupont, H. Brøseth, J. Kindberg, J. A. Royle, and R. Bischof. 2018. Using partial aggregation in Spatial Capture Recapture. Methods in Ecology and Evolution 9:1896-1907.

Milleret, C., P. Dupont, J. Chipperfield, D. Turek, H. Brøseth, O. Gimenez, P. de Valpine, and R. Bischof. Estimating abundance with interruptions in data collection using open population spatial capture-recapture models. Ecosphere (in press).

Royle, J. A., R. B. Chandler, R. Sollmann, and B. Gardner. 2013. Spatial

Capture-Recapture. Academic Press.

Royle, J. A., and R. M. Dorazio. 2012. Parameter-expanded data augmentation for Bayesian analysis of capture–recapture models. Journal of Ornithology 152:521–537.

Royle, J. A., and K. V. Young. 2008. A hierarchical model for spatial capture–recapture data. Ecology 89:2281–2289.

Schaub, M., and J. A. Royle. 2014. Estimating true instead of apparent survival using spatial Cormack–Jolly–Seber models. Methods in Ecology and Evolution 5:1316–1326.

de Valpine, P., D. Turek, C. J. Paciorek, C. Anderson-Bergman, D. T. Lang, and R. Bodik. 2017. Programming With Models: Writing Statistical Algorithms for General Model Structures With NIMBLE. Journal of Computational and Graphical Statistics 26:403–413.

Walther, B. A., and J. L. Moore. 2005. The concepts of bias, precision and accuracy, and their use in testing the performance of species richness estimators, with a literature review of estimator performance. Ecography 28:815–829.

Appendix 1: Open-Population Spatial Capture-Recapture models – R and Nimble scripts

R simulation and NIMBLE analysis script can be found here or go to: https://github.com/PierreDupont/SpatialDeadRecovery/blob/master/Simulations_SpatialDeadRecovery.R

Data, R and NIMBLE scripts for the wolverine analysis can be found here or go to: https://github.com/PierreDupont/SpatialDeadRecovery/blob/master/Wolverines_SpatialDeadRecovery.R

Appendix 2: Supplementary information for the simulation study

Table S1: *Parameter values used in the simulation study.*

	Simulation parameters	**Simulated values**
Demographic	Survival	$\Phi = 0.6$
	Per capita recruitment	$\rho = 0.4$
	Initial population size	$N_1 \in [40, 120]$
Movement	Movement scale parameter	$\tau = 3$
Detection	Baseline detection probability	$p_0 \in [0.1, 0.5]$
	Detection scale parameter	$\sigma = 1.2$
	Recovery probability	$r \in [0, 0.25, 0.5, 0.75, 1]$

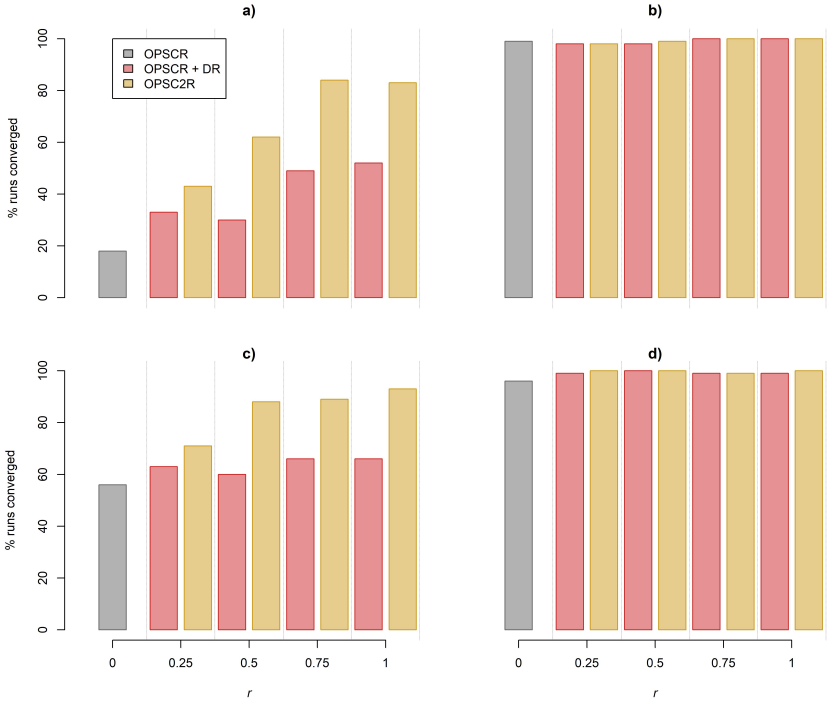

Figure S1: *Proportion of simulation runs that reached convergence (R-hat < 1.1 and good mixing of the MCMC chains) with increasing proportion of dead individuals recovered (r) for a traditional OPSCR model (OPSCR), a model integrating non-spatial dead recovery (OPSCR+DR), and a model integrating spatial dead recovery information (OPSC2R) for the different simulation scenarios; a) low detectability ($p_0 = 0.1$) and small population size ($N = 40$), b) high detectability ($p_0 = 0.5$) and small population size, c) low detectability and large population size ($N = 120$), d) high detectability and large population size.*

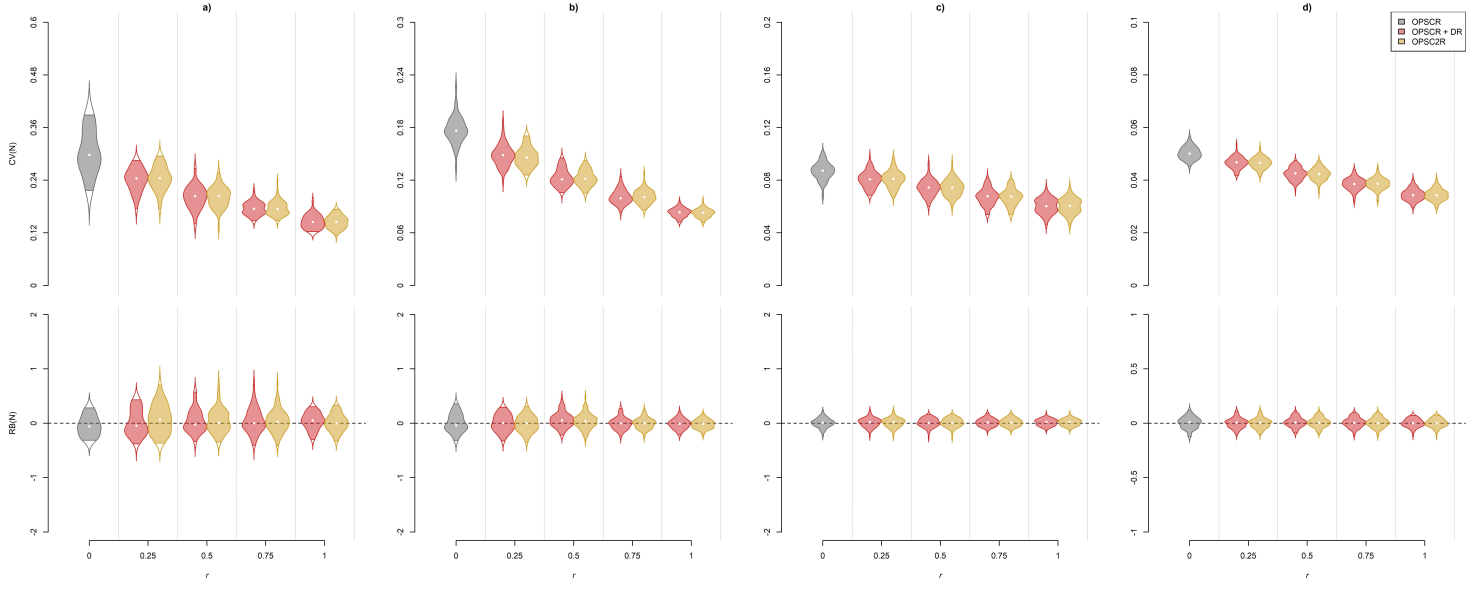

Figure S2: *Coefficient of variation (upper row) and relative bias (lower row) of the population size estimate for the 1st capture occasion with increasing proportion of dead individuals recovered (r) for a traditional OPSCR model (OPSCR), a model integrating non-spatial dead recovery (OPSCR+DR), and a model integrating spatial dead recovery information (OPSC2R) for the different simulation scenarios; a) low detectability ($p_0 = 0.1$) and small population size ($N = 40$), b) high detectability ($p_0 = 0.5$) and small population size, c) low detectability and large population size ($N = 120$), d) high detectability and large population size. NB: y-axes scales are different among plots.*

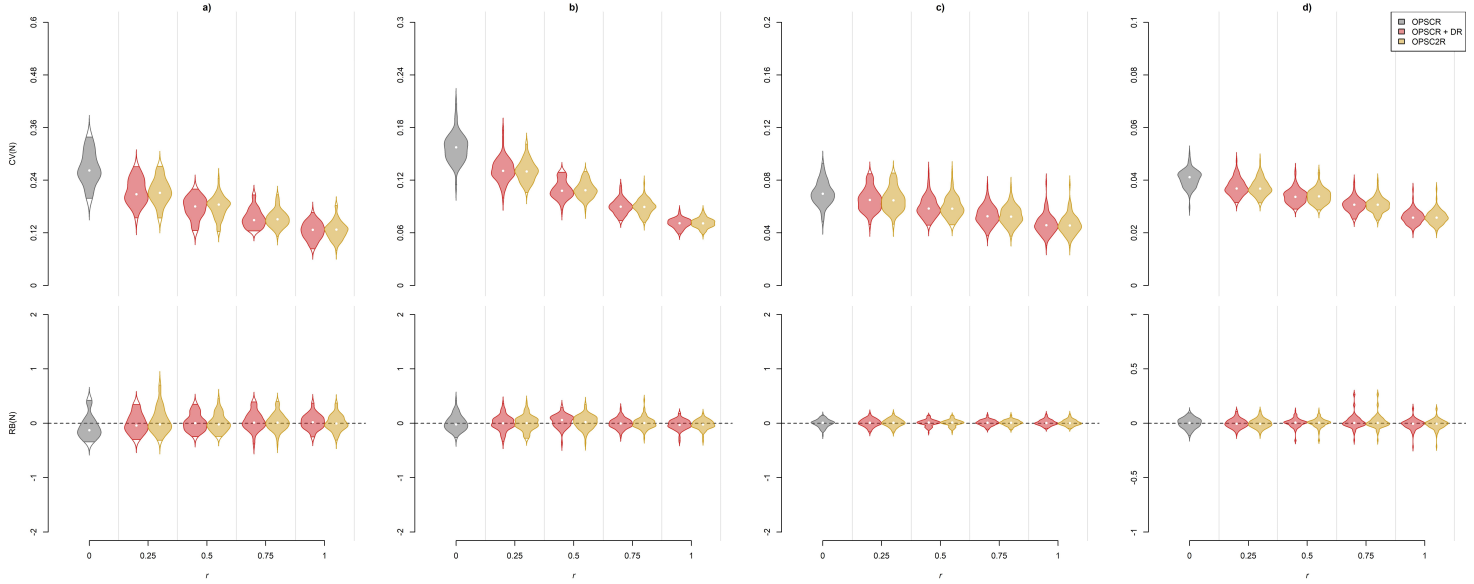

Figure S3: *Coefficient of variation (upper row) and relative bias (lower row) of the population size estimate for the 2nd capture occasion with increasing proportion of dead individuals recovered (r) for a traditional OPSCR model (OPSCR), a model integrating non-spatial dead recovery (OPSCR+DR), and a model integrating spatial dead recovery information (OPSC2R) for the different simulation scenarios; a) low detectability ($p_0 = 0.1$) and small population size ($N = 40$), b) high detectability ($p_0 = 0.5$) and small population size, c) low detectability and large population size ($N = 120$), d) high detectability and large population size. NB: y- axes scales are different among plots.*

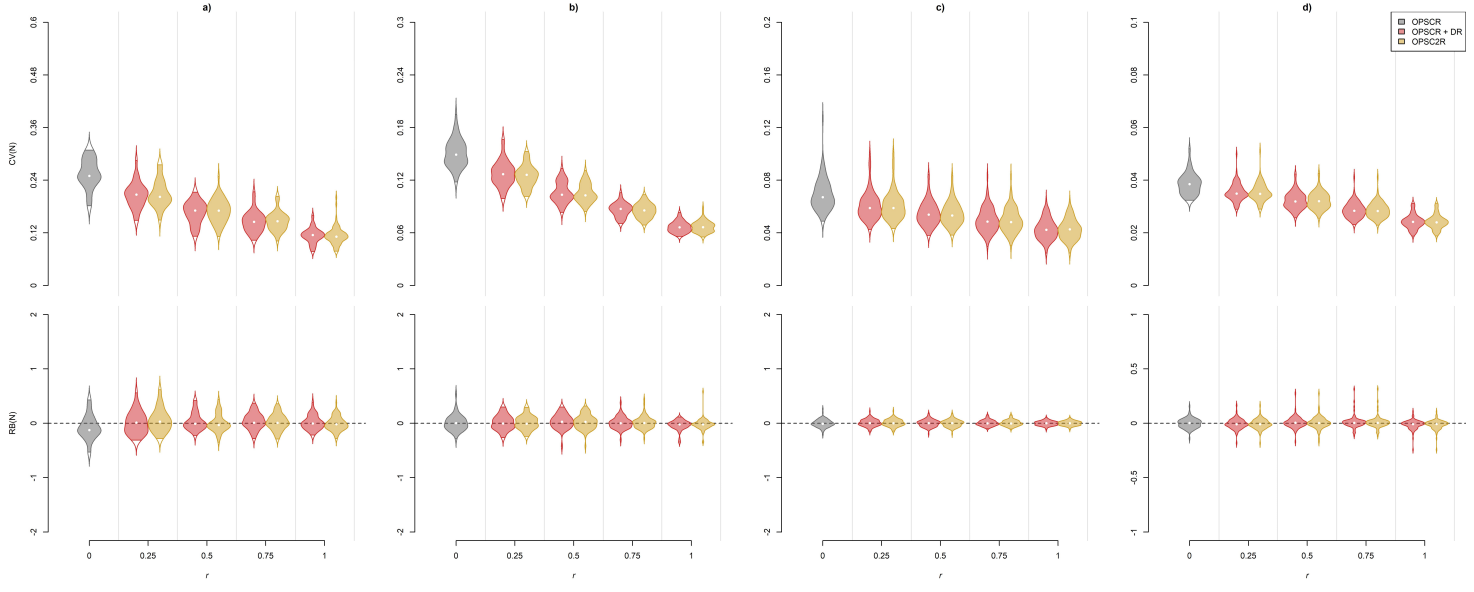

Figure S4: *Coefficient of variation (upper row) and relative bias (lower row) of the population size estimate for the 3rd capture occasion with increasing proportion of dead individuals recovered (r) for a traditional OPSCR model (OPSCR), a model integrating non-spatial dead recovery (OPSCR+DR), and a model integrating spatial dead recovery information (OPSC2R) for the different simulation scenarios; a) low detectability ($p_0 = 0.1$) and small population size ($N = 40$), b) high detectability ($p_0 = 0.5$) and small population size, c) low detectability and large population size ($N = 120$), d) high detectability and large population size. NB: y-axes scales are different among plots.*

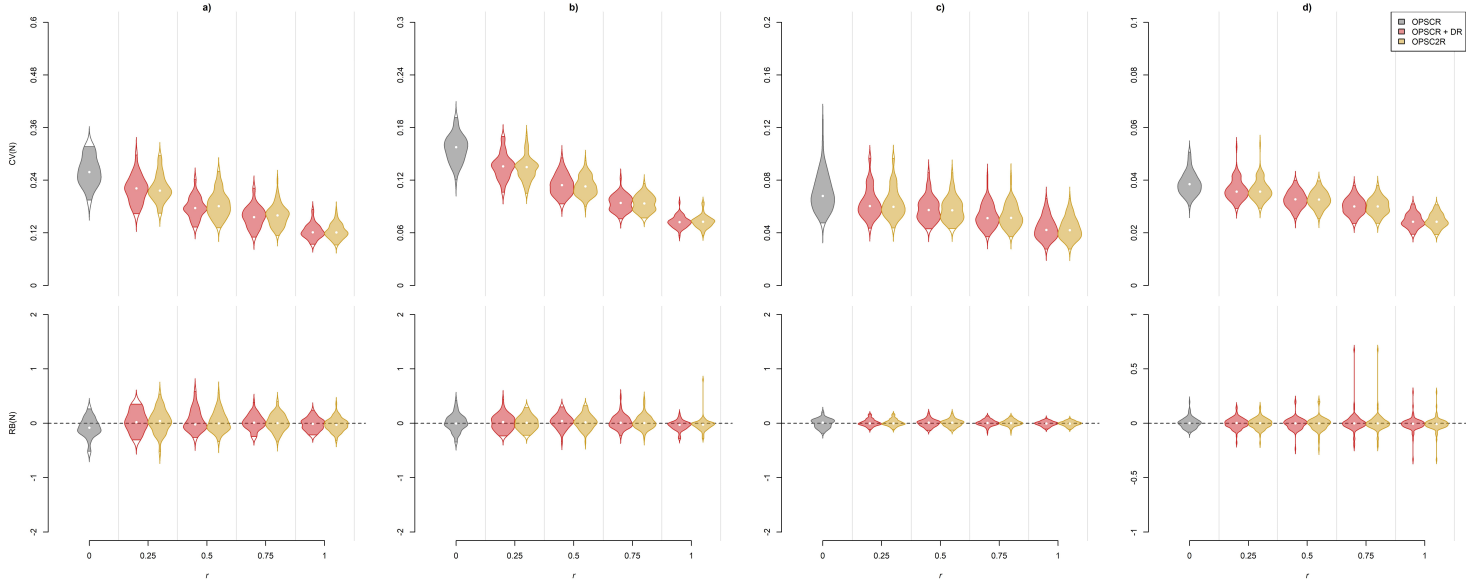

Figure S5: *Coefficient of variation (upper row) and relative bias (lower row) of the population size estimate for the 4th capture occasion with increasing proportion of dead individuals recovered (r) for a traditional OPSCR model (OPSCR), a model integrating non-spatial dead recovery (OPSCR+DR), and a model integrating spatial dead recovery information (OPSC2R) for the different simulation scenarios; a) low detectability ($p_0 = 0.1$) and small population size ($N = 40$), b) high detectability ($p_0 = 0.5$) and small population size, c) low detectability and large population size ($N = 120$), d) high detectability and large population size. NB: y-axes scales are different among plots.*

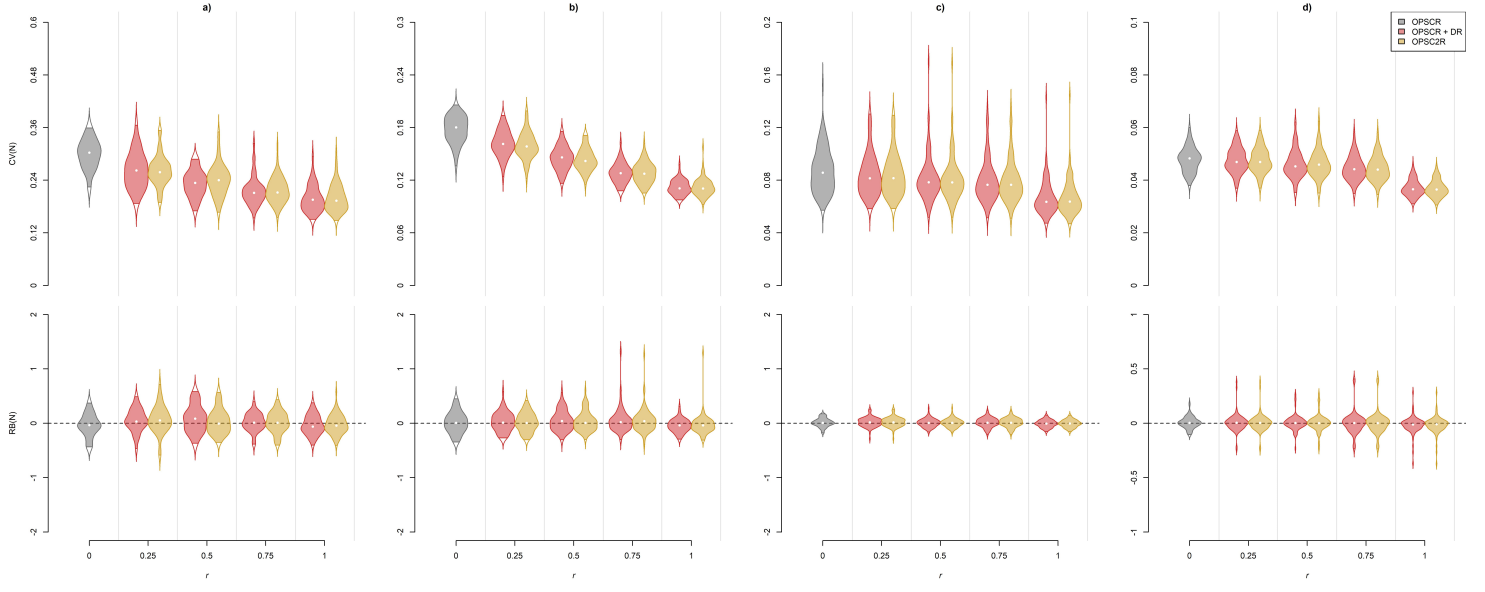

Figure S6: *Coefficient of variation (upper row) and relative bias (lower row) of the population size estimate for the 5th capture occasion with increasing proportion of dead individuals recovered (r) for a traditional OPSCR model (OPSCR), a model integrating non-spatial dead recovery (OPSCR+DR), and a model integrating spatial dead recovery information (OPSC2R) for the different simulation scenarios; a) low detectability ($p_0 = 0.1$) and small population size ($N = 40$), b) high detectability ($p_0 = 0.5$) and small population size, c) low detectability and large population size ($N = 120$), d) high detectability and large population size. NB: y- axes scales are different among plots.*

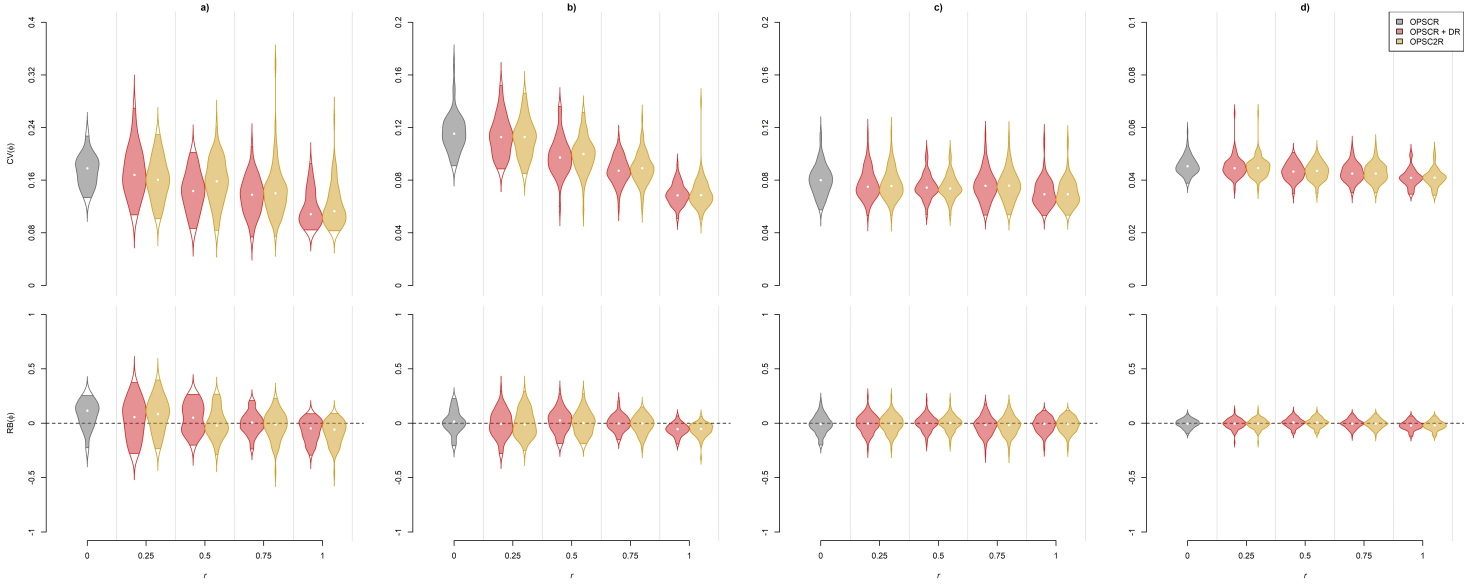

Figure S7: *Coefficient of variation (upper row) and relative bias (lower row) of the survival probability estimate (Φ) with increasing proportion of dead individuals recovered (r) for a traditional OPSCR model (OPSCR), a model integrating non-spatial dead recovery (OPSCR+DR), and a model integrating spatial dead recovery information (OPSC2R) for the different simulation scenarios; a) low detectability ($p_0 = 0.1$) and small population size ($N = 40$), b) high detectability ($p_0 = 0.5$) and small population size, c) low detectability and large population size ($N = 120$), d) high detectability and large population size. NB: y-axes scales are different among plots.*

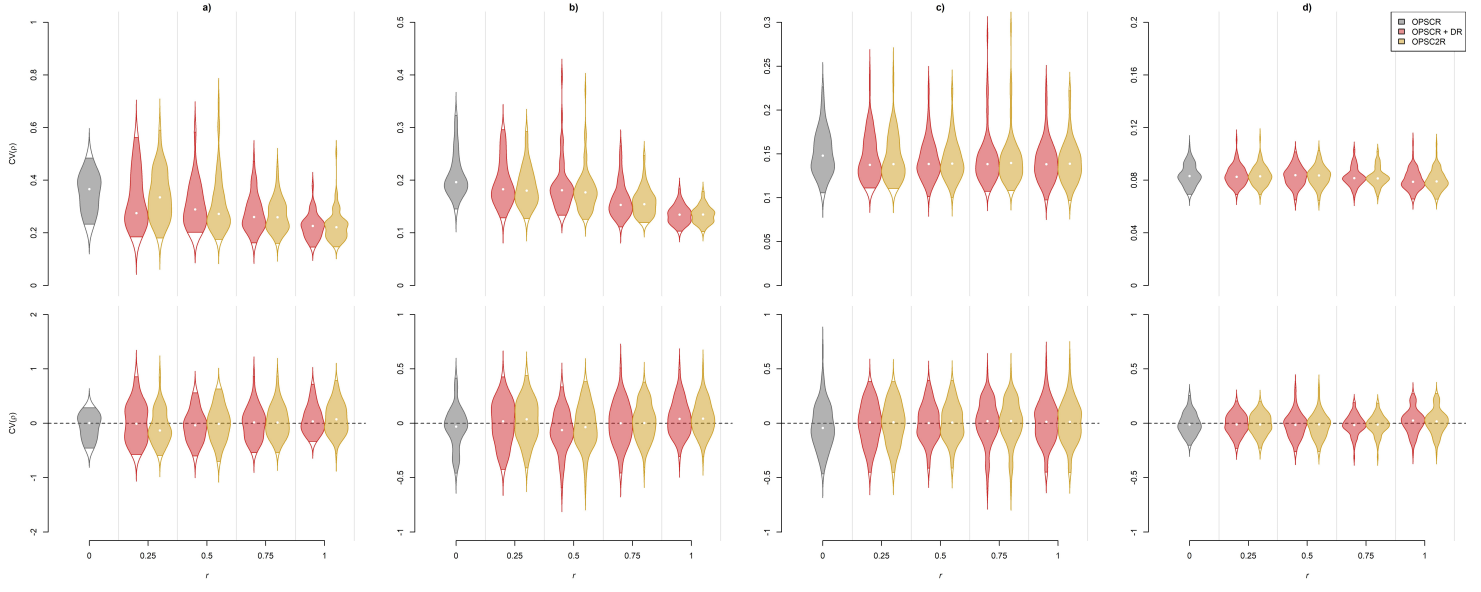

Figure S8: *Coefficient of variation (upper row) and relative bias (lower row) of the per capita recruitment rate estimate (ρ) with increasing proportion of dead individuals recovered (r) for a traditional OPSCR model (OPSCR), a model integrating non-spatial dead recovery (OPSCR+DR), and a model integrating spatial dead recovery information (OPSC2R) for the different simulation scenarios; a) low detectability ($p_0 = 0.1$) and small population size ($N = 40$), b) high detectability ($p_0 = 0.5$) and small population size, c) low detectability and large population size ($N = 120$), d) high detectability and large population size. NB: y-axes scales are different among plots.*

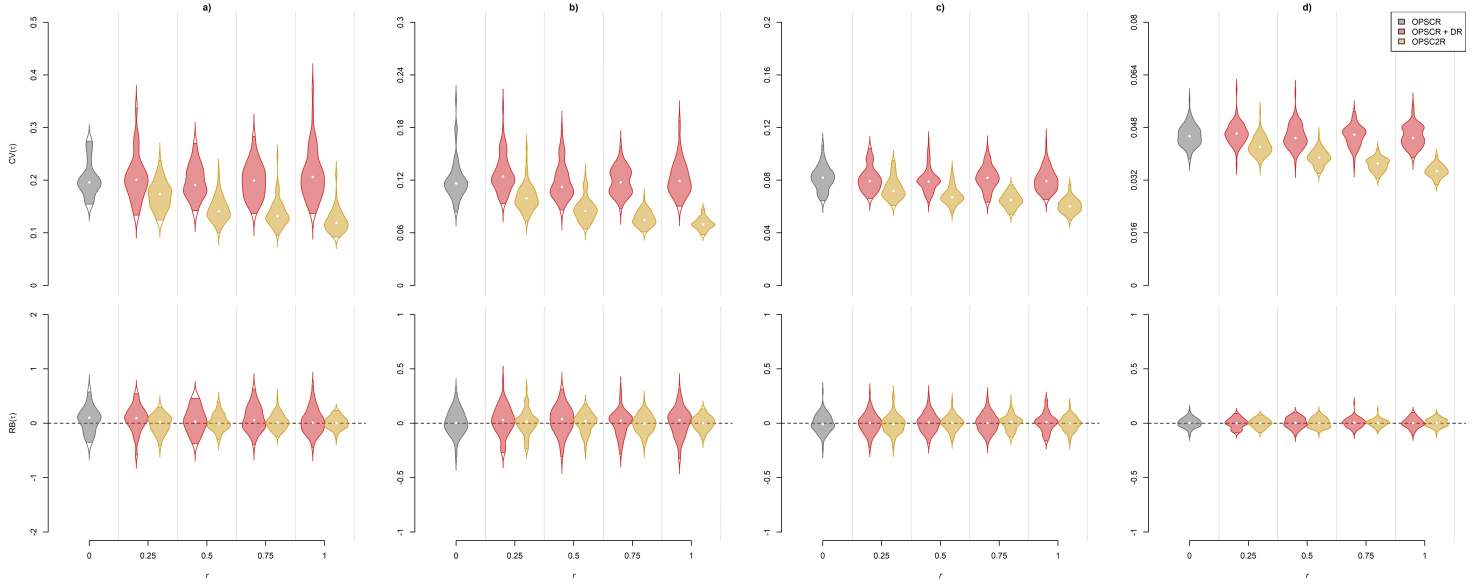

Figure S9: *Coefficient of variation (upper row) and relative bias (lower row) of the movement parameter estimate (τ) with increasing proportion of dead individuals recovered (r) for a traditional OPSCR model (OPSCR), a model integrating non-spatial dead recovery (OPSCR+DR), and a model integrating spatial dead recovery information (OPSC2R) for the different simulation scenarios; a) low detectability ($p_0 = 0.1$) and small population size ($N = 40$), b) high detectability ($p_0 = 0.5$) and small population size, c) low detectability and large population size ($N = 120$), d) high detectability and large population size. NB: y-axes scales are different among plots.*

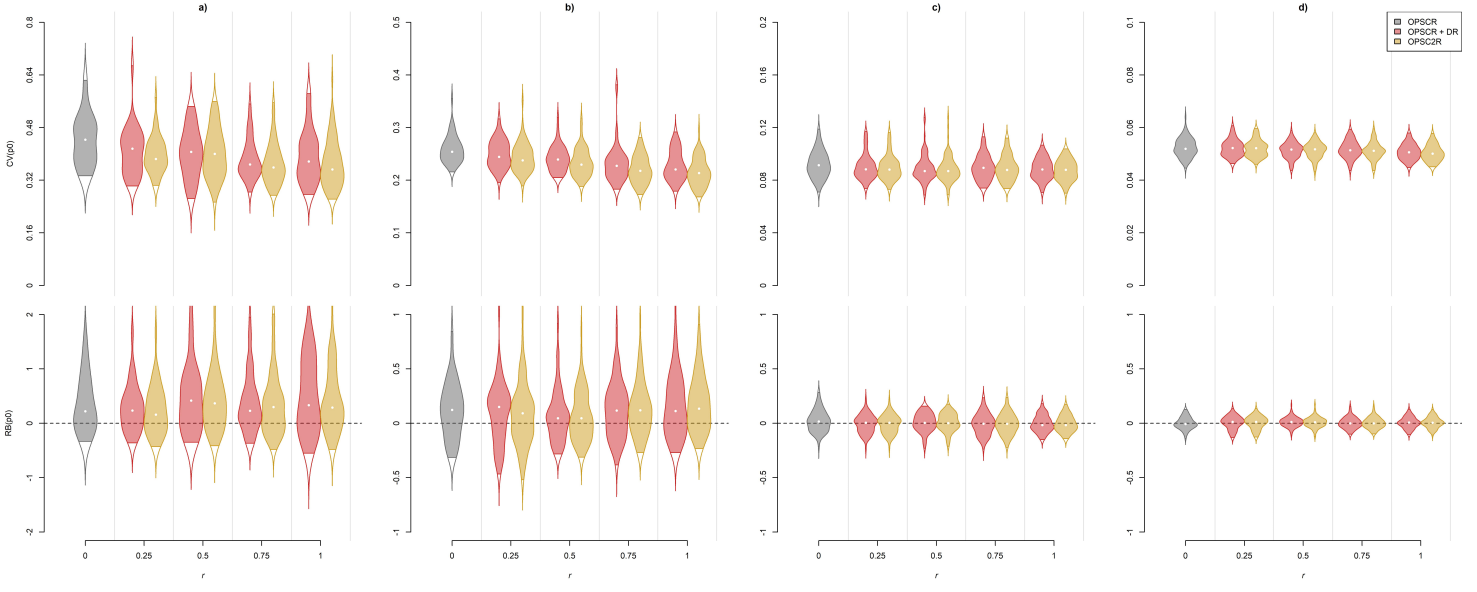

Figure S10: *Coefficient of variation (upper row) and relative bias (lower row) of the baseline detection probability estimate (p_0) with increasing proportion of dead individuals recovered (r) for a traditional OPSCR model (OPSCR), a model integrating non-spatial dead recovery (OPSCR+DR), and a model integrating spatial dead recovery information (OPSC2R) for the different simulation scenarios; a) low detectability ($p_0 = 0.1$) and small population size ($N = 40$), b) high detectability ($p_0 = 0.5$) and small population size, c) low detectability and large population size ($N = 120$), d) high detectability and large population size. NB: y-axes scales are different among plots.*

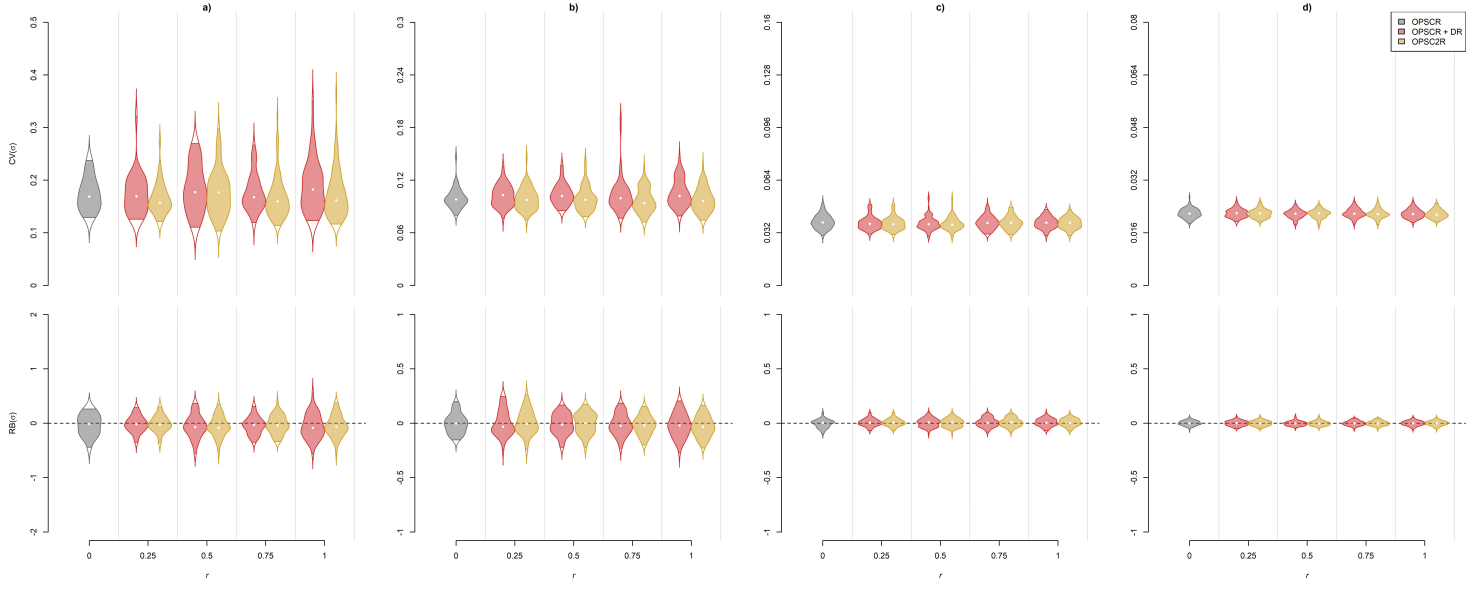

Figure S11: *Coefficient of variation (upper row) and relative bias (lower row) of the scale parameter of the detection function (σ) with increasing proportion of dead individuals recovered (r) for a traditional OPSCR model (OPSCR), a model integrating non-spatial dead recovery (OPSCR+DR), and a model integrating spatial dead recovery information (OPSC2R) for the different simulation scenarios; a) low detectability ($p_0 = 0.1$) and small population size ($N = 40$), b) high detectability ($p_0 = 0.5$) and small population size, c) low detectability and large population size ($N = 120$), d) high detectability and large population size. NB: y-axes scales are different among plots.*

Appendix 3: Supplementary information for the wolverine study

For the wolverine case study, we used data available in the Scandinavian large carnivore database Rovbase 3.0 (`http://rovbase.se/`or `http://rovbase.no/`). This database is used jointly by Norway and Sweden to record detailed information associated with large carnivore monitoring, including, but not limited to, non-invasive genetic sampling (NGS) data, dead recoveries, GPS search tracks and carnivore observations. Here, we restricted our analysis to the NGS and GPS tracks collected during winters 2012/13 to 2018/19 (December to June) in the Norwegian counties of Hedmark, Oppland and parts of Sør-Trøndelag (Fig. S12; Flagstad et al. 2004, Brøseth et al. 2010, Gervasi et al. 2015). If available, we also used dead recovery data for all individuals ever detected in the aforementioned study area, which led us to consider a 60 km surrounding buffer leading to a habitat area of 145,533 km^2 (Fig. S12). The dataset was composed of 1,011 alive detections and 70 dead recoveries from 232 individually identified female wolverines and 1,635 alive detections and 80 dead recoveries from 250 individually identified male wolverines.

To account for the specificity of the wolverine monitoring, the models fitted to the wolverine data extended on those used in the simulation study in four places: i) the definition of the detectors, ii) the definition of the baseline detection probability, iii) the definition of the mortality parameters in the OPSC2R, and iv) the definition of the spatial model for ACs distribution and movement.

Detectors. As is common practice in SCR studies using NGS search encounter data, we defined detectors as the center of grid cells overlaid over the entire study area, i.e. the area considered to have been searched for NGS samples. We used a grid cell resolution of 10x10 km, further subdivided into 25 sub-cells of 2x2 km for use in the partially aggregated binomial observation model (Milleret et al. 2018) leading to a total of 707 detector grid cells where DNA samples could be detected. We considered a buffer of 60 km around this study area to define the habitat S, i.e. the spatial extent where individual ACs can be located. Because the process by which dead recoveries are recorded is mostly independent from the DNA searches and can take place even where non-invasive DNA samples are collected, we defined a second set of detectors with a resolution of 10×10 km covering the entirety of the habitat S, leading to 1468 detectors for dead recoveries (Fig. S12).

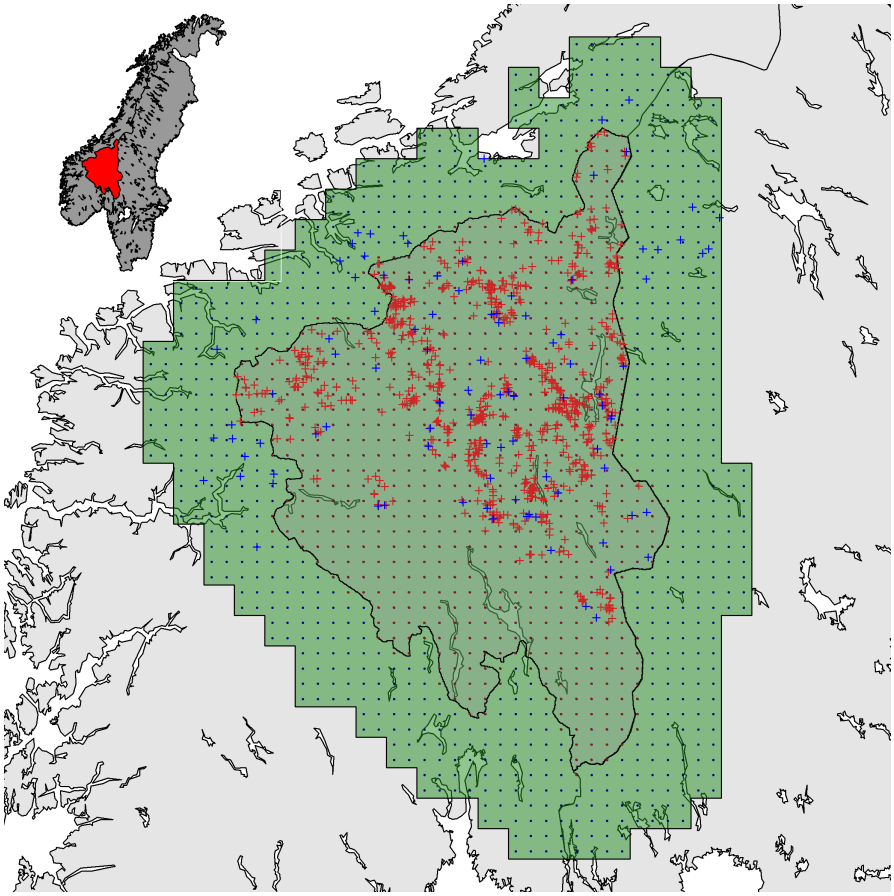

Figure S12: *Distribution of individual detections (non-invasive DNA sample; red crosses) and dead recoveries (blue crosses) used in the wolverine case study collected during monitoring periods 2012/13 to 2018/19. The area considered as searched for NGS is represented by the red polygon in the map in the upper left corner. Detector locations (separated by 10 km) considered in the analysis for live detections are represented by small red dots. Potential dead recovery locations are represented by all small dots (red and blue) and extend into the buffer area surrounding the detector grid*

Baseline detection probability. To account for the spatial and temporal variation in search effort and individual detectability, we used a set of covariates to model the individual, year and detector-specific detection probability (Bischof et al. 2019). These covariates included:

- the length of GPS search tracks logged by searchers within each detector grid cell in each monitoring period (*tracks*).

- the average distance to the nearest primary and secondary roads. This variable represents accessibility, which we predict to facilitate detectability (*roads*).

- the average percentage of snow cover (*snow*) in each detector grid cell (MODIS at 0.1 degrees resolution, `www.neo.sci.gsfc.nasa.gov`, accessed 2019-10-11). As NGS during winter relies heavily on the presence of snow, we predicted that greater snow cover increases detectability.

- the county identity. This was incorporated to control for differences in monitoring regimes between jurisdictions (*Hedmark, Oppland and Sør-Trondelag*).

- Previous detection could be expected to positively influence the probability of being detected at subsequent occasions. To account for this potential "trap-happiness" (Williams et al. 2002), we used an indicator of whether an individual was detected or not during the previous monitoring season as a linear predictor of the baseline detection probability (*trap-response*).

- Year. We estimated different baseline detection probabilities for each annual monitoring period to control for temporal variation in search effort.

Mortality parameters. As all dead recoveries in the analysis came from legally killed animals (e.g. legal hunting, management kills, defense of life and property) that must be reported to the management authorities (Fylkesmannen or SNO in Norway and Länsstyrelserna or the police in Sweden), we were able to reformulate the demographic model to distinguish between two mortality probabilities. An individual alive at time $t-1 (z_{it-1} = 2)$ can either survive and stay in state 2, die from legal culling with probability h and be reported with probability 1 (transition to state 3), or die from all other causes (including natural deaths) without being recovered (transition to state 4), so that $z_{it} \sim Categorical(0, \Phi, h, w)$. This formulation is equivalent to the one used in the simulation study in that $h = (1-\Phi)r$ and $w = (1-\Phi)(1-r)$, where r is the recovery probability conditional on being dead.

Spatial model. To account for the fact that wolverine density is most likely

inhomogeneous in space, we used an inhomogeneous point process (Illian et al. 2008) to model both the distribution of ACs during the first occasion and AC movements. Under this specification, a spatial intensity function describes movement as a series of isotropic Gaussian random walks (see also Gardner et al. 2018) weighted by the spatial covariate considered. We constructed a spatial covariate for density by applying a smoothing kernel to the locations of known dens for wolverines and estimated B_{dens} the effect of the number of dens in a given habitat cell on the probability that an individual has its AC located in this same cell.

We fitted separate sex-specific models because male and female wolverines are expected to have different vital rates and space-use patterns and fitted the OPSCR and OPSC2R models using Markov chain Monte Carlo (MCMC) simulations with NIMBLE (de Valpine et al. 2017) in R version 3.5.2 (R core team, 2017). To reduce computation time, we implemented the LESS approach (Milleret et al. 2019), i.e. we reduced the number of calculations to be performed by removing unnecessary evaluation of the likelihood whenever the distance between a detector and an individual activity center location was larger than a distance threshold (120 km) and built custom NIMBLE distributions (see Appendix S1). We ran four chains of 20,000 iterations including an initial burn-in phase of 5,000 iterations and considered models to have reached convergence if all R-hat value were ≤ 1.1 and visual inspections of trace plots revealed good mixing of the chains (Brooks and Gelman 1998). Mean parameter estimates for both models and sexes, with the associated 95% credible intervals, coefficients of variation and R-hat are provided in tables S2 and S3.

References

Bischof, R., C. Milleret, P. Dupont, J. Chipperfield, H. Brøseth, and J. Kindberg. 2019. RovQuant: Estimating density, abundance and population dynamics of bears, wolverines and wolves in Scandinavia. 79 pp.

Brooks, S. P., and A. Gelman. 1998. General Methods for Monitoring Convergence of Iterative Simulations. Journal of Computational and Graphical Statistics 7:434–455.

Brøseth, H., Ø. Flagstad, C. Wärdig, M. Johansson, and H. Ellegren. 2010. Large-scale noninvasive genetic monitoring of wolverines using scats reveals density dependent adult survival. Biological Conservation 143:113–120.

Flagstad, Ø., E. Hedmark, A. Landa, H. Brøseth, J. Persson, R. Andersen, P. Segerström, and H. Ellegren. 2004. Colonization History and Noninvasive Monitor-

ing of a Reestablished Wolverine Population. Conservation Biology 18:676–688.

Gardner, B., R. Sollmann, N. S. Kumar, D. Jathanna, and K. U. Karanth. 2018. State space and movement specification in open population spatial capture-recapture models. Ecology and Evolution 8(20):10336-10344.

Gervasi, V., H. Brøseth, E. B. Nilsen, H. Ellegren, Ø. Flagstad, and J. D. C. Linnell. 2015. Compensatory immigration counteracts contrasting conservation strategies of wolverines (*Gulo gulo*) within Scandinavia. Biological Conservation 191:632–639.

Illian, D. J., P. A. Penttinen, D. H. Stoyan, and D. D. Stoyan. 2008. Statistical Analysis and Modelling of Spatial Point Patterns. John Wiley & Sons.

Milleret, C., P. Dupont, C. Bonenfant, H. Brøseth, Ø. Flagstad, C. Sutherland, and R. Bischof. 2019. A local evaluation of the individual state-space to scale up Bayesian spatial capture–recapture. Ecology and Evolution 9:352–363.

Milleret, C., P. Dupont, H. Brøseth, J. Kindberg, J. A. Royle, and R. Bischof. 2018. Using partial aggregation in Spatial Capture Recapture. Methods in Ecology and Evolution 9:1896–1907.

de Valpine, P., D. Turek, C. J. Paciorek, C. Anderson-Bergman, D. T. Lang, and R. Bodik. 2017. Programming With Models: Writing Statistical Algorithms for General Model Structures With NIMBLE. Journal of Computational and Graphical Statistics 26:403–413.

Williams, B. K., J. D. Nichols, and M. J. Conroy. 2002. Analysis and management of animal populations: modeling, estimation, and decision making. Academic Press.

Table S2: *Parameter estimates for the female portion of the wolverine population in eastern Norway during winters 2012/2013 to 2018/2019 returned by the open-population spatial capture-recapture model (OPSCR, left) and the open-population spatial capture-recapture-recovery model (OPSC2R, right)*

Parameters		OPSCR					OPSC2R				
		mean	2.5%CI	97.5%CI	CV	Rhat	mean	2.5%CI	97.5%CI	CV	Rhat
Pop. size	$N_{2012/13}$	90	70	116	0.13	1.03	96	76	121	0.12	1.01
	$N_{2013/14}$	143	111	178	0.12	1.04	136	110	167	0.11	1.00
	$N_{2014/15}$	113	89	144	0.12	1.02	111	93	135	0.10	1.00
	$N_{2015/16}$	137	111	168	0.11	1.01	135	113	162	0.09	1.01
	$N_{2016/17}$	132	107	164	0.11	1.02	128	107	154	0.10	1.00
	$N_{2017/18}$	147	118	183	0.11	1.00	146	119	180	0.11	1.00
	$N_{2018/19}$	163	134	196	0.10	1.01	158	130	193	0.10	1.00
Spatial	B_{dens}	0.60	0.47	0.73	0.11	1.10	0.51	0.40	0.62	0.11	1.01
	τ	0.47	0.41	0.53	0.07	1.01	0.61	0.55	0.68	0.06	1.04
Demographic	γ_{2012}	0.24	0.14	0.34	0.22	1.03	0.21	0.13	0.32	0.23	1.00
	γ_{2013}	0.06	0.00	0.16	0.66	1.01	0.06	0.00	0.16	0.66	1.00
	γ_{2014}	0.24	0.13	0.38	0.26	1.01	0.22	0.12	0.34	0.26	1.00
	γ_{2015}	0.13	0.02	0.29	0.54	1.02	0.11	0.01	0.24	0.53	1.00
	γ_{2016}	0.37	0.18	0.61	0.30	1.01	0.37	0.20	0.59	0.27	1.00
	γ_{2017}	0.58	0.27	0.94	0.30	1.07	0.52	0.25	0.89	0.31	1.00
	Φ_{2012}	0.73	0.54	0.90	0.13	1.01	0.70	0.54	0.84	0.11	1.00
	Φ_{2013}	0.68	0.52	0.85	0.12	1.00	0.70	0.56	0.83	0.10	1.01
	Φ_{2014}	0.71	0.55	0.86	0.11	1.00	0.74	0.62	0.84	0.08	1.00
	Φ_{2015}	0.79	0.64	0.93	0.09	1.00	0.79	0.66	0.91	0.08	1.00
	Φ_{2016}	0.68	0.54	0.82	0.11	1.00	0.66	0.52	0.79	0.10	1.00
	Φ_{2017}	0.73	0.58	0.87	0.10	1.00	0.71	0.56	0.85	0.10	1.00

Table S2: *Continue*

Parameters		OPSCR					OPSC2R				
		mean	2.5%CI	97.5%CI	CV	Rhat	mean	2.5%CI	97.5%CI	CV	Rhat
	h_{2012}	-	-	-	-	-	0.12	0.06	0.20	0.29	1.00
	h_{2013}	-	-	-	-	-	0.07	0.03	0.12	0.34	1.00
	h_{2014}	-	-	-	-	-	0.18	0.11	0.26	0.22	1.00
	h_{2015}	-	-	-	-	-	0.07	0.03	0.12	0.34	1.00
	h_{2016}	-	-	-	-	-	0.12	0.07	0.19	0.25	1.00
	h_{2017}	-	-	-	-	-	0.07	0.03	0.12	0.32	1.00
	w_{2012}	0.27	0.10	0.46	0.34	1.01	0.18	0.05	0.34	0.43	1.00
	w_{2013}	0.32	0.15	0.48	0.26	1.00	0.24	0.11	0.38	0.29	1.01
	w_{2014}	0.29	0.14	0.45	0.28	1.00	0.08	0.01	0.20	0.59	1.00
	w_{2015}	0.21	0.07	0.36	0.35	1.00	0.14	0.03	0.27	0.45	1.00
	w_{2016}	0.32	0.18	0.46	0.23	1.00	0.22	0.10	0.35	0.30	1.00
	w_{2017}	0.27	0.13	0.42	0.27	1.00	0.22	0.08	0.37	0.33	1.00
Detection	${p_0^{Hedmark}}_{2012/13}$	0.03	0.00	0.13	1.18	1.01	0.03	0.00	0.14	1.18	1.00
	${p_0^{Hedmark}}_{2013/14}$	0.03	0.01	0.05	0.33	1.00	0.02	0.01	0.04	0.34	1.00
	${p_0^{Hedmark}}_{2014/15}$	0.03	0.02	0.03	0.16	1.00	0.02	0.02	0.03	0.16	1.00
	${p_0^{Hedmark}}_{2015/16}$	0.04	0.01	0.12	0.70	1.00	0.05	0.01	0.13	0.71	1.00
	${p_0^{Hedmark}}_{2016/17}$	0.01	0.00	0.02	0.33	1.00	0.01	0.00	0.01	0.33	1.00
	${p_0^{Hedmark}}_{2017/18}$	0.01	0.01	0.01	0.16	1.00	0.01	0.01	0.01	0.16	1.00
	${p_0^{Hedmark}}_{2018/19}$	0.02	0.00	0.09	1.02	1.00	0.02	0.00	0.08	0.94	1.00

Table S2: *Continue*

Parameters	OPSCR					OPSC2R				
	mean	2.5%CI	97.5%CI	CV	Rhat	mean	2.5%CI	97.5%CI	CV	Rhat
$p_0^{Oppland}{}_{2012/13}$	0.01	0.01	0.02	0.30	1.00	0.01	0.01	0.02	0.30	1.00
$p_0^{Oppland}{}_{2013/14}$	0.01	0.01	0.01	0.19	1.00	0.01	0.01	0.01	0.18	1.00
$p_0^{Oppland}{}_{2014/15}$	0.03	0.00	0.07	0.69	1.00	0.02	0.00	0.07	0.73	1.00
$p_0^{Oppland}{}_{2015/16}$	0.02	0.01	0.03	0.23	1.00	0.02	0.01	0.03	0.24	1.00
$p_0^{Oppland}{}_{2016/17}$	0.01	0.01	0.01	0.16	1.00	0.01	0.01	0.01	0.16	1.00
$p_0^{Oppland}{}_{2017/18}$	0.04	0.01	0.11	0.72	1.00	0.04	0.01	0.12	0.76	1.00
$p_0^{Oppland}{}_{2018/19}$	0.02	0.01	0.03	0.24	1.00	0.02	0.01	0.03	0.23	1.00
$p_0^{SØr-TrØndelag}{}_{2012/13}$	0.01	0.01	0.01	0.18	1.00	0.01	0.01	0.01	0.18	1.00
$p_0^{SØr-TrØndelag}{}_{2013/14}$	0.01	0.00	0.03	1.14	1.00	0.01	0.00	0.03	1.16	1.00
$p_0^{SØr-TrØndelag}{}_{2014/15}$	0.02	0.01	0.03	0.26	1.00	0.01	0.01	0.02	0.26	1.00
$p_0^{SØr-TrØndelag}{}_{2015/16}$	0.01	0.01	0.02	0.15	1.00	0.01	0.01	0.01	0.15	1.00
$p_0^{SØr-TrØndelag}{}_{2016/17}$	0.02	0.00	0.05	0.82	1.00	0.02	0.00	0.05	0.83	1.00
$p_0^{SØr-TrØndelag}{}_{2017/18}$	0.02	0.01	0.03	0.25	1.00	0.02	0.01	0.03	0.25	1.00
$p_0^{SØr-TrØndelag}{}_{2018/19}$	0.02	0.01	0.02	0.14	1.00	0.02	0.01	0.02	0.14	1.00
σ	0.35	0.33	0.37	0.03	1.00	0.34	0.33	0.36	0.03	1.00
B_{tracks}	0.60	0.52	0.68	0.07	1.00	0.61	0.53	0.69	0.07	1.00
B_{roads}	-0.03	-0.12	0.05	1.29	1.00	-0.02	-0.11	0.07	2.70	1.00
B_{snow}	0.03	-0.10	0.16	2.05	1.00	0.01	-0.12	0.14	6.62	1.00
$B_{trap\ response}$	0.36	0.18	0.56	0.27	1.01	0.41	0.22	0.61	0.24	1.00

Table S3: *Parameter estimates for the male portion of the wolverine population in eastern Norway during winters 2012/2013 to 2018/2019 returned by the open-population spatial capture-recapture model (OPSCR, left) and the open-population spatial capture-recapture-recovery model (OPSC2R, right).*

Parameters		OPSCR					OPSC2R				
		mean	2.5%CI	97.5%CI	CV	Rhat	mean	2.5%CI	97.5%CI	CV	Rhat
Pop. size	$N_{2012/13}$	84	66	106	0.12	1.04	90	73	112	0.11	1.05
	$N_{2013/14}$	92	75	113	0.11	1.03	94	79	114	0.10	1.04
	$N_{2014/15}$	78	63	96	0.11	1.03	88	76	104	0.08	1.01
	$N_{2015/16}$	78	66	93	0.09	1.01	84	74	97	0.07	1.01
	$N_{2016/17}$	75	64	90	0.09	1.00	78	68	92	0.08	1.00
	$N_{2017/18}$	104	88	123	0.09	1.01	102	87	119	0.08	1.00
	$N_{2018/19}$	127	107	149	0.09	1.01	126	106	149	0.09 6 1.00	
Spatial	B_{dens}	0.51	0.39	0.63	0.12	1.04	0.47	0.37	0.58	0.11	1.03
	τ	0.74	0.65	0.83	0.06	1.06	0.83	0.74	0.93	0.06	1.02
Demographic	γ_{2012}	0.15	0.09	0.22	0.21	1.02	0.14	0.09	0.21	0.21	1.03
	γ_{2013}	0.10	0.05	0.16	0.28	1.02	0.11	0.06	0.17	0.26	1.01
	γ_{2014}	0.11	0.06	0.18	0.27	1.01	0.10	0.05	0.16	0.30	1.00
	γ_{2015}	0.11	0.05	0.18	0.30	1.00	0.11	0.05	0.17	0.29	1.00
	γ_{2016}	0.28	0.18	0.38	0.18	1.03	0.26	0.18	0.36	0.18	1.01
	γ_{2017}	0.39	0.25	0.56	0.21	1.04	0.39	0.25	0.56	0.20	1.02
	Φ_{2012}	0.46	0.31	0.61	0.17	1.01	0.48	0.34	0.62	0.15	1.01
	Φ_{2013}	0.52	0.38	0.67	0.14	1.01	0.59	0.45	0.72	0.12	1.01
	Φ_{2014}	0.60	0.45	0.75	0.13	1.01	0.64	0.52	0.76	0.09	1.00
	Φ_{2015}	0.63	0.49	0.77	0.11	1.00	0.62	0.48	0.74	0.11	1.00
	Φ_{2016}	0.57	0.42	0.71	0.13	1.00	0.55	0.41	0.68	0.13	1.00
	Φ_{2017}	0.61	0.48	0.73	0.11	1.00	0.60	0.47	0.73	0.11	1.00

Table S3: *Continue*

Parameters		OPSCR					OPSC2R				
		mean	2.5%CI	97.5%CI	CV	Rhat	mean	2.5%CI	97.5%CI	CV	Rhat
	h_{2012}	-	-	-	-	-	0.15	0.08	0.24	0.27	1.01
	h_{2013}	-	-	-	-	-	0.08	0.04	0.15	0.35	1.00
	h_{2014}	-	-	-	-	-	0.23	0.15	0.33	0.20	1.00
	h_{2015}	-	-	-	-	-	0.20	0.12	0.29	0.23	1.00
	h_{2016}	-	-	-	-	-	0.17	0.10	0.27	0.25	1.00
	h_{2017}	-	-	-	-	-	0.12	0.06	0.19	0.28	1.00
	w_{2012}	0.54	0.39	0.69	0.15	1.01	0.37	0.22	0.52	0.21	1.02
	w_{2013}	0.48	0.33	0.62	0.16	1.01	0.33	0.20	0.48	0.22	1.02
	w_{2014}	0.40	0.25	0.55	0.19	1.01	0.13	0.04	0.24	0.40	1.00
	w_{2015}	0.37	0.23	0.51	0.20	1.00	0.19	0.08	0.31	0.31	1.00
	w_{2016}	0.43	0.29	0.58	0.17	1.00	0.28	0.16	0.42	0.24	1.00
	w_{2017}	0.39	0.27	0.52	0.17	1.00	0.28	0.17	0.41	0.22	1.00
Detection	${p_0^{Hedmark}}_{2012/13}$	0.03	0.00	0.09	0.82	1.00	0.02	0.00	0.07	0.82	1.00
	${p_0^{Hedmark}}_{2013/14}$	0.01	0.01	0.02	0.29	1.01	0.01	0.00	0.01	0.30	1.01
	${p_0^{Hedmark}}_{2014/15}$	0.01	0.01	0.02	0.13	1.01	0.01	0.01	0.02	0.13	1.00
	${p_0^{Hedmark}}_{2015/16}$	0.01	0.00	0.02	1.05	1.00	0.01	0.00	0.02	1.03	1.00
	${p_0^{Hedmark}}_{2016/17}$	0.02	0.01	0.03	0.23	1.00	0.02	0.01	0.03	0.23	1.00
	${p_0^{Hedmark}}_{2017/18}$	0.01	0.01	0.01	0.14	1.01	0.01	0.01	0.01	0.14	1.00
	${p_0^{Hedmark}}_{2018/19}$	0.00	0.00	0.02	1.11	1.00	0.00	0.00	0.02	1.10	1.00

Table S3: *Continue*

Parameters	OPSCR					OPSC2R				
	mean	2.5%CI	97.5%CI	CV	Rhat	mean	2.5%CI	97.5%CI	CV	Rhat
$p_0^{Oppland}{}_{2012/13}$	0.01	0.01	0.02	0.28	1.00	0.01	0.01	0.02	0.28	1.00
$p_0^{Oppland}{}_{2013/14}$	0.01	0.01	0.01	0.14	1.01	0.01	0.00	0.01	0.14	1.00
$p_0^{Oppland}{}_{2014/15}$	0.02	0.01	0.05	0.56	1.00	0.02	0.01	0.05	0.56	1.00
$p_0^{Oppland}{}_{2015/16}$	0.02	0.01	0.03	0.22	1.00	0.01	0.01	0.02	0.22	1.00
$p_0^{Oppland}{}_{2016/17}$	0.01	0.01	0.02	0.11	1.00	0.01	0.01	0.01	0.12	1.00
$p_0^{Oppland}{}_{2017/18}$	0.03	0.01	0.07	0.47	1.00	0.03	0.01	0.07	0.47	1.00
$p_0^{Oppland}{}_{2018/19}$	0.02	0.01	0.03	0.21	1.00	0.02	0.01	0.02	0.21	1.00
$p_0^{Sør-Trøndelag}{}_{2012/13}$	0.01	0.01	0.01	0.13	1.00	0.01	0.01	0.01	0.13	1.00
$p_0^{Sør-Trøndelag}{}_{2013/14}$	0.00	0.00	0.02	1.07	1.00	0.00	0.00	0.02	1.03	1.00
$p_0^{Sør-Trøndelag}{}_{2014/15}$	0.01	0.01	0.02	0.24	1.00	0.01	0.01	0.02	0.24	1.00
$p_0^{Sør-Trøndelag}{}_{2015/16}$	0.01	0.01	0.02	0.10	1.00	0.01	0.01	0.02	0.10	1.00
$p_0^{Sør-Trøndelag}{}_{2016/17}$	0.01	0.00	0.03	0.64	1.00	0.01	0.00	0.03	0.64	1.00
$p_0^{Sør-Trøndelag}{}_{2017/18}$	0.03	0.02	0.04	0.17	1.00	0.03	0.02	0.04	0.17	1.00
$p_0^{Sør-Trøndelag}{}_{2018/19}$	0.01	0.01	0.01	0.11	1.00	0.01	0.01	0.01	0.11	1.00
σ	0.52	0.51	0.54	0.02	1.00	0.52	0.50	0.54	0.02	1.00
B_{tracks}	0.53	0.48	0.59	0.06	1.00	0.55	0.49	0.61	0.05	1.00
B_{roads}	0.04	-0.03	0.11	0.96	1.00	0.02	-0.05	0.09	1.46	1.00
B_{snow}	0.00	-0.10	0.10	80.44	1.00	-0.01	-0.11	0.08	3.85	1.00
$B_{trap\ response}$	0.55	0.40	0.70	0.14	1.02	0.57	0.42	0.73	0.13	1.01

ISBN: 978-82-575-1726-7
ISSN: 1894-6402

Norwegian University
of Life Sciences

Postboks 5003
NO-1432 Ås, Norway
+47 67 23 00 00
www.nmbu.no

108094 / ANDVORDGRAFISK.NO